AD-A080 606 AUBURN UNIV ALA DEPT OF AEROSPACE ENGINEERING F/G 19/4
AN ANALYSIS OF THE EFFECTS OF TRANSVERSE VIBRATION ON THE ATTIT--ETC(U)
DEC 79 J E COCHRAN, G A CASTLEBERRY, S D REW DAAK40-79-C-0030
UNCLASSIFIED DRSMI/RL-CR-80-2 NL

1 OF 2
AD
A080606

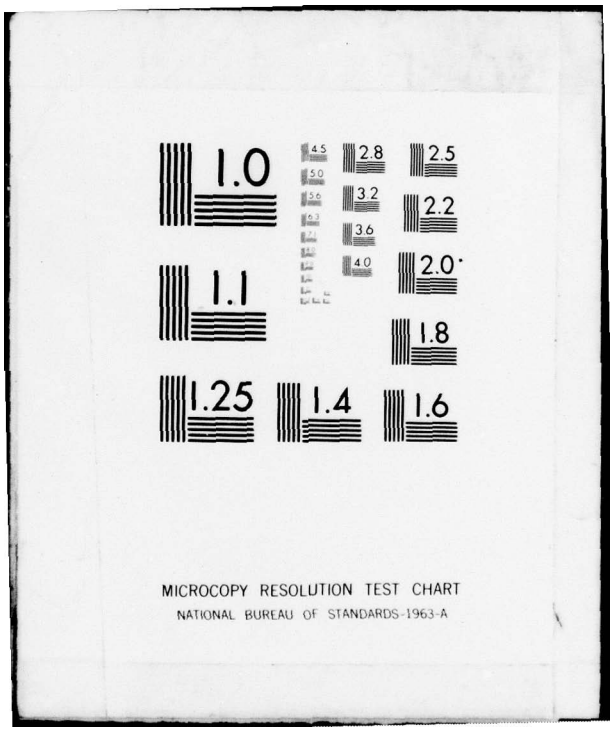
1.0
1.1
1.25
1.4
1.6
1.8
2.0
2.2
2.5
2.8
3.2
3.6
4.0
4.5
5.0
5.6
6.3
MICROCOPY RESOLUTION TEST CHART
NATIONAL BUREAU OF STANDARDS-1963-A

TECHNICAL REPORT RL-CR-80-2

# AN ANALYSIS OF THE EFFECTS OF TRANSVERSE VIBRATION ON THE ATTITUDE MOTION OF FREE-FLIGHT ROCKETS

by

John E. Cochran, Jr.; Grant A. Castleberry; Stephen D. Rew
Aerospace Engineering Department
Auburn University
Auburn, Alabama 36830

FINAL REPORT
under
Contract DAAK40-79-C-0030

administered through

Engineering Experiment Station
Auburn University
Auburn, Alabama 36830



U.S. ARMY MISSILE COMMAND
Redstone Arsenal, Alabama 35809

14 December 1979

## DISPOSITION INSTRUCTIONS

DESTROY THIS REPORT WHEN IT IS NO LONGER NEEDED. DO NOT RETURN IT TO THE ORIGINATOR.

## DISCLAIMER

THE FINDINGS IN THIS REPORT ARE NOT TO BE CONSTRUED AS AN OFFICIAL DEPARTMENT OF THE ARMY POSITION UNLESS SO DESIGNATED BY OTHER AUTHORIZED DOCUMENTS.

## TRADE NAMES

USE OF TRADE NAMES OR MANUFACTURERS IN THIS REPORT DOES NOT CONSTITUTE AN OFFICIAL INDORSEMENT OR APPROVAL OF THE USE OF SUCH COMMERCIAL HARDWARE OR SOFTWARE.

SECURITY CLASSIFICATION OF THIS PAGE *(When Data Entered)*

## REPORT DOCUMENTATION PAGE

READ INSTRUCTIONS BEFORE COMPLETING FORM

| | |
|---|---|
| 1. REPORT NUMBER: Technical Report RL-CR-80-2 | 2. GOVT ACCESSION NO. |
| 3. RECIPIENT'S CATALOG NUMBER: (9) | |
| 4. TITLE *(and Subtitle)*: (4) AN ANALYSIS OF THE EFFECTS OF TRANSVERSE VIBRATION ON THE ATTITUDE MOTION OF FREE-FLIGHT ROCKETS. | 5. TYPE OF REPORT & PERIOD COVERED: FINAL rept. 15 Dec 1978-15 Dec 1979 |
| | 6. PERFORMING ORG. REPORT NUMBER |
| 7. AUTHOR(s): (10) John E. Cochran, Jr.; Grant A. Castleberry; Stephen D. Rew | 8. CONTRACT OR GRANT NUMBER(s): (15) DAAK40-79-C-0030 JDR |
| 9. PERFORMING ORGANIZATION NAME AND ADDRESS: Engineering Experiment Station, Auburn University, Auburn, Alabama 36830 | 10. PROGRAM ELEMENT, PROJECT, TASK AREA & WORK UNIT NUMBERS: (12) 143 |
| 11. CONTROLLING OFFICE NAME AND ADDRESS: (11) Commander, US Army Missile Command, Attn: DRSMI-RPT, Redstone Arsenal, AL 35809 | 12. REPORT DATE: 14 December 1979 |
| | 13. NUMBER OF PAGES: 98 |
| 14. MONITORING AGENCY NAME & ADDRESS *(if different from Controlling Office)*: Commander, US Army Missile Command, Attn: DRSMI-RLH, Redstone Arsenal, AL 35809 | 15. SECURITY CLASS. *(of this report)*: Unclassified |
| | 15a. DECLASSIFICATION/DOWNGRADING SCHEDULE: N/A |

16. DISTRIBUTION STATEMENT *(of this Report)*

Approved for public release; distribution unlimited

17. DISTRIBUTION STATEMENT *(of the abstract entered in Block 20, if different from Report)*

(18) DRSMI/RL

(19) CR-80-2

18. SUPPLEMENTARY NOTES

The findings of this report are not to be construed as an official Department of the Army position unless so designated by other authorized documents.

19. KEY WORDS *(Continue on reverse side if necessary and identify by block number)*

Free-Flight Rockets
Flexible Rockets
Spinning Rockets
Mallaunch of Free Rockets
Assumed Modes
Coulomb Friction

20. ABSTRACT *(Continue on reverse side if necessary and identify by block number)*

The results of an analysis of the effects of transverse vibration of a spinning, flexible, free-flight rocket during its guidance phase on its attitude motion subsequent to end of guidance (EOG) are presented. Two models of a spinning, flexible, free-flight rocket are described. One is a simple two-body model. The other is a "continuous" model. A physical explanation is given for the way transverse vibration during the guidance phase causes the appearance of a transverse angular rate at EOG. The two-body model is

DD FORM 1 JAN 73 1473 EDITION OF 1 NOV 65 IS OBSOLETE

SECURITY CLASSIFICATION OF THIS PAGE *(When Data Entered)*

401 926

JOB

20. (Continued)

used to obtain a simple equation from which estimates of the transverse angular rate can be found. Typical results from the two models are presented and agreement between the results is shown. Optical lever data for a free-flight rocket which was vibrating transversely at EOG is analyzed using three methods: (1) a graphical method which ignores transverse vibration effects, (2) a method based on the use of graphical results and results from the two-body model, and (3) a method in which the data is fitted in a least-squares sense by a two-body model solution. This part of the analysis reveals that the transverse angular rate of this rocket at EOG due to vibration was on the order of 70 mrad/sec. Two probable causes of transverse vibration, multiple (more than two) supports and friction, are studied using a modified continuous model and an extended (to include friction) two-body model, respectively. Each cause is shown capable of producing transverse vibrations which result in significant transverse angular rates at EOG.

## PREFACE

This report contains a description of the research accomplished under U.S. Army Contract DAAK40-79-C-0030, during the period 15 December 1978 to 15 December 1979, for the U.S. Army Missile Command, Redstone Arsenal, Alabama. Mr. Dean E. Christensen, the Contracting Officer's Technical Representative, was of great assistance during this effort. His encouragement and technical suggestions are truly appreciated.

The authors, other than the first, contributed to the contractual effort in the following ways. Mr. Grant Castleberry assisted in programming and in preparation of the manuscript of this report. Mr. Stephen Rew assisted in programming, particularly in obtaining comparisons of theoretical results and optical lever data, and in the preparation of the manuscript.

In addition to the authors, Mr. Gene Holloway contributed to the development of computer codes and Mr. Mark Maschoff assisted in the preparation of graphic materials. Finally, Mrs. Marjorie McGee deserves special recognition for her superb typing of the manuscript.

John E. Cochran, Jr.
Project Leader

TABLE OF CONTENTS


PREFACE . . . . . i

LIST OF FIGURES . . . . . iv

LIST OF TABLES . . . . . vi

SECTION 1. INTRODUCTION . . . . . 1

SECTION 2. EFFECTS OF TRANSVERSE VIBRATION . . . . . 4

2.1 Description of models . . . . . 4

2.2 Causes of Transverse Angular Rates . . . . . 8

2.3 How Transverse Vibration Causes Transverse Angular Rates . . . . . 9

2.4 Results from Mathematical Models . . . . . 14

SECTION 3. ANALYSIS OF OPTICAL LEVER DATA . . . . . 27

3.1 Introduction . . . . . 27

3.2 Transverse Vibration Effects Ignored . . . . . 28

3.3 Transverse Vibration Effects Included . . . . . 34

SECTION 4. PROBABLE CAUSES OF TRANSVERSE VIBRATION . . . . . 40

4.1 Introduction . . . . . 40

4.2 Multiple Supports . . . . . 41

4.3 Flexible Supports and Friction . . . . . 43

SECTION 5. CONCLUSIONS AND RECOMMENDATIONS . . . . . 53

5.1 Conclusions . . . . . 53

5.2 Recommendations . . . . . 55

REFERENCES . . . . . 56

APPENDIX A. TWO-BODY MATHEMATICAL MODEL FOR FREE FLIGHT . . . . . 57

APPENDIX B. ASSUMED-MODES MATHEMATICAL MODEL . . . . . 64

TABLE OF CONTENTS (CONTINUED)

APPENDIX C. PRINCIPAL AXES ROTATION DUE TO TRANSVERSE VIBRATION . . . . . 75

APPENDIX D. TWO-BODY MATHEMATICAL MODEL WITH FLEXIBLE SUPPORTS . . . . . 81

LIST OF FIGURES


| Figure No. | | Page No. |
|---|---|---|
| 1 | Two-body physical model. (a) On launcher. (b) Off launcher | 5 |
| 2 | Continuous physical model. (a) On launcher. (b) Off launcher | 7 |
| 3 | Angular momentum of a spinning flexible rocket | 10 |
| 4 | Transverse angular rate as a function of forward support location | 14 |
| 5 | Two-body results - effects of bending | 16 |
| 6 | Thrust misalignment angles | 17 |
| 7 | Two-body results - effects of thrust misalignment. | 18 |
| 8 | Two-body results - combined effects. | 19 |
| 9 | Assumed-modes results - effects of bending | 21 |
| 10 | Assumed-modes results - effects of thrust misalignment | 22 |
| 11 | Assumed-modes and two-body results - combined effects. | 23 |
| 12 | Assumed-modes results - effects of bending with different guidance lengths | 24 |
| 13 | Assumed-modes results - "simulated" optical lever data | 25 |
| 14 | Optical lever data (reduced) for GEM #8 | 26 |
| 15 | Pitch and yaw angles when thrust misalignment is present | 30 |
| 16 | Comparison of theoretical results and data - bending effects ignored | 32 |
| 17 | Comparison of theoretical results and data - bending effects included using first method | 33 |

LIST OF FIGURES (CONTINUED)


| Figure No. | | Page No. |
|---|---|---|
| 18 | Comparison of theoretical results and data - bending effects included using least-squares method, Case 1 | 37 |
| 19 | Comparison of theoretical results and data - bending effects included using least-squares method, Case 2 | 39 |
| 20 | Effect of "intermittent" third support | 42 |
| 21 | Effect of flexible supports | 44 |
| 22 | Effects of flexible supports and friction - $\mu_P = \mu_Q = 0.05$ | 46 |
| 23 | Effects of flexible supports and friction - $\mu_P = \mu_Q = 0.1$ | 47 |
| 24 | Effects of flexible supports, friction and clearance - $\mu_P = \mu_Q = 0.05$ and $\varepsilon = 0.31$ mm | 49 |
| 25 | Effect of forward support location | 50 |
| 26 | A combined effects example | 51 |
| C.1 | Principal axes of the two-body model | 76 |
| D.1 | Two-body model in flexible tube | 82 |
| D.2 | Displacement of point P | 86 |
| D.3 | Normal and frictional forces | 87 |

LIST OF TABLES


| Table No. | | Page No. |
|---|---|---|
| 1 | Physical Characteristics of GEM #7 . . . . . | 15 |
| 2 | Characteristics of Two-Body Model of GEM #7 . . . . . | 15 |
| 3 | Data for Assumed-Modes Model of GEM #7 . . . . . | 20 |
| 4 | Physical Characteristics of GEM #8 . . . . . | 31 |

## SECTION 1. INTRODUCTION

The accuracy of a free-flight rocket depends significantly on the transverse angular rate of the rocket at the time it is no longer physically constrained by the launcher guidance mechanism, i.e., at end of guidance (EOG). If the causes of such angular rates cannot be accurately predicted and proper allowances made for them, an accurate free-flight rocket system cannot be constructed, except perhaps by trial and error. Historically, launcher motion and guidance mechanism imperfections have been considered principal causes of transverse angular rates of free-flight rockets at EOG. Dynamic imbalance of spinning rockets and thrust misalignment have also been recognized as resulting in what are effectively secular transverse angular rates at EOG.

Due to difficulties in interpreting optical lever data in the light of only the recognized error sources mentioned above, and to the fact that the data in question evidenced considerable transverse bending of rockets, both during and subsequent to guidance,[1] it was suspected that there was a strong correlation between transverse vibration of a free-flight rocket during guidance and its transverse angular rate subsequent to EOG. Through a previous research effort,[2] it was shown, on the basis of a simple two-body model of a spinning flexible rocket, that if such a rocket is vibrating transversely at EOG then, in general, it will possess a non-zero transverse angular rate subsequent to EOG. Furthermore, two-body model results indicate that the transverse angular rate attributable solely to transverse vibration may be on the order of

100 mrad/sec. To put this in perspective, it is desirable that the initial transverse angular rate of a free-flight rocket (which cannot be treated as a bias) be no greater than, say 10 mrad/sec. It follows that the problem of transverse vibrations must be dealt with if such a system is to be achieved.

Recent research has provided a more detailed model (assumed-modes model) of a spinning flexible rocket which has been used[3] to validate the two-body model and also to obtain certain results presented herein. In addition to the development of the aforesaid model, the following objectives were established at the beginning of this effort: (1) to gain a better understanding of the mechanism whereby transverse vibrations are transformed into transverse angular rates, (2) to determine probable causes of transverse vibration and (3) to recommend ways of reducing transverse vibration during guidance and/or its adverse effects. The following sections of this report describe the approaches taken in pursuit of these objectives and the principal results of this study.

In Section 2, the effects of transverse vibration which is present at EOG are considered without regard for the cause, or causes, of such vibration. The two models mentioned above are described, and physical explanations for the post-launch transverse angular rate generally associated with transverse vibration are given. Some results obtained using the mathematical models based on the two-body and assumed-modes models are presented. Methods for analyzing optical lever data not considering vibration, and also considering it, are described in Section 3. Probable causes of transverse vibration of a free-flight rocket during guidance are discussed in Section 4. Results are presented for two probable causes,

support imperfections and friction. Conclusions and recommendations follow in Section 5. Most of the mathematical details are relegated to appendices.

The term "mallaunch" is avoided in this report, because the meanings attributed to it by various individuals are not the same. Instead, we shall use the expression, "transverse angular rate at end of guidance" in which "transverse angular rate" refers to the magnitude of the angular velocity of the instantaneous centroidal principal axes of the vibrating rocket and "end of guidance" is an event which occurs at the time of last intended physical contact between the rocket and its launcher.

## SECTION 2. EFFECTS OF TRANSVERSE VIBRATION

### 2.1 Description of Models

As stated previously, two models of a spinning flexible rocket have been developed and used to study the effects of transverse vibration of such a rocket during the guidance phase of its flight on its motion subsequent to EOG. One, the two-body model, is fairly simple - as simple as possible, it is felt, if the effects of transverse vibration are to be modeled. The other, which we call the continuous model and also the assumed-modes model, is more detailed.

#### The Two-Body Model

The two-body model consists, as its name implies, of two "cylindrical" rigid bodies (see Fig. 1) which are connected by torsional springs, viscous dampers and a "hinge". Then allow "transverse" angular rotation of the bodies relative to each other. Here, "transverse" is used to indicate motion orthogonal to the longest axis of either body. In most of the work which has been done, both bodies have been assumed to be axisymmetric and homogeneous. These assumptions could have been avoided, but to do so would have resulted in a more complex mathematical model, and they are very proper for the type of rockets considered.

As shown in Fig. 1, the aft body is denoted by Body 1 and the other by Body 2. Body j's center of mass is $C_j$. The hinge point is R and the points P and Q are points on the geometric centerlines of Bodies 1 and 2, respectively. The points P and Q are constrained to move rectilinearly while the rocket is on the launcher, if the mechanism which supports the rocket is rigid. If the supporting mechanism is flexible, as is assumed

to obtain some of the results given in Section 4, then the points P and Q are constrained in another manner (see Appendix D).

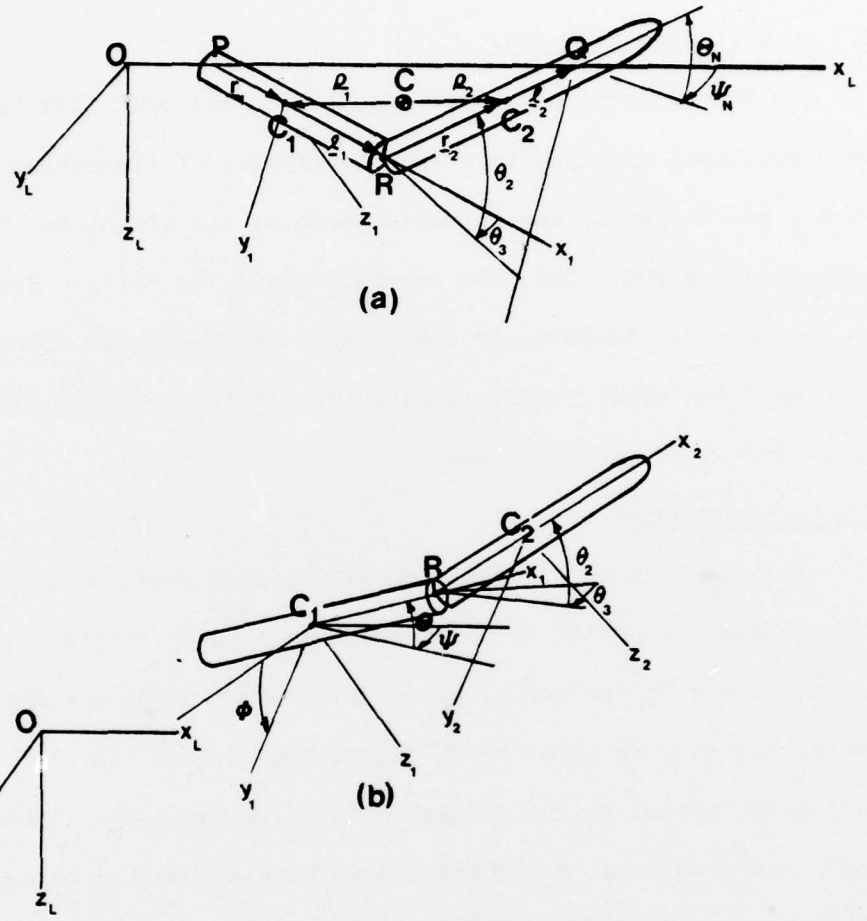


Fig. 1. Two-body physical model. (a) On launcher. (b) Off launcher.

The bodies are truly rigid in that their masses are constant. Since the time period considered is that from ignition to shortly after EOG, this assumption is a good one if the rocket's mass does not change substantially during this short time period. The constant mass assumption is also necessary if the closed-form solution to the equations of rotational motion given in Appendix A is to be obtained. Although the mass is assumed constant, a constant magnitude thrust force ($\underline{F}_T$) is assumed present. The thrust

acts through point P and is not necessarily aligned with the longitudinal axis of Body 1. That is, mechanical thrust misalignment may be modeled. Another basic assumption which allows the closed-form solution to be obtained is that aerodynamic reactions (force and moment) are negligible during the time of interest. This assumption is a good one if the magnitude of the velocity of the rocket's center of mass is "sufficiently" small in magnitude, say less than 100 m/sec.

The spin rate of the rocket is also assumed constant to obtain the closed-form solution, But it is modeled as variable when the effects of friction (Section 4 and Appendix D) are considered.

The Assumed-Modes Model

The name "assumed-modes model" was coined because certain mode shapes were "assumed" in mathematically modeling (see Appendix B) the transverse vibrations of the rocket, which is modeled physically as a continuous flexible body. Two sketches of the continuous physical model are shown in Fig. 2. Figure 2a shows how during the guidance phase two points, P and Q, on the deformed centerline of the rocket model are constrained to move rectilinearly. After EOG (see Fig. 2b) the points P and Q may move arbitrarily. The rocket's mass is assumed to be constant and a thrust force (possibly time varying) acts on the rocket. The axial component of this force is assumed to act at the head end of the rocket motor section; however, the effects of transverse vibration in turning the flow of the rocket exhaust gases as they exit and mechanical misalignment of the rocket nozzle are modeled by transverse thrust components which act at point P. An additional characteristic of the continuous, or assumed-modes, model is that the undeformed shape of the rocket can be "nonstraight,"

thereby allowing for imperfections in motor section to warhead section connections or "non-straightness" of the rocket for other reasons.

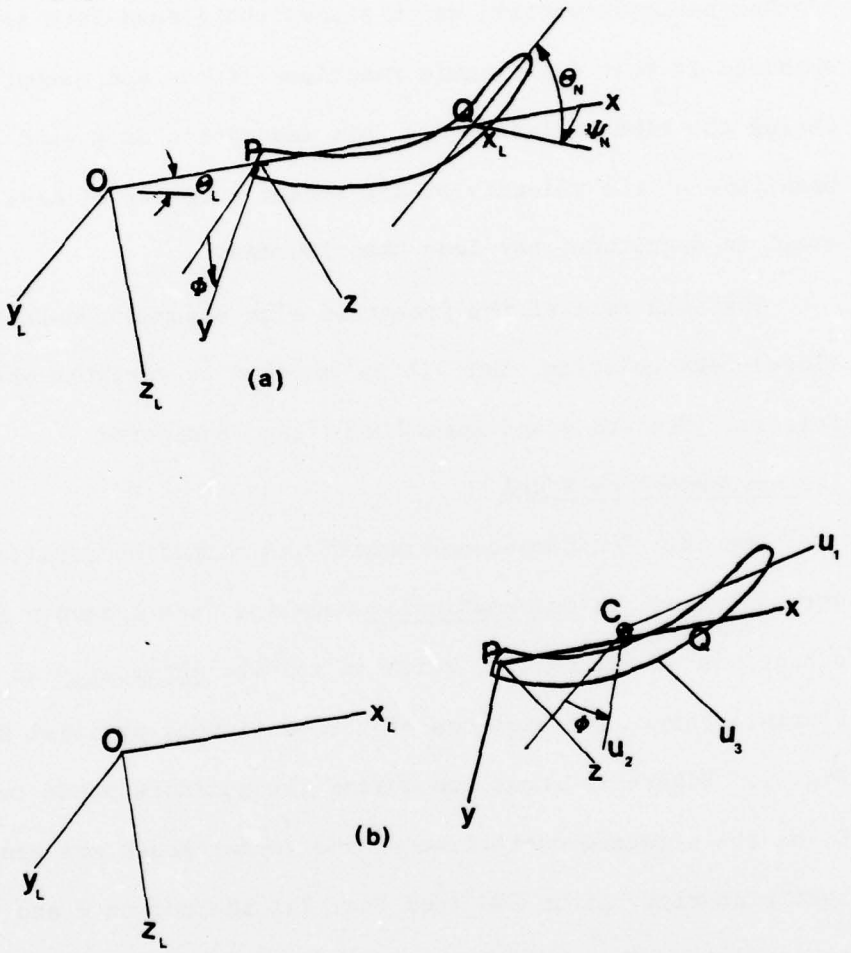


Fig. 2. Continuous physical model. (a) On launcher. (b) Off launcher.

The transverse vibration of the continuous rocket model during guidance is modeled mathematically using pinned-pinned-free normal mode shapes of a uniform beam.[2] At EOG, a transformation is made so that free-free bending mode shapes of a uniform beam can be used for the free-flight portion of the rocket's flight.[2]

In the assumed-modes model, the spin torque may be time varying. Thus, a spin producing device such as an eroding spin turbine[4] can be modeled.

In Section 4, the effects of supporting the rocket at three points during guidance are studied. Although this could be done by using pinned-pinned-pinned-free normal mode shapes for a uniform beam, the approach taken was to constrain a third point (between P and Q) to follow a predetermined path as the rocket moves longitudinally.

## 2.2 Causes of Transverse Angular Rates

There are numerous possible causes of transverse angular rates of free-flight rockets. Some are:

1. Exhaust flow interference, including "blow-by" and blast impingement from a previously launched rocket on the launcher.
2. Dynamic imbalance of the rocket.
3. Rocket thrust anomalies due to mechanical misalignment of the rocket nozzle and unsteady flow within the rocket.
4. Elastic deformations of the rocket.
5. Elastic deformations of the launcher.
6. Guidance mechanism imperfections.

Forces caused by flow interference in the form of blow-by may be sufficient to produce transverse angular rates on the order of 100 mrad/sec according to Booker.[4] Dynamic imbalance can cause a long period precessional motion of the unbalanced rocket which appears in attitude data to be a secular transverse angular rate of considerable magnitude, say 57 mrad/sec for a spin rate of 9 rps and a 1 mrad angular misalignment of the principal axis of least inertia (PALI). Thrust misalignment of a mechanical nature may

produce similar rates. As mentioned, elastic vibration of a spinning flexible rocket may result in rates on the order of 100 mrad/sec, while elastic deformations of the launcher itself, especially the launch rail or tube, may produce similar magnitude rates.

In the effort reported here, elastic deformations of the rocket were considered of principal interest. For purposes of comparison and to match optical lever data, we also consider thrust misalignment. We note that thrust misalignment may, in fact, be caused by a static elastic deformation of the rocket. Hence, thrust misalignment and elastic deformations of the rocket are sometimes related. Also, the effects of dynamic imbalance, which could be caused by static bending of the rocket, are much like those of thrust misalignment. If the thrust and spin rate of the rocket are essentially constant, or there is available attitude data over only a short time period, the two are generally indistinguishable.

With these thoughts as background, we now consider transverse vibrations as "causes" of transverse angular rates.

## 2.3 How Transverse Vibration Causes Transverse Angular Rates

A physical explanation for the way in which transverse vibration of a rocket during the guidance phase results in a transverse angular rate of the rocket at EOG is first given in what follows. On the basis of this physical explanation, the two-body physical and mathematical models are used to obtain a simple mathematical expression for the transverse angular rate which results from transverse vibration.

Physical Explanation

Assume that a rocket is vibrating transversely prior to EOG. The rocket then has angular momentum due to motion about its center of mass. This angular momentum has a transverse component (see Fig. 3) that is time varying. It is the resultant of the transverse angular momenta of infinitely many segments of the rocket (considered as a continuous flexible body) due to rotation of each segment about its center of mass and of the angular momenta due to the motion of the segments' centers of mass relative to the center of mass of the rocket.

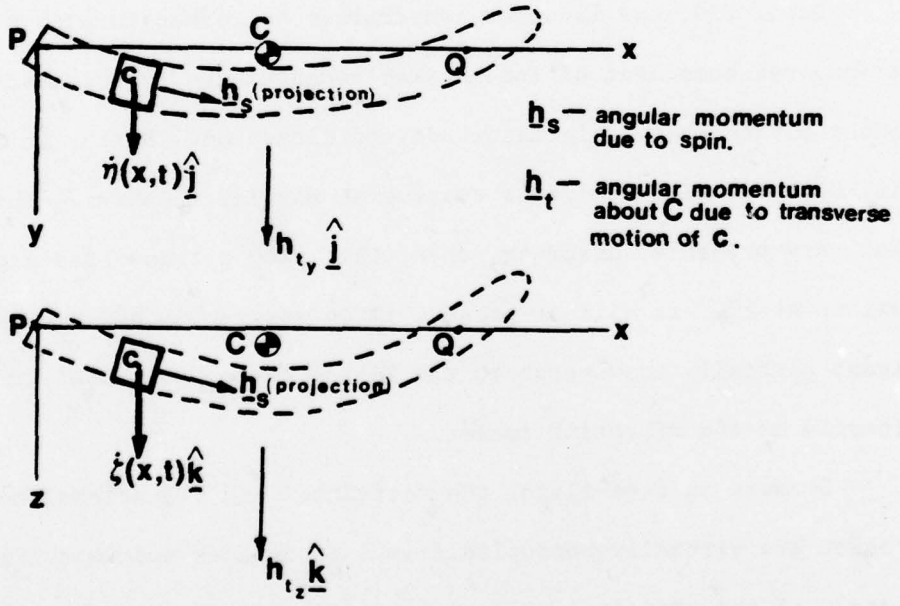


Fig. 3. Angular momentum of a spinning flexible rocket.

The angular momentum of each segment due to rotation about its center of mass has a transverse component because each element is, in general, rotating transversely to the line segment which forms a portion of the

centroidal axis of the rocket. It also normally has a component transverse to the launch axis which is due to the fact that angular momentum resulting from spin is (because the rocket is bending transversely) not directed along that axis.

If the rocket is slender and is not bent severely, the resultant of the angular momenta of the rocket segments about their respective centers of mass is much less than that due to the motion of the segments' centers of mass relative to the rocket's center of mass. The latter can be (as will be seen later) a substantial part of the total angular momentum of the rocket.

Until EOG, the launcher constrains the rocket in such a manner that the transverse component of its angular momentum due to transverse (to the launch axis) motion changes in magnitude and direction. Hence, it is possible that at EOG there will be little transverse angular momentum. This is, however, not very probable. Assuming, then, that such a transverse angular momentum exists at EOG, it will be present immediately after EOG and will generally be at least partially transverse to the instantaneous principal axis of least inertia of the vibrating rocket.

Because in free-flight the rotational and vibrational motions of the rocket are virtually uncoupled (i.e., it behaves somewhat like a free-free beam), if the principal axis of least inertia of the rocket is rotating transversely at EOG, it will continue to do so until an external torque stops it. This rotation is a precession and is periodic if no external torques are present and there is no energy dissipation. However, the period of the precession is very long for slender rockets, since it is approximately equal to $2\pi\ I_T/(\Omega_x I_A)$, where $I_T$ is the transverse moment of inertia of the

rocket, and $\Omega_x$ is its spin rate and $I_A$ is the rocket's axial moment of inertia. Hence, it appears to be constant near EOG.

An important point is that the transverse rate due to transverse vibration of the rocket is not created subsequent to EOG as a rate due to blow-by would be. It is the result of energy being input into the rocket for a period of time before EOG, perhaps from the time of ignition. Another important point is that if the transverse vibration is such that the PALI of the vibrating rocket is not rotating transversely at EOG, then there is essentially no transverse angular rate of that axis due to the vibration subsequent to EOG.

Approximate Transverse Angular Rate Due to Vibration

An approximate expression for $\omega_t$, the transverse angular rate at EOG which is the result of transverse vibration, is derived in Appendix C. There, the two-body physical model and the constraints used in the two-body mathematical model are used to determine the transverse components of the angular momentum of the centroidal principal axes of the rocket at EOG in terms of model physical characteristics and the pitch and yaw rates of the rocket's nose at end of guidance, $\dot{\Theta}_{NO}$ and $\dot{\Psi}_{NO}$, respectively. Note that in this model, $\dot{\Theta}_{NO}$ and $\dot{\Psi}_{NO}$ are due to bending only.

Let $B_1$ and $B_2$ be the axial and transverse moments of inertia, respectively, of Body 2; $\sigma = m_1 m_2/m$, where $m_j$ is the mass of Body j and $m = m_1+m_2$; $r_1$, $\ell_1$, $r_2$ and $\ell_2$ be the axial components of the vectors from P to $C_1$, $C_1$ to R, R to $C_2$ and $C_2$ to Q, respectively. Then,

$$\omega_t = (\delta k_1 - k_1/k_2)\sqrt{\dot{\Theta}_{NO}^2 + \dot{\Psi}_{NO}^2} \quad , \tag{1}$$

where $\delta = [B_2 + \sigma r_2(\ell_1+r_2)-B_1]/(I_T-I_A)$, $k_1 = d/(\ell_1+r_1)$, $k_2 = d/(\ell_2+r_2)$,

and $d = \ell_1 + r_1 + \ell_2 + r_2$. We note here that the curves on page 37 of Ref. 2 are not all correct, since incorrect initial conditions were used to obtain them. The correct initial conditions are given in Appendix A.

Equation (1) implies that $\omega_t$ is directly proportional to the transverse angular rate of the rocket's nose. Regardless of the transverse angular rate of the rocket's nose, $\omega_t$ will be zero when the factor $\delta k_1 - k_1/k_2$ is zero. This may be the case if either the mass and inertia characteristics of the two bodies are altered so that $\delta = 1/k_2$, or the support points of the rocket are changed. The latter possibility will be considered shortly. First, we shall see what size transverse angular rate may be expected.

From the physical characteristics of the rocket GEM #7 (see Table 1, infra) the following values needed to determine the constant factor in Eq. (1) can be obtained (see Table 2, infra): $B_1 = 0.29$ kg-m$^2$, $B_2 = 11.86$ kg-m$^2$, $\sigma = 28.37$ kg, $I_A = 0.406$ kg-m$^2$, $I_T = 99.7$ kg-m$^2$, $k_1 = 1.22$, and $k_2 = 5.64$. The constant factor is approximately 0.32. Bending oscillations of amplitudes up to 0.5 milliradians have been observed by optical lever techniques. Assuming such an amplitude and a first mode bending frequency of 60 Hz, we get $\omega_t \simeq 60$ mrad/sec, a <u>substantial</u> transverse angular rate.

If we replace the second factor in Eq. (1) with $A\omega_v$, where A is the amplitude of the transverse vibration just prior to EOG and where $\omega_v$ is the dominant (probably first-mode) bending frequency, then we can plot $\omega_t/A\omega_v$ as a function of $\ell_2/r_2$. (Note that $\ell_2$ may be negative; indeed, it is in the above example!) The curve (see Fig. 4) obtained is virtually a straight line, which has a zero crossing at $\ell_2/r_2 \simeq 0.73$. Thus, if $\ell_2 = 0.73\ r_2$ had been used in the above example, the transverse rate predicted by Eq. (1) would have been approximately zero.

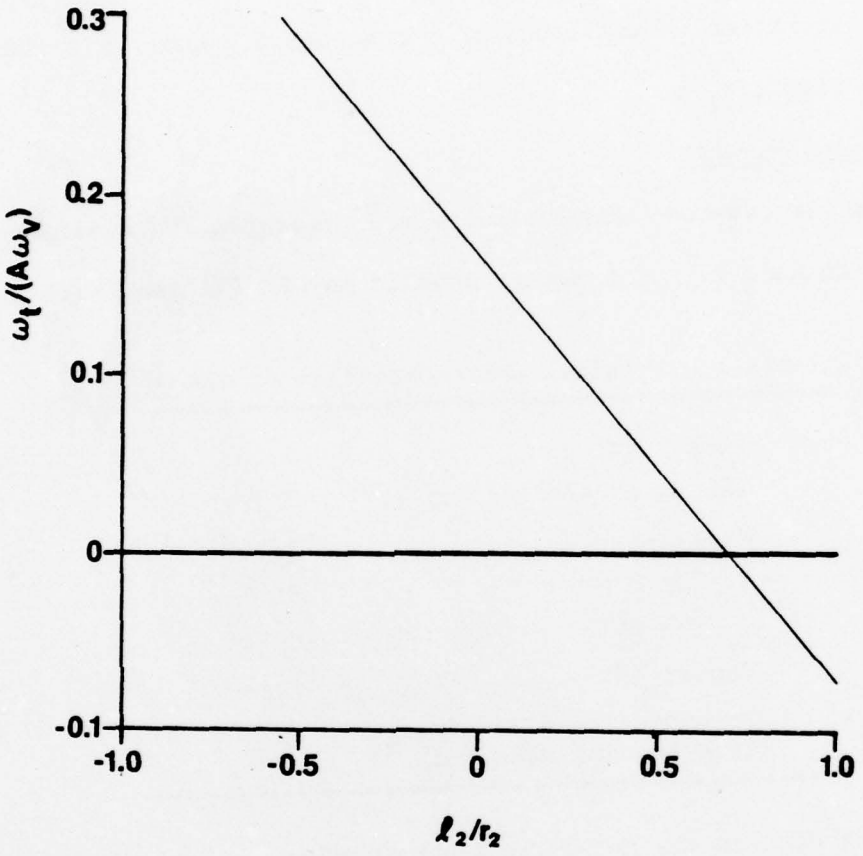


Fig. 4. Transverse angular rate as a function of forward support location.

Although Eq. (1) does not include the effects of higher-order bending modes, it still yields reasonably good estimates of the transverse angular rate which may occur. It does include the effects of support placement and the results presented emphasize the importance of choosing the locations of supports judiciously.

## 2.4 Results from Mathematical Models

To illustrate the type of post-launch attitude motion which is caused by transverse vibration prior to EOG, we present here some results obtained

using the two-body and assumed modes mathematical models. In addition to transverse vibration, the effects of thrust misalignment on a flexible rocket are illustrated.

Two-Body Model Results

Only a few two-body model results are presented, because others have been given in Ref. 2.† The rocket modeled is GEM #7 (see Table 1).

Table 1. Physical Characteristics of GEM #7

| | |
|---|---|
| Length (m) | 3.353 |
| Radius at aft end (m) | 0.076 |
| Mass (kg) | 114.76 |
| $I_T$ (kg-m$^2$) | 99.7 |
| $I_x$ (kg-m$^2$) | 0.406 |
| Thrust (Nt) | 46720 |
| Frequency of first free-free bending mode (Hz) | ≈67 |

The data used in the two-body model is given in Table 2. It should be pointed out that this data is such that the center of mass of the undeformed rocket model is located at the hinge point R.

Table 2. Characteristics of Two-Body Model of GEM #7.

| | | | | | |
|---|---|---|---|---|---|
| $m_1$ (kg) | 50.466 | $m_2$ (kg) | 64.286 | k (Nt-m) | $1.491 \times 10^6$ |
| $\ell_1$ (m) | 0.9376 | $\ell_2$ (m) | -0.3354 | $F_T$ (Nt) | 46720 |
| $r_1$ (m) | 0.9376 | $r_2$ (m) | 0.7393 | $I_T$ (kg-m$^2$) | 99.7 |
| Radius (m) | 0.095 | Radius (m) | 0.095 | $I_A$ (kg-m$^2$) | 0.406 |
| $A_1$ (kg-m$^2$) | 0.1681 | $B_1$ (kg-m$^2$) | 0.1789 | $\Omega_1$ (rad/sec) | 47 |
| $A_2$ (kg-m$^2$) | 10.996 | $B_2$ (kg-m$^2$) | 5.274 | | |

† Although the results given in Ref. 2 are not exactly correct due to the error in initial conditions mentioned previously, the error had very little effect on the results given there, except for those on page 37.

The initial conditions $\Theta_{NO}$ = -.25 mrad, $\Psi_{NO}$ = 0.25 mrad, $\dot{\Theta}_{NO}$ = 0.364 rad/sec and $\dot{\Psi}_{NO}$ = 0 were used along with $\Omega_1$ = 47 rad/sec to obtain the time histories of $\Theta_N$ and $\Psi_N$ shown in Fig. 5. Both $\Theta_N$ and $\Psi_N$ have the form of a lightly damped periodic oscillation superimposed on a linear function of time The slope of the mean value of $\Psi_N$ is essentially zero, while the slope of the mean value of $\Theta_N$ is about 0.118 rad/sec. Equation (1) can be used to obtain $\omega_t$ = 0.117 rad/sec; hence, for the two-body model (on which it is based), Eq. (1) yields the proper transverse rate.

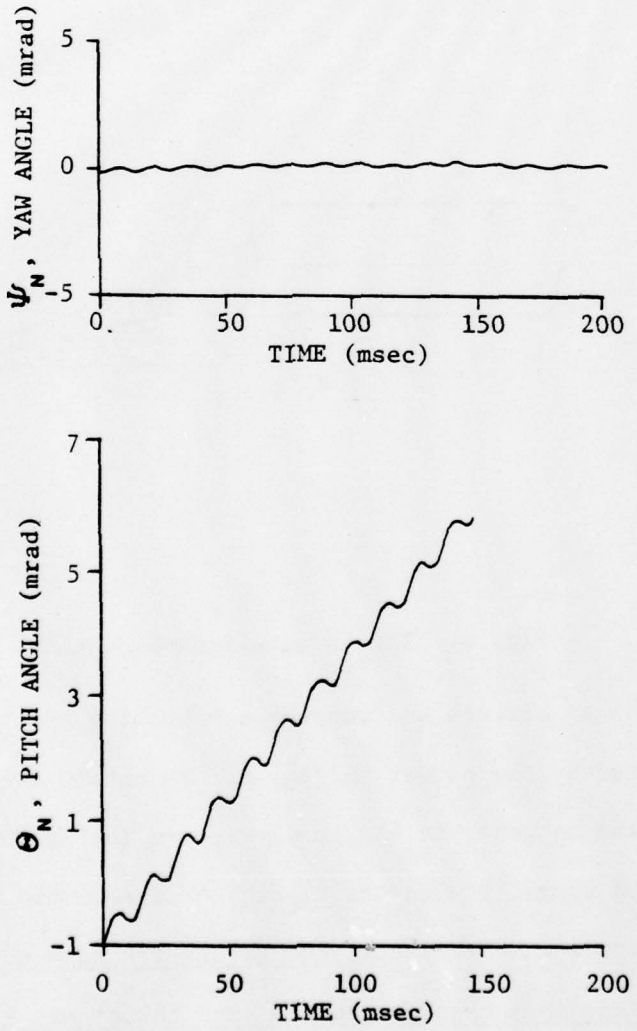


Fig. 5. Two-body results - effects of bending.

If there is no transverse vibration at EOG, but there is thrust misalignment defined (see Fig. 6) by $\alpha_y$ = 0.677 mrad and $\alpha_z$ = 4.6 mrad, the time histories shown in Fig. 7 are obtained. The thrust misalignment causes only a small amount of bending so that the curves look essentially like those obtained using a rigid-body model for the rocket. The slope of the mean value of $\Theta_N$ is about -80 mrad/sec.

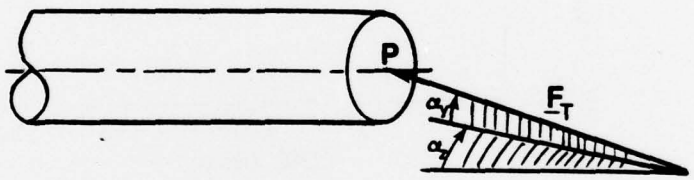


Fig. 6. Thrust misalignment angles.

The combined effects of transverse vibration and thrust misalignment are illustrated by the curves in Fig. 8. To obtain these curves, the initial conditions used to generate the results shown in Fig. 5 and the thrust misalignment used to get the curves in Fig. 6 were combined. It is clear from the $\Theta_N$ curve in Fig. 7 that the transverse rate due to vibration is more significant than that due to a 4 mrad thrust misalignment.

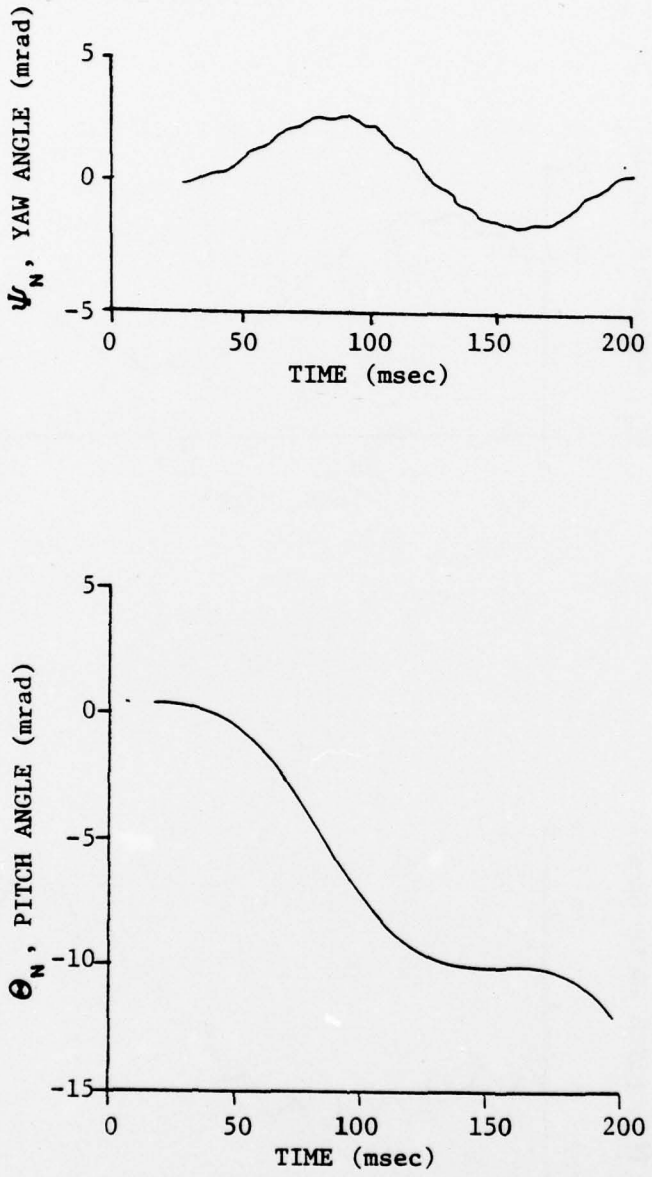


Fig. 7. Two-body results - effects of thrust misalignment.

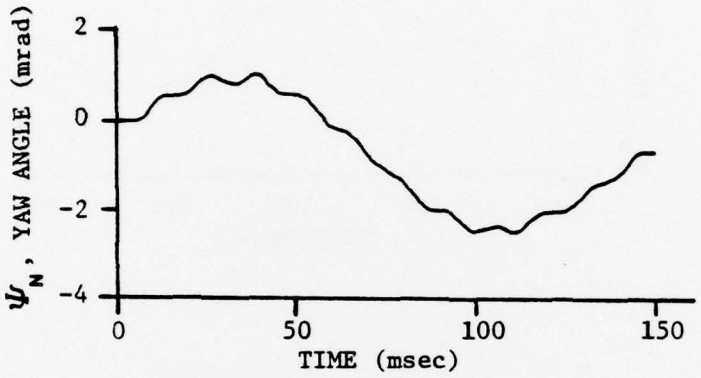


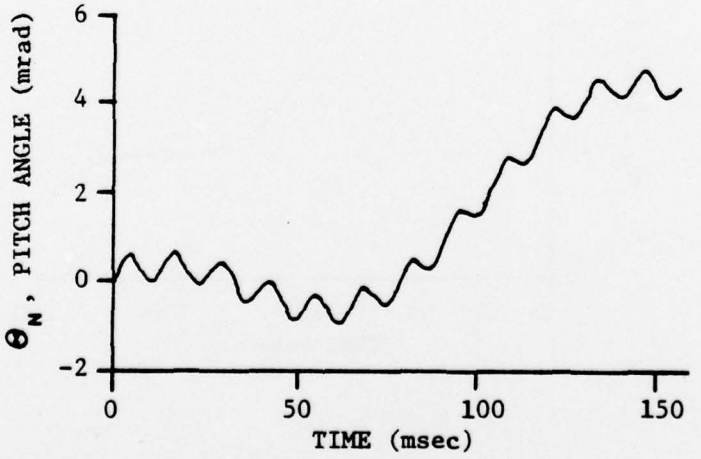


Fig. 8. Two-body results - combined effects.

Assumed-Modes Model Results

At this point we are considering the effects of transverse vibration regardless of the cause. Hence, for purposes of illustration, a bending oscillation of the rocket model was induced while it was "on the launcher" and $\Theta_N$ and $\Psi_N$ as functions of time were generated by numerically integrating the assumed-mode model equations of motion. The data used is given in Table 3.

Table 3. Data for Assumed-Modes Model of GEM #7

| | |
|---|---|
| L (m) | 3.353 |
| EI (Nt-m$^2$) | $1.652 \times 10^6$ |
| $\sigma$ (kg/m) | $\begin{cases} 26.93, & 0 \leq x \leq x_M \\ 43.49, & x_M \leq x \leq L \end{cases}$ |
| $x_M$(m) | 1.875 |
| $x_Q$(m) | 2.236 |
| $I_A$ (kg-m$^2$) | 0.406 |
| $I_T$ (kg-m$^2$) | 99.7 |
| $F_T$ (Nt) | 46720 $(0.0 \leq t \leq 0.25)$ |
| $T_A$ (Nt-m) | 284.2 $(0.0 \leq t \leq 0.0647)$ |
| $y_0 \equiv z_0 \equiv 0$ | |

End of guidance occurred (see Fig. 9) at about 0.0647 seconds, as the nose of the rocket model was pitching up. The transition from on-the-launcher motion to free-flight is characterized by (1) a change in the slope of the mean value of $\Theta_N$ and (2) changes in the amplitude and dominant frequency of the bending oscillations. Such changes are observable in optical lever data. The natural frequencies of the first bending mode of the model for this example are approximately 41 Hz during guidance and 70 Hz during free flight.

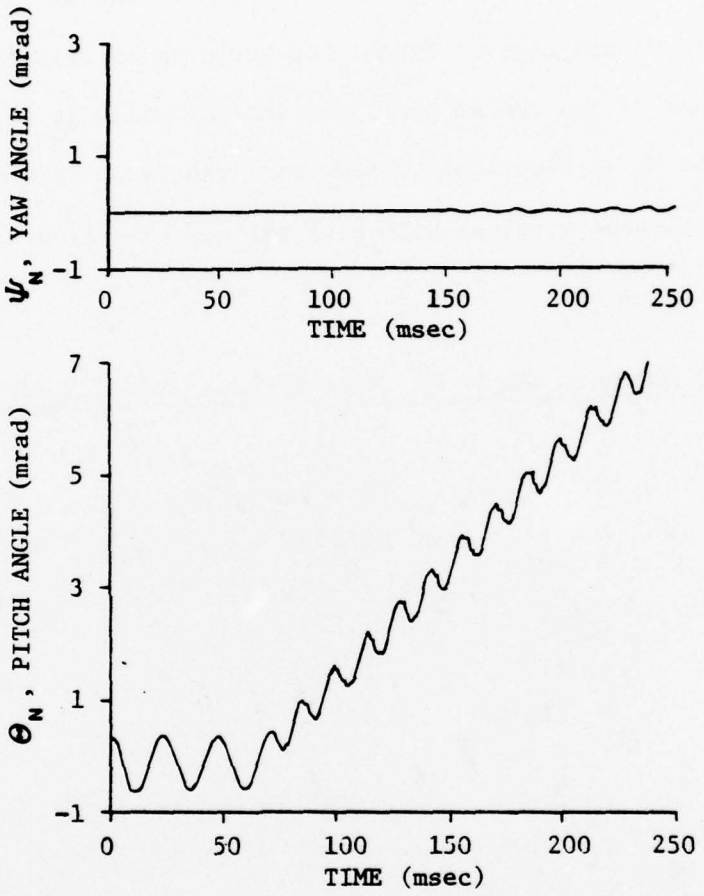


Fig. 9. Assumed-modes results - effects of bending.

The effect of thrust misalignment is qualitatively the same when the two-body or assumed-modes model is used. The time histories shown in Fig. 10 were generated by using $\alpha_y$ and $\alpha_z$ values stated above in connection with the two-body model. The curves shown in Fig. 10 differ from those shown in Fig. 7, primarily because the assumed-modes model of the rocket had rotated through approximately 60 degrees at EOG. Hence, the corresponding two-body thrust misalignment angles are $\alpha \simeq 4.32$ mrad and $\alpha_z \simeq -1.72$ mrad. (The roll angle in the two-body mathematical model is

zero at EOG.) When the proper thrust misalignment angles are used in the two-body model and the pitch and yaw angles and rates of the rocket model's nose at EOG (as taken from the assumed-modes model results with vibration present) are used, the results for $\Psi_N$ and $\Theta_N$ as functions of time obtained using the two models agree very well (see Fig. 11). Since the computer codes used to obtain the results given were developed at different points in time and are different in many respects, the agreement achieved implies that both codes are correct.

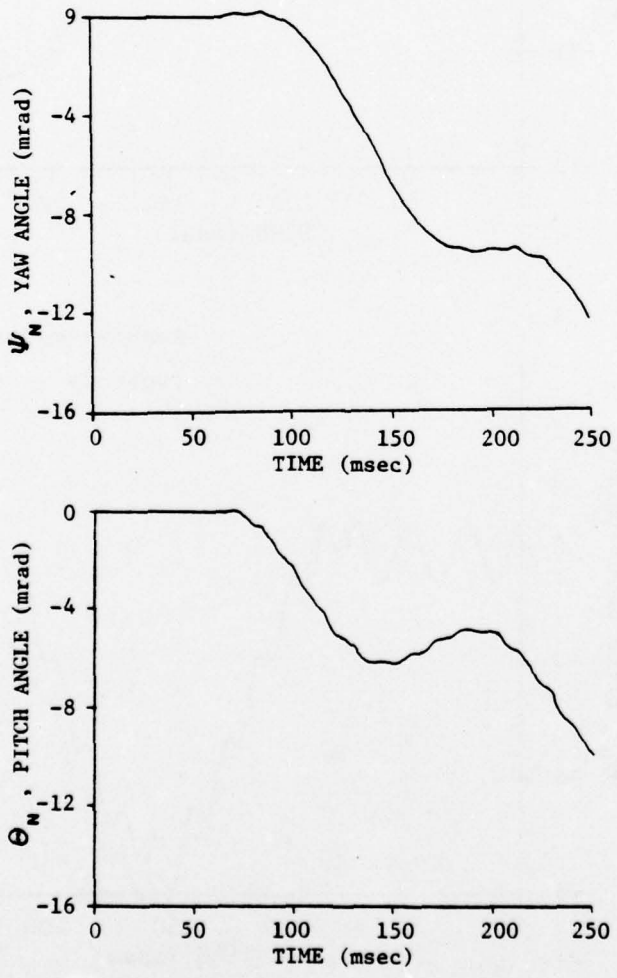


Fig. 10. Assumed-modes results - effects of thrust misalignment.

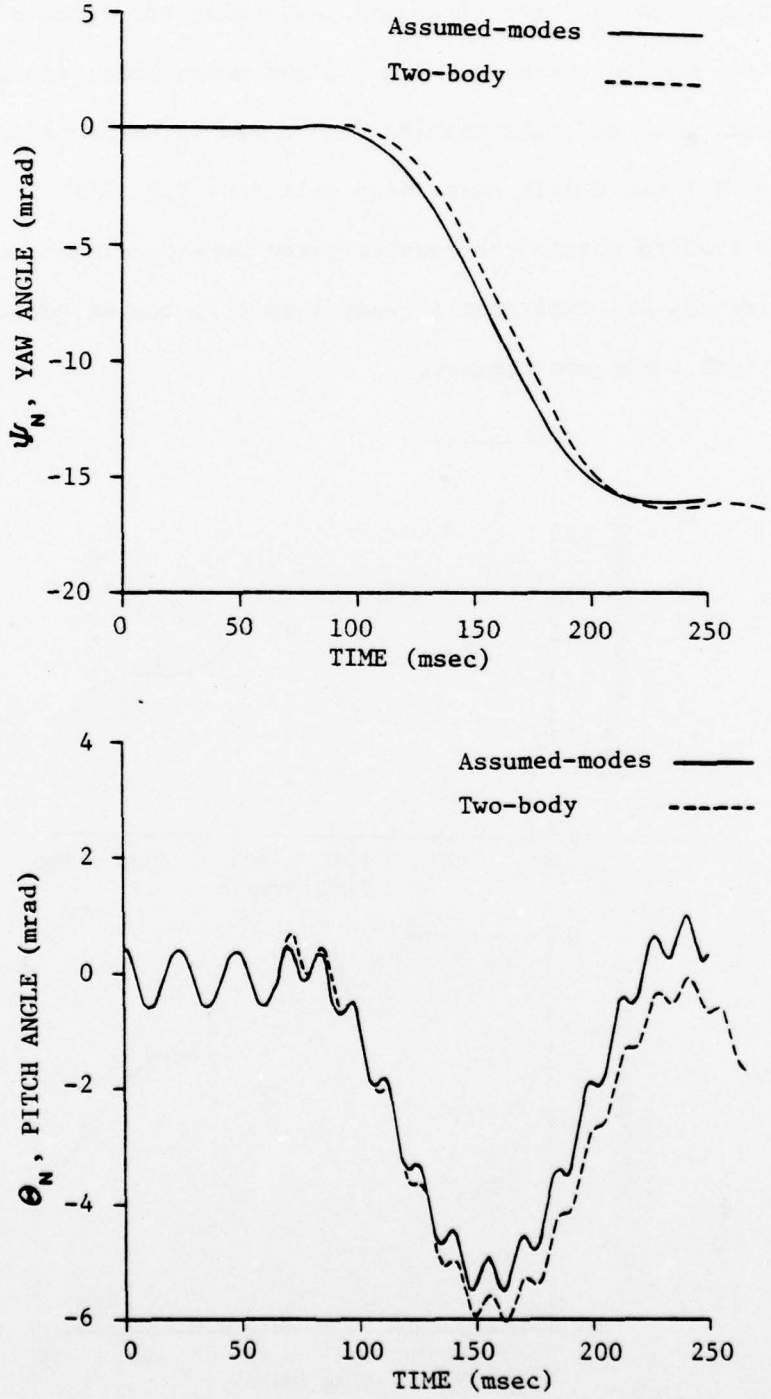


Fig. 11. Assumed-modes and two-body results - combined effects.

The rates at which $\Theta_N$ and $\Psi_N$ are changing at EOG determine, according to Eq. (1), the transverse angular rate of the rocket after EOG which is due to bending. To see if this is true for the assumed-modes model, the guidance length was changed so that EOG occurred at times when $\dot{\Theta}_N$ was negative, essentially zero, and positive. The results for $\Theta_N(t)$ are shown in Fig. 12. They are in agreement with the two-body model results.

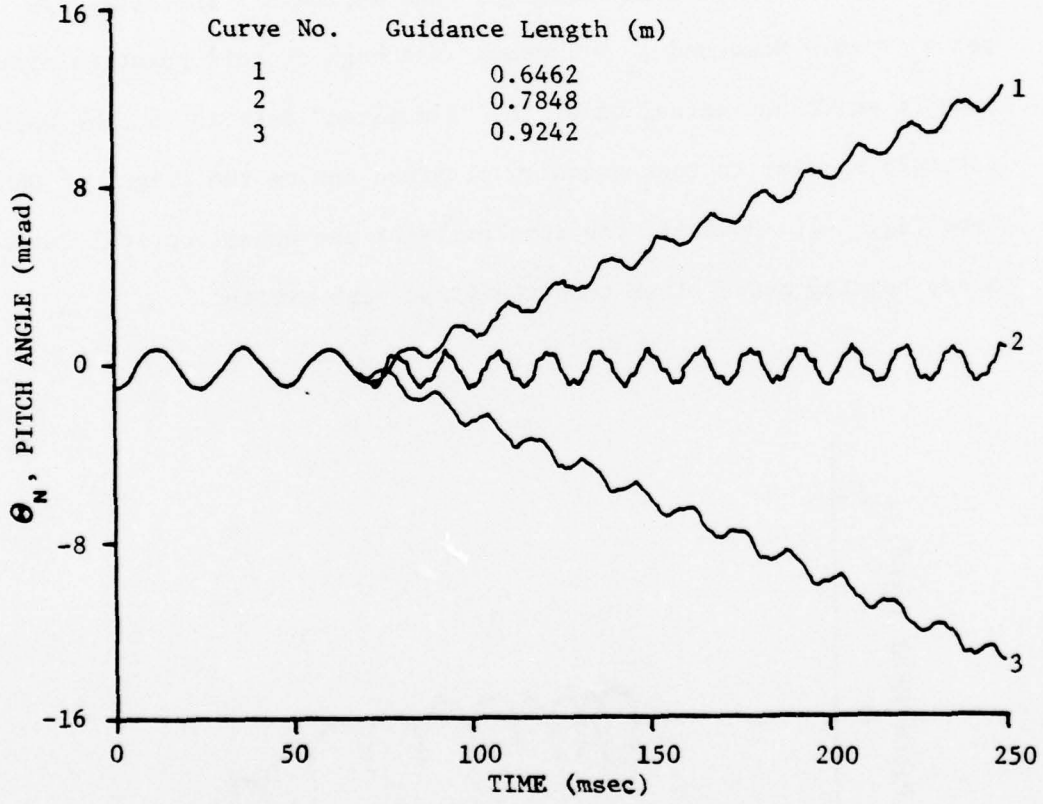


Fig. 12. Assumed-modes results - effects of bending with different guidance lengths.

A constant factor analogous to that in Eq. (1) can be obtained from assumed-modes model results by measuring the mean slopes of the $\Theta_N(t)$ and $\Psi_N(t)$ curves after EOG and using the values of $\dot{\Theta}_N$ and $\dot{\Psi}_N$ at EOG. For this model of GEM #7, we get the factor 0.33 which is in close agreement with the two-body value of 0.32.

As a final illustrative result, we offer Fig. 13, which depicts the pitch and yaw angles of a flexible spinning rocket represented using the assumed-modes model. This plot of $\Theta_N$ vs. $\Psi_N$ can be considered as "simulated" optical lever data. To obtain this result, we used the data in Table 3, forced $\Theta_N$ to be -1 mrad and $\dot{\Psi}_N$ to be -120 mrad/sec at t=0, by picking the proper first mode generalized coordinate $q_1$ and the proper value of the time rate of change $p_1$ (see Appendix B for details). We also set $\alpha_y$ = -0.5 mrad and $\alpha_z$ = 1 mrad. Although at this point no attempt was made to match any actual data, the "simulated" data is in some ways qualitatively similar to that actually obtained during the flight of GEM #8 (see Fig. 14). However, the complexity of the actual optical lever data shows bending modes other than the first were excited.

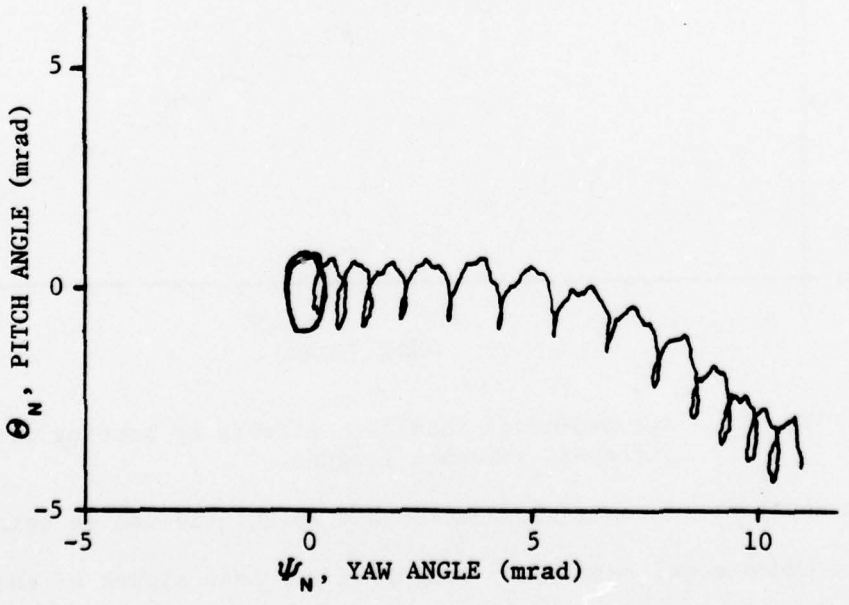


Fig. 13. Assumed-modes results - "simulated" optical lever data.

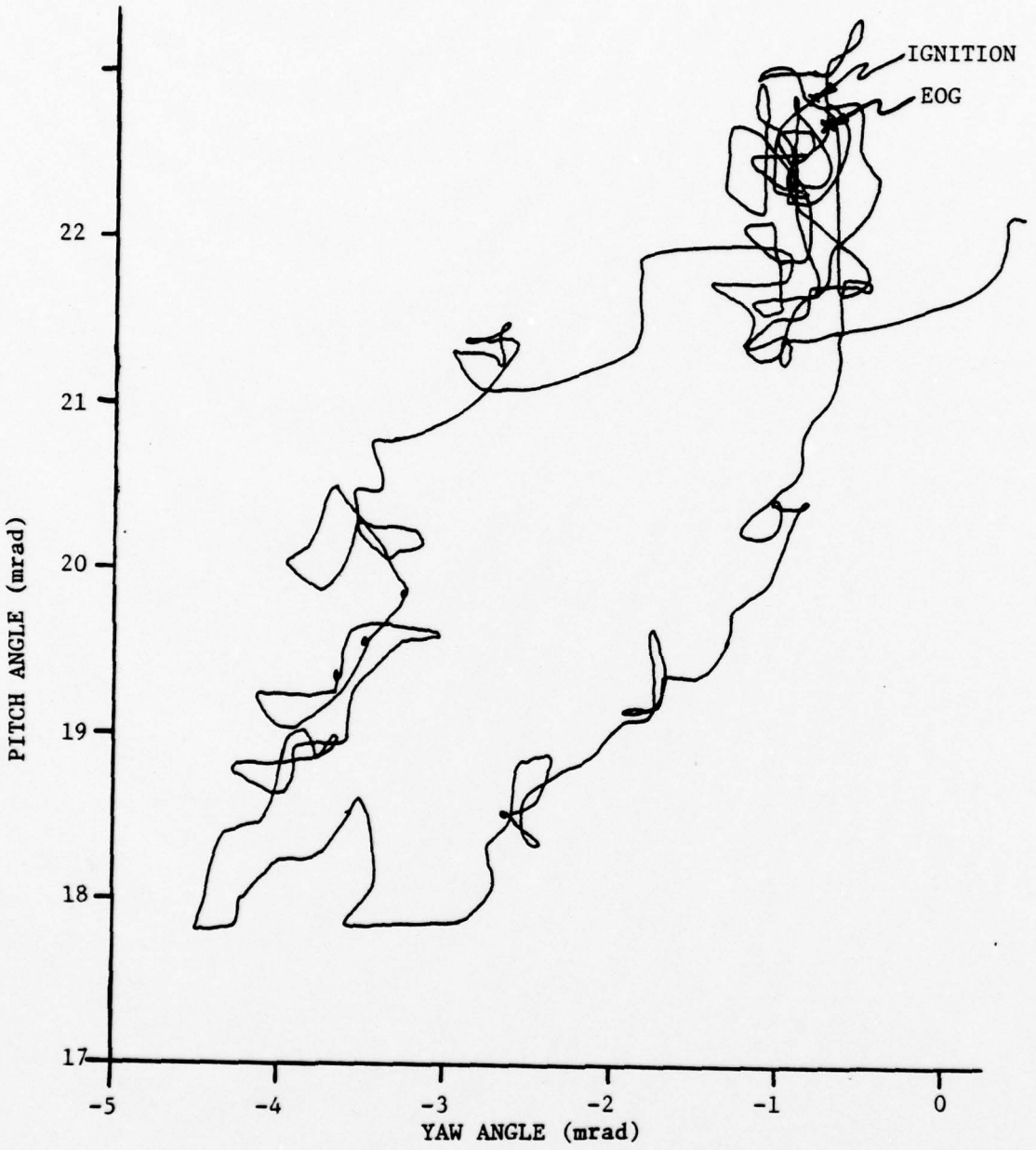


Fig. 14. Optical lever data (reduced) for GEM #8.

## SECTION 3. ANALYSIS OF OPTICAL LEVER DATA

### 3.1 Introduction

The optical lever is the most accurate, commonly-used means of obtaining attitude time histories of free-flight rockets. Optical lever data is usually acquired during the guidance phase and a short portion of the free-flight phase. Through appropriate processing, the raw data is converted into pitch and yaw angles of the rocket's nose as functions of time. If the rocket is not vibrating transversely during the data acquisition time, the pitch and yaw angles of the rocket's nose are, of course, those of the rocket. However, if it is vibrating transversely, this is clearly not so. In fact, if the rocket is vibrating transversely, there arises the question of what coordinate frame should be used in specifying the "attitude of the rocket."

The coordinate frames most commonly used in specifying the attitude of an unconstrained flexible body are: (1) a coordinate frame rigidly fixed in an essentially rigid portion of the body, (2) principal axes of the deformed body, and (3) so-called "mean axes" which are such that the angular momentum with respect to the mean axes due to vibration is zero at all times. As mentioned previously, principal axes of the deformed rocket are used in the assumed-modes mathematical model during the free-flight phase.

If the transverse vibrations are assumed to have no effect on the rocket's gross attitude motion subsequent to EOG, the data can be analyzed by assuming that the variation in the attitude of the rocket is due to:

(1) an initial transverse angular velocity due to unspecified factors, (2) the action of a body-fixed torque due to thrust misalignment, (3) dynamic imbalance of the rocket, and (4) space-fixed torques arising from, for example, blow-by and gravity (if a tip-off launcher is used). If the dynamic imbalance of a rocket which is spinning at a constant rate is also constant, it produces variations in rocket attitude which are of the same form as those produced by an "equivalent" constant body-fixed torque. Thus, if a constant spin rate model is used in the analysis process, constant dynamic imbalance and constant thrust misalignment effects are not distinguishable. Furthermore, since the torque due to blow-by acts approximately impulsively, it is difficult to distinguish its effects from those of the otherwise present initial angular velocity. For these reasons, in the analysis presented here, only the effects of initial transverse angular velocity due to unspecified factors and thrust misalignment are considered when the effects of transverse vibrations are ignored. When the effects of transverse vibration are not ignored, the initial (at EOG) angular velocity due to it and possibly an additional initial angular velocity due to other factors (launcher vibration, for example) as well as thrust misalignment is considered. The effects of blow-by are not considered because pressure data[4] taken during the guidance phase of the rocket of interest indicated blow-by was not significant.

### 3.2 Transverse Vibration Effects Ignored

If the rocket is modeled as a rigid body, which is spinning at a constant rate $\Omega_x$ and is acted upon by a constant body-fixed torque due to a constant magnitude thrust, $\underline{F}_T$, that is not aligned with the longitudinal axis (x-axis) of the rocket, Euler's equations and Poisson's kinematic

equations can be solved to obtain closed-form solutions for the yaw, pitch and roll angles of its centroidal principal reference frame. Furthermore, if the rocket is slender, so that $I_A << I_T$, and the pitch and yaw angles are small, the solutions for $\Theta_N$ and $\Psi_N$ can be well approximated for a short period of time (say one-half a second) by the expressions given on Fig. 15. In Fig. 15, $\alpha_y$ and $\alpha_z$ are "pitch" and "yaw" angles of the thrust vector with respect to the rocket's x-axis. Also, $\Omega_{y0}$ and $\Omega_{z0}$ are the initial transverse angular velocity components. The curves in Fig. 16 are typical ones. Certain geometric characteristics of the curves are defined in Fig. 15. These are expressed analytically in terms of $\Omega_x$, $\Omega_{y0}$, $\Omega_{z0}$, $I_T$, $I_A$, $\alpha_y$, $\alpha_z$, $F_T$ and $\ell_C$, the distance from the intersection of $\underline{F}_T$ with the x-axis and the rocket's center of mass. By labeling plots of $\Theta_N$ and $\Psi_N$ versus time obtained from optical lever data as shown in Fig. 15, if $\Omega_x$, $F_T$, $\ell_c$, $I_T$ and $I_A$ are known, $\alpha_y$, $\alpha_z$, $\Omega_{y0}$ and $\Omega_{z0}$ can be obtained graphically.

To give an example of this "graphical analysis," we use optical lever based data for GEM #8. The physical characteristics of GEM #8 are given in Table 4. From the appropriately labeled curves, we get: $\beta_y \simeq -18$ mrad/sec, $\Delta_y \simeq 0.945$ mrad, $\beta_z \simeq 20$ mrad/sec, $\Delta_z \simeq 2.41$ mrad, and $A = 2.6$ mrad.

For GEM #8, $I_T \simeq 99.5$ kg-m$^2$, $I_A \simeq 0.421$ kg-m$^2$, $\ell_c \simeq 1.874$ m, $\Omega_x \simeq 30$ rad/sec[†] and $F_T \simeq 40940$ Nt. Hence, $K \simeq 0.8642$. It follows from the definitions of $\beta_y$, $\Delta_y$, $\beta_z$ and $\Delta_z$ that $\Omega_{y0} \simeq -90$ mrad/sec, $\Omega_{z0} \simeq 48.5$ mrad/sec, $\alpha_y \simeq 1.104$ mrad and $\alpha_z \simeq 2.79$ mrad.

---

[†]This is an average value of $\Omega_x$, since GEM #8 was spun via an eroding spin turbine. It is actually lower than a simple average, because the nutational frequency does not instantaneously become $(I_T - I_A)\Omega_x/I_T$.

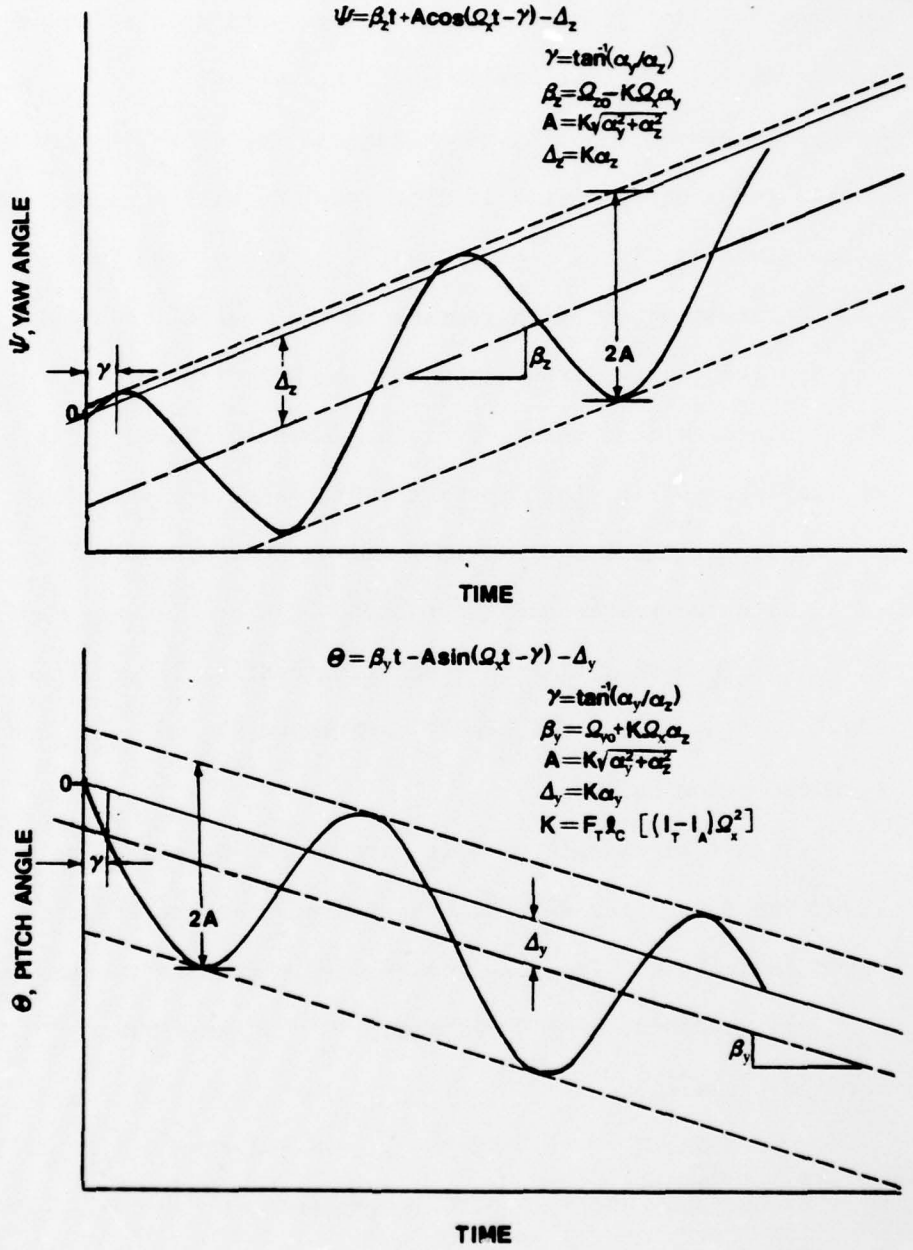


Fig. 15. Pitch and yaw angles when thrust misalignment is present.

Table 4. Physical Characteristics of GEM #8

| | |
|---|---|
| Length (m) | 3.353 |
| Radius at aft end (m) | 0.076 |
| Mass (kg) | 114.5 |
| $I_T$ (kg-$m^2$) | 99.5 |
| $I_A$ (kg-$m^2$) | 0.421 |
| Thrust (Nt) | 40940 |
| Frequency of first free-free bending mode | $\simeq$ 67 |
| Spin rate at EOG (rad/sec) | $\simeq$ 30 |
| Distance from aft end to initial center of mass (m) | 1.874 |

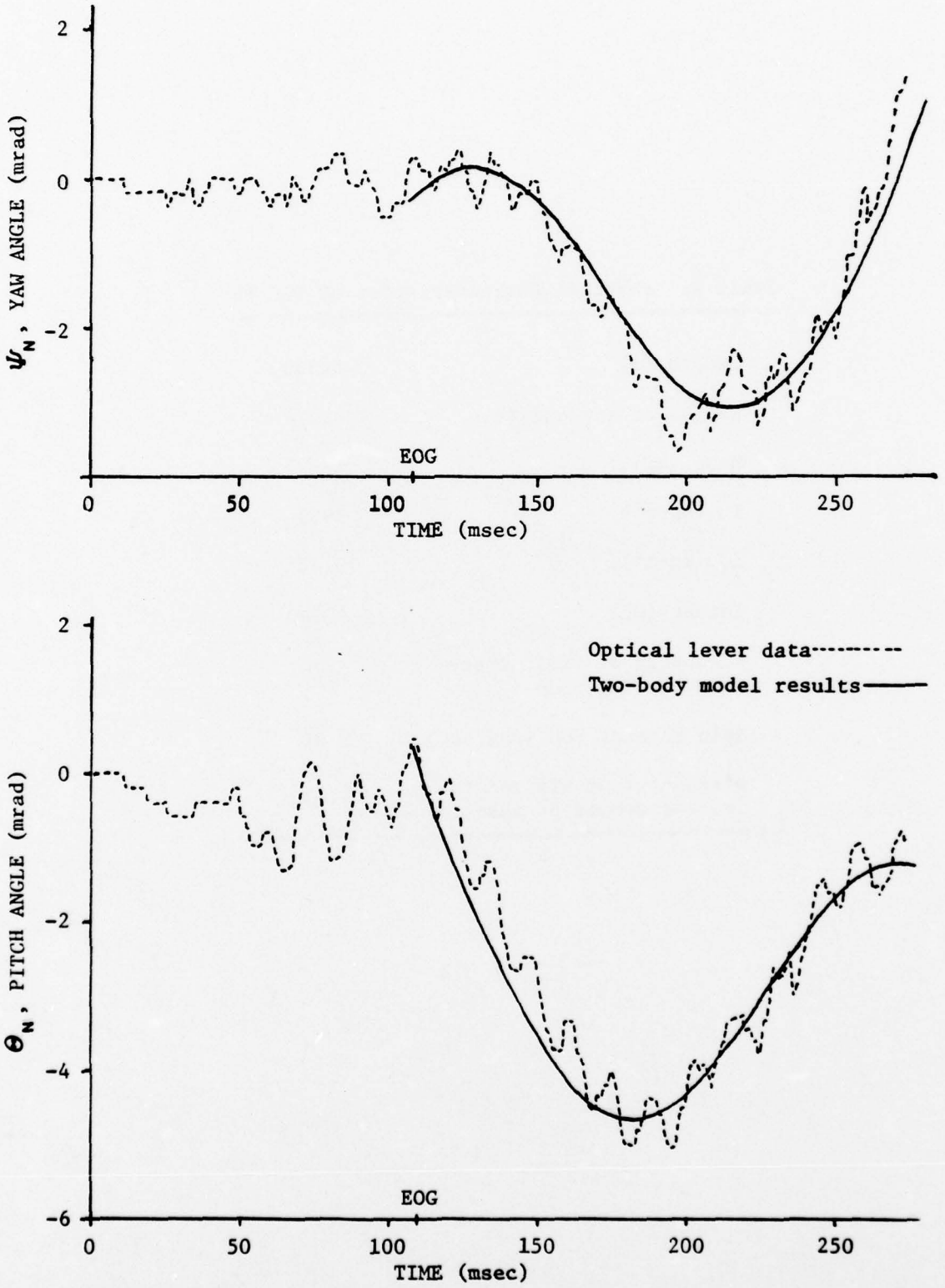


Fig. 16. Comparison of theoretical results and data - bending effects ignored.

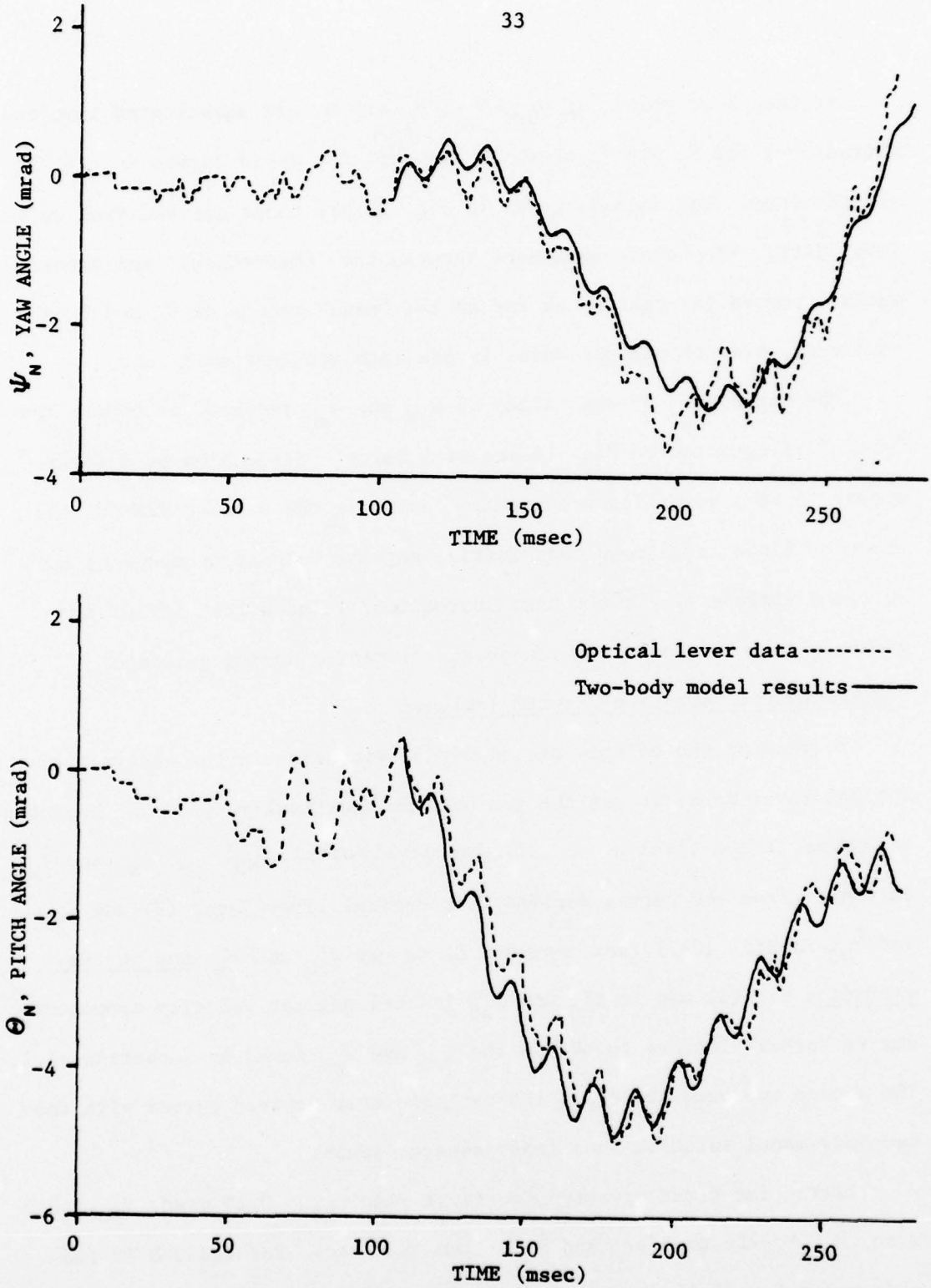


Fig. 17. Comparison of theoretical results and data - bending effects included using first method.

If the above values of $\Omega_{y0}$, $\Omega_{z0}$, $\alpha_y$ and $\alpha_z$ are substituted into the expressions for $\Theta_N$ and $\Psi_N$ shown in Fig. 15, the solid curves in Fig. 16 are obtained. The dashed curves in Fig. 16 are those derived from optical lever data. Very close agreement between the theoretical and experimental curves is apparent as far as the "mean" values of $\Theta_N$ and $\Psi_N$ are concerned, even though the model is one with constant spin rate.

The magnitudes of the values of $\Omega_{y0}$ and $\Omega_{z0}$ required to obtain the "match" illustrated in Fig. 16 are very large. Since blow-by did not appear to be a significant causative factor in the case of GEM #8, the cause of these large magnitude initial angular velocity components must be found elsewhere. In the next subsection, we show that it is very probable that one cause was transverse vibration during guidance.

3.3 Transverse Vibration Effects Included

To include the effects of transverse vibration in the analysis of optical lever data, we use the two-body mathematical model. Two approaches are taken. In the first we : (1) graphically obtain $\Theta_{NO}$, $\Psi_{NO}$, $\dot{\Theta}_{NO}$ and $\dot{\Psi}_{NO}$ estimates from the curves derived from optical lever data, (2) use $\dot{\Theta}_{NO}$ and $\dot{\Psi}_{NO}$ in Eqs. (C-7) (see Appendix C) to get $\omega'_{20}$ and $\omega'_{30}$ due to the vibration and (3) add to $\omega'_{20}$ and $\omega'_{30}$ initial angular velocity components due to "other" factors to obtain the $\Omega_{y0}$ and $\Omega_{z0}$ found in subsection 3.2. The second approach is to fit the optical lever derived curves with the two-body model solution in a least-squares sense.

Taking the first approach, we first find $\Theta_{NO} \simeq 0.25$ mrad, $\Psi_{NO} \simeq 0.0$ mrad, $\dot{\Theta}_{NO} \simeq -220$ mrad/sec and $\dot{\Psi}_{NO} \simeq 140$ mrad/sec. For the GEM #8 two-body model $B_1 \simeq 0.194$ kg-m$^2$, $B_2 \simeq 5.088$ kg-m$^2$, $m_1 \simeq 50.51$ kg and $m_2 \simeq 64.35$ kg. Hence, $\sigma \simeq 28.22$ kg and the constant factor $(\delta k_1 - k_1/k_2) =$

0.2733. From Eqs. (C-7), $\omega'_{20} \simeq -60$ mrad/sec and $\omega'_{30} \simeq 38$ mrad/sec due to transverse vibration. The total transverse rate due to bending is, therefore, approximately 70 mrad/sec.

Care must be exercised to maintain consistency when using the graphical method. Note that $A = \sqrt{\Delta_y^2 + \Delta_z^2}$ ; so, the values of $\Delta_y$ and $\Delta_z$ and A must be consistent. Also, the equation, $\gamma = \tan^{-1}(\Delta_y/\Delta_z)$, must be approximately satisfied by the measured value of $\gamma$. Attaining such consistency generally requires several attempts at drawing the enclosing lines and centerlines of the oscillations.

It is obviously no small problem to determine exactly what $\Theta_{NO}$, $\Psi_{NO}$, $\dot{\Theta}_{NO}$ and $\dot{\Psi}_{NO}$ are from the optical lever data. Again, the theoretical results must be consistent in that the amplitudes of the bending oscillations in the theoretical results must match well with those in the optical lever data. The results shown in Fig. 17 (see page 33) do, in fact, agree well.

The second approach involves considerably more labor than the graphical approach, unless the optical lever data is available in a form suitable for input into a digital computer. It is a standard least-squares procedure in which influence functions obtained from the two-body model computer code are used. The influence functions are found by setting all but one of the initial conditions and thrust misalignment angles successively to zero. The nonzero quantity is set equal to the same constant in each case. We used the values of 1 mrad for angles and 1 mrad/sec for rates to obtain the influence functions used to get the results which follow in this section.

To put the method in mathematical terms, we let $\underline{y}$ be a nx1 matrix of angles extracted from optical lever data. We also let $\underline{x} = (\Theta_{NO}\ \dot{\Theta}_{NO}\ \Psi_{NO}\ \dot{\Psi}_{NO}\ \alpha_y\ \alpha_z)^T$ and $\underline{\underline{A}}$ denote a nx6 matrix of influence coefficients, i.e.,

values of the influence functions evaluated at times after EOG corresponding to the data points. Then, if the two-body model were assumed to give exact results, we would have

$$\underline{y} = \underline{\underline{A}}\,\underline{x} \ . \tag{2}$$

Since the two-body model cannot be reasonably expected to give exact results and since we would like to use more than six pieces of data, we let the error involved be

$$\underline{\epsilon} = \underline{y} - \underline{\underline{A}}\,\underline{x} \ . \tag{3}$$

We then choose, as our "answer" for $\underline{x}$, the vector (6x1 matrix) $\hat{\underline{x}}$, such that $\underline{\epsilon}^T\underline{\epsilon}$ is minimized when $\hat{\underline{x}}$ is substituted for $\underline{x}$ in Eq. (3). The vector $\hat{\underline{x}}$ is given by the equation,

$$\hat{\underline{x}} = (\underline{\underline{A}}^T\,\underline{\underline{A}})^{-1}\,\underline{\underline{A}}^T\,\underline{y} \ . \tag{4}$$

By using 25 values of $\Psi_N$, 22 values of $\Theta_N$ and the appropriate influence coefficients from the two-body model computer code (in which $\Omega_x$ is set equal to 30 rad/sec) in Eq. (4), the following values may be obtained: $\hat{\Theta}_{NO} = 0.8722$ mrad, $\hat{\dot{\Theta}}_{NO} = -387$ mrad/sec, $\hat{\Psi}_{NO} = 0.1947$ mrad, $\hat{\dot{\Psi}}_{NO} = 128.5$ mrad/sec, $\hat{\alpha}_y = 0.685$ mrad, $\hat{\alpha}_z = 3.214$ mrad. These estimates are in reasonably close agreement with those obtained using the graphical procedure. One difference is that in obtaining the former we have not considered causes of transverse angular rates at EOG other than transverse bending. It turns out that if one attempts to solve for transverse angular velocity components due to "other" factors, the matrix $\underline{\underline{A}}^T\underline{\underline{A}}$ cannot be inverted.

When the estimates given immediately above are substituted into the two-body model computer code, the results shown as solid lines in Fig. 18

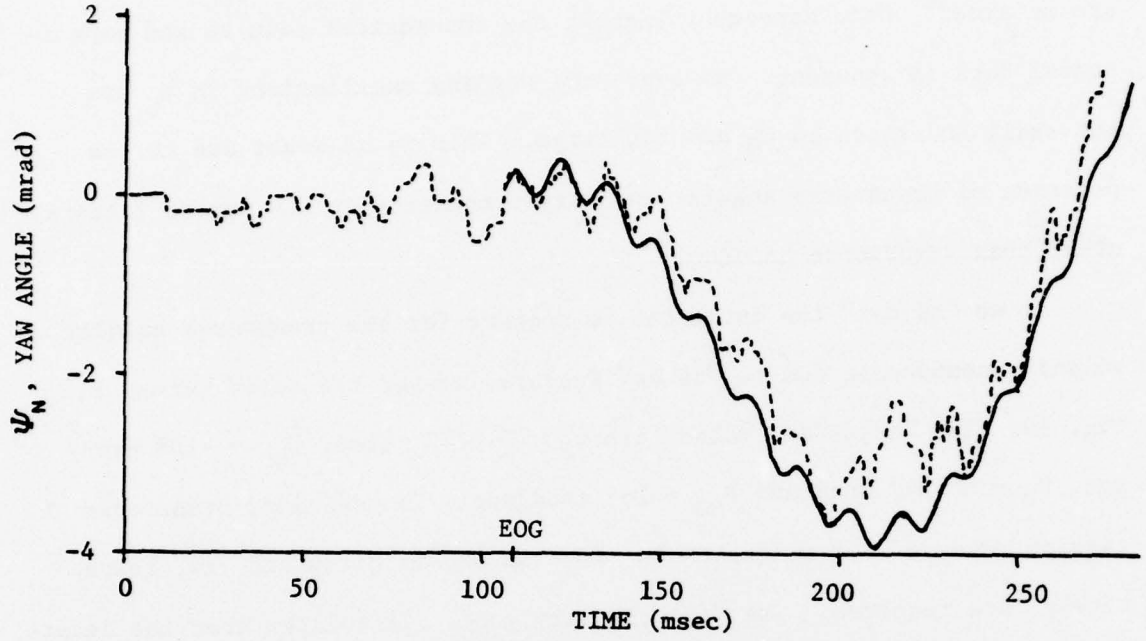


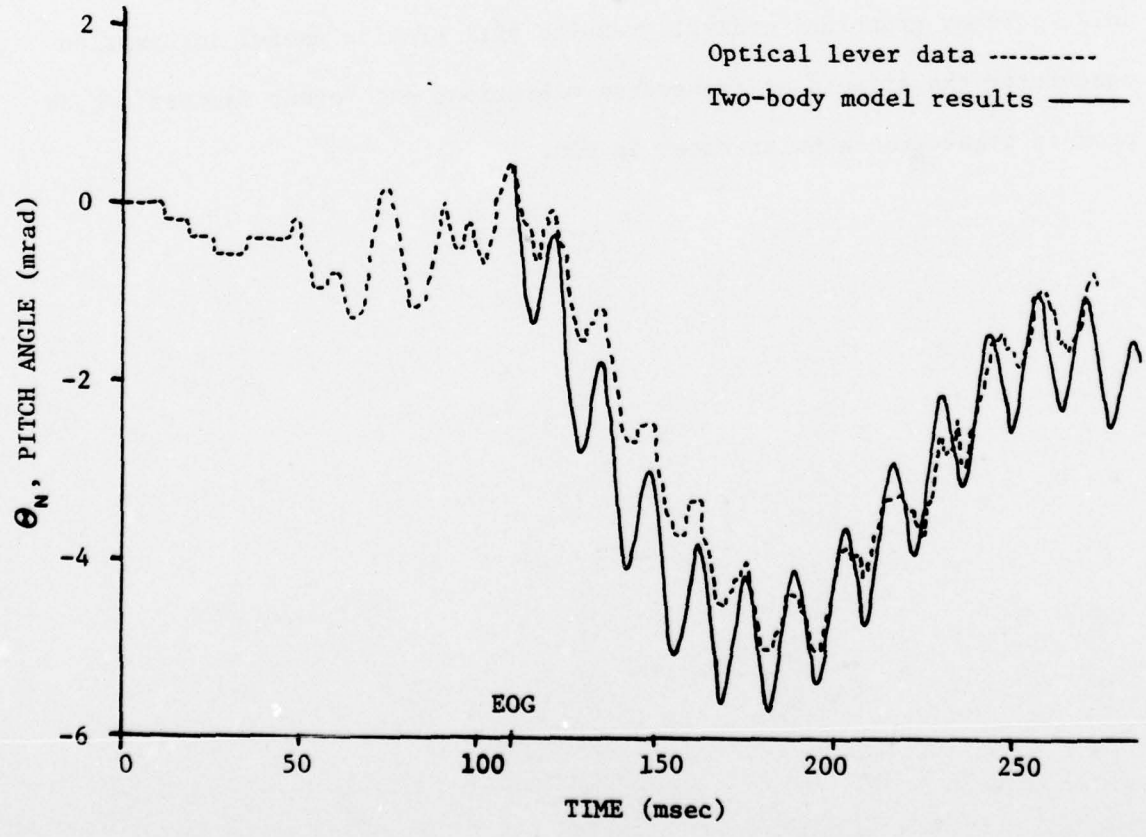


Fig. 18. Comparison of theoretical results and data - bending effects included using least-squares method, Case 1.

are obtained. Good agreement between the theoretical results and experimental data is apparent. However, the bending oscillations in $\Psi_N$ are too small and those in $\Theta_N$ are too large. This is no doubt due to the presence of transverse angular velocity components at EOG due to factors other than transverse bending.

If we "adjust" the estimates to account for the transverse angular velocity components due to "other" factors, we get the solid curves in Fig. 19. The "adjusted" values are $\psi_N = 0.8722$ mrad, $\hat{\dot{\Theta}}_{NO} = -208$ mrad/sec, $\theta_N = 0.1947$ mrad and $\hat{\dot{\Psi}}_{NO} = 166$ mrad/sec. In addition, transverse angular rates of -49 mrad/sec and 10 mrad/sec in pitch and yaw, respectively, are required. The "fit" is very good. It follows that the least-squares method combined with a little "engineering judgment," perhaps influenced by graphical analysis results will provide useful information concerning the effects of transverse vibrations and "other factors" which produce transverse angular rates at EOG.

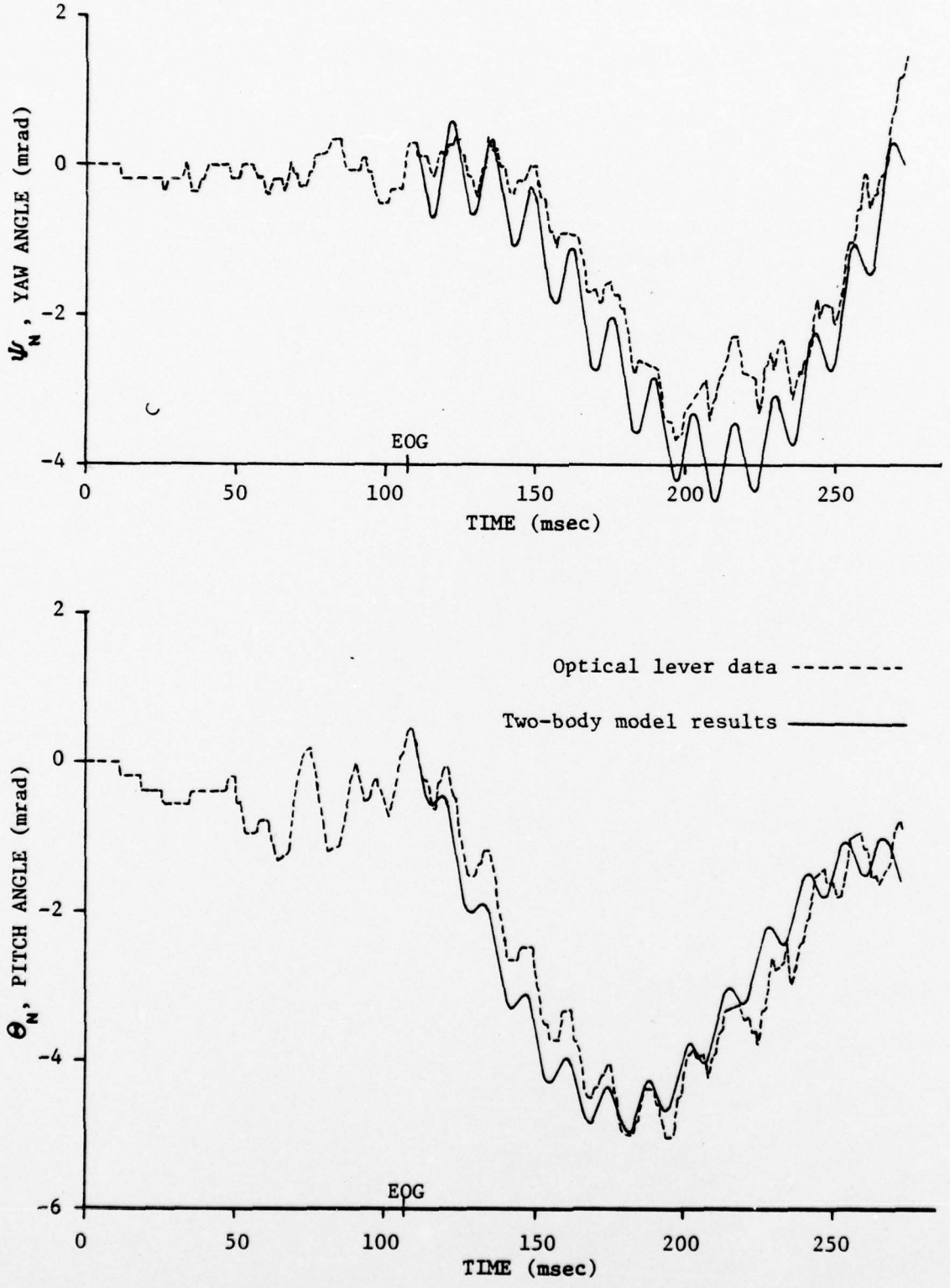


Fig. 19. Comparison of theoretical results and data - bending effects included using least-squares method, Case 2.

## SECTION 4. PROBABLE CAUSES OF TRANSVERSE VIBRATION

### 4.1 Introduction

It is clear from the results given in the previous sections that if transverse vibration of a free-flight rocket is occurring at EOG there will generally be an associated transverse angular rate. The exact cause, or causes, of the bending evidenced in GEM series flight test data has not been determined during the current research effort. However, several "probable" causes have been identified and studied by the authors and/or by U.S. Army Missile Laboratory personnel or U.S. Army contractors.

Soon after the search for causes of transverse bending began, it was discovered that some of the GEM series rockets were supported during portions of their guidance phases at three longitudinal points rather than two points. Hence, it is probable that this "intermittent" third support caused bending of the rocket.

A second cause of bending was suggested by Golden.[5] As the rocket begins to spin within the tube, transverse frictional forces act at support points. These forces may alternate in direction and hence cause bending.

A third cause of bending has been studied briefly by Smith.[6] If the thickness of the rocket motor case is not uniform circumferentially, the pressurization of the motor case during ignition of the rocket motor, and the axial forces on the rocket as it travels on the launcher will generally cause the rocket motor case to bend. Since the axial forces which act during detent and guidance are not constant, it is reasonable to believe that transverse vibration of the rocket with an eccentric motor case will occur.

In the following subsections, we treat the first two of the causes discussed above. We first consider the effects of "multiple" (more than two) supports.

## 4.2 Multiple Supports

The computer code which contains the assumed-modes mathematical model was modified so that three points of support could be modeled. This was done by forcing, mathematically, a point $x_3$ on the centerline of the rocket to follow a prescribed path for a prescribed amount of the total guidance length. The path chosen was a ramp. That is, the rocket travels within the launch tube for a certain distance. Then, the point $x_3$ on the centerline of the rocket is forced to follow a straight-line path which is not collinear with the launch axis, i.e., the ramp. After the rocket travels a certain additional distance within the launch tube, the "third support" ceases to support the rocket; however, the other two supports are still present until EOG. Hence, the rocket is forced to bend and is then released (partially). The resulting transverse vibration of the rocket model exists until and subsequent to EOG.

Only typical results are presented here to illustrate the possible effects of more than two longitudinal support locations. The curves in Fig. 20 were obtained using the data given in Table 3. The sequence of events is as follows. The point $x_M$ corresponding to the head end of the motor case of GEM #7 is forced to move vertically down 0.0254 cm during 0.1524 m of travel in the $x_L$-direction. The "third support" which caused the displacement of $x_M$ is then removed. The induced deflection of the rocket model's nose is about 0.8 mrad when the third support is removed. The rocket model then begins to vibrate and a transverse rate of about 61 mrad/sec is present at EOG. Hence, a small displacement of $x_M$ during guidance is sufficient to produce a large transverse rate at EOG.

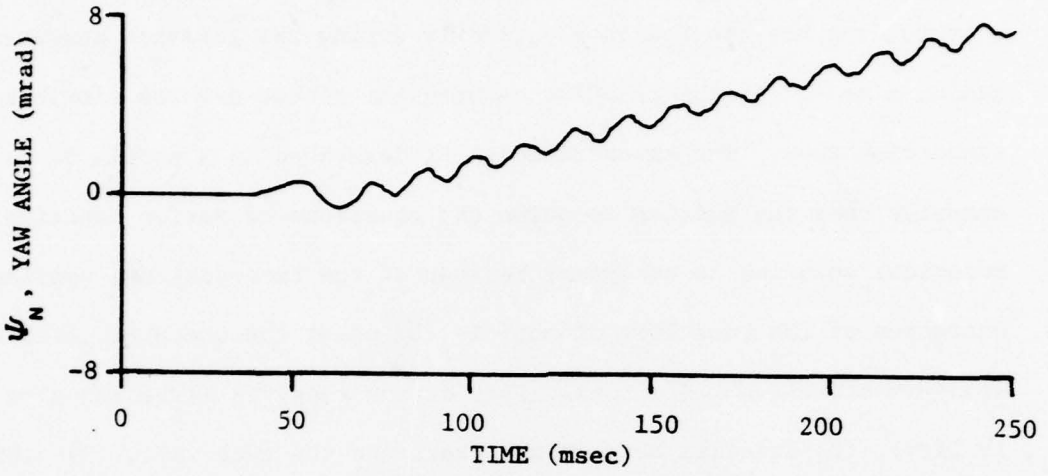


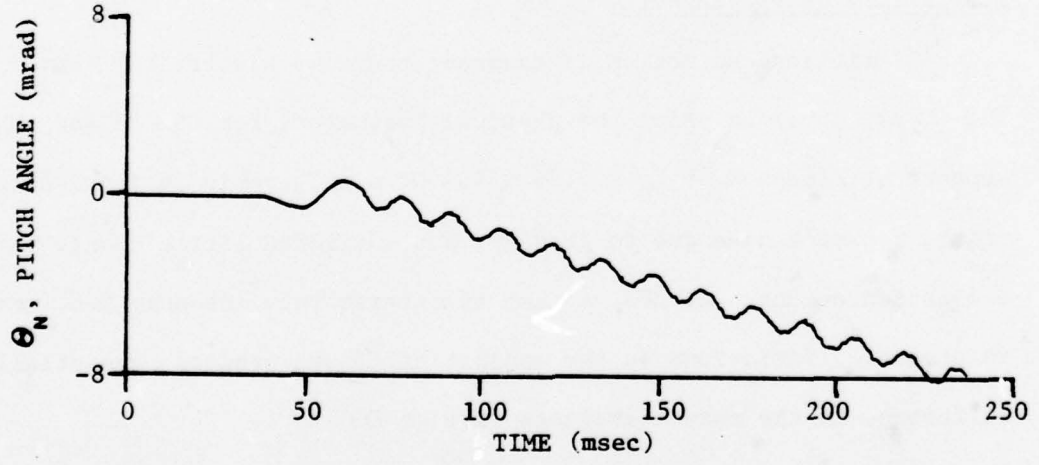


Fig. 20. Effect of "intermittent" third support.

## 4.3 Flexible Supports and Friction

The two-body model of a spinning flexible rocket was extended by constraining the two bodies elastically during the guidance phase and adding a model for the friction between the rocket and the flexible supporting tube. The extended model is described in Appendix D. A computer code was written to solve the equations of motion numerically. Numerical solution is necessary because of the time-varying, nonlinear character of the equations of motion. By using the computer code, one may study the effects of: (1) flexibility of the supports (tube and shoe flexibility), (2) friction between the shoes and the tube wall, (3) clearance, or "dead space," between the shoes and wall, (4) forward support location, (5) spin torque magnitude and (6) tipoff. Only the first four of the above will be discussed in what follows.

### Flexibility of the Supports

If frictionless motion is assumed, the time histories $\Theta_N$ and $\Psi_N$ shown in Fig. 21 are obtained using the physical parameters for GEM #8 and the support stiffness $K_P = K_Q = 8.76 \times 10^7$ Nt/m. There is an initial deflection of the rocket's nose due to gravity, but until EOG little change in this deflection occurs. At EOG, a mean transverse rate† of only 0.67 mrad/sec is present. Variations in the support stiffness produce essentially no difference in the mean transverse rate at EOG.

### Friction

When non-zero coefficients of friction, $\mu_P$ and $\mu_Q$, are introduced into the equations of motion, the rocket generally begins to "whirl" as the spin rate increases and the frictional forces cause transverse vibration. This

---

†Here, "mean transverse rate" is the square root of the sum of the squares of the mean values (bending oscillations not included) of $\dot{\Theta}_N$ and $\dot{\Psi}_N$.

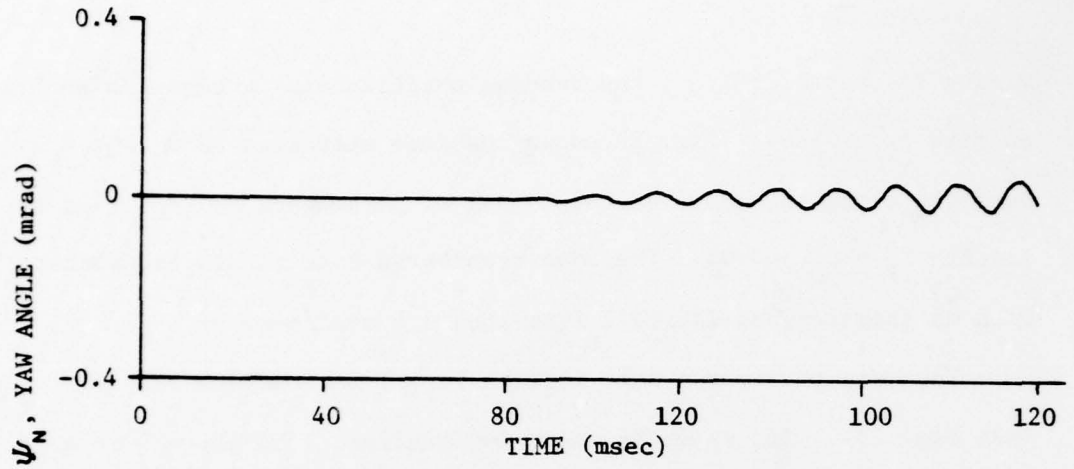


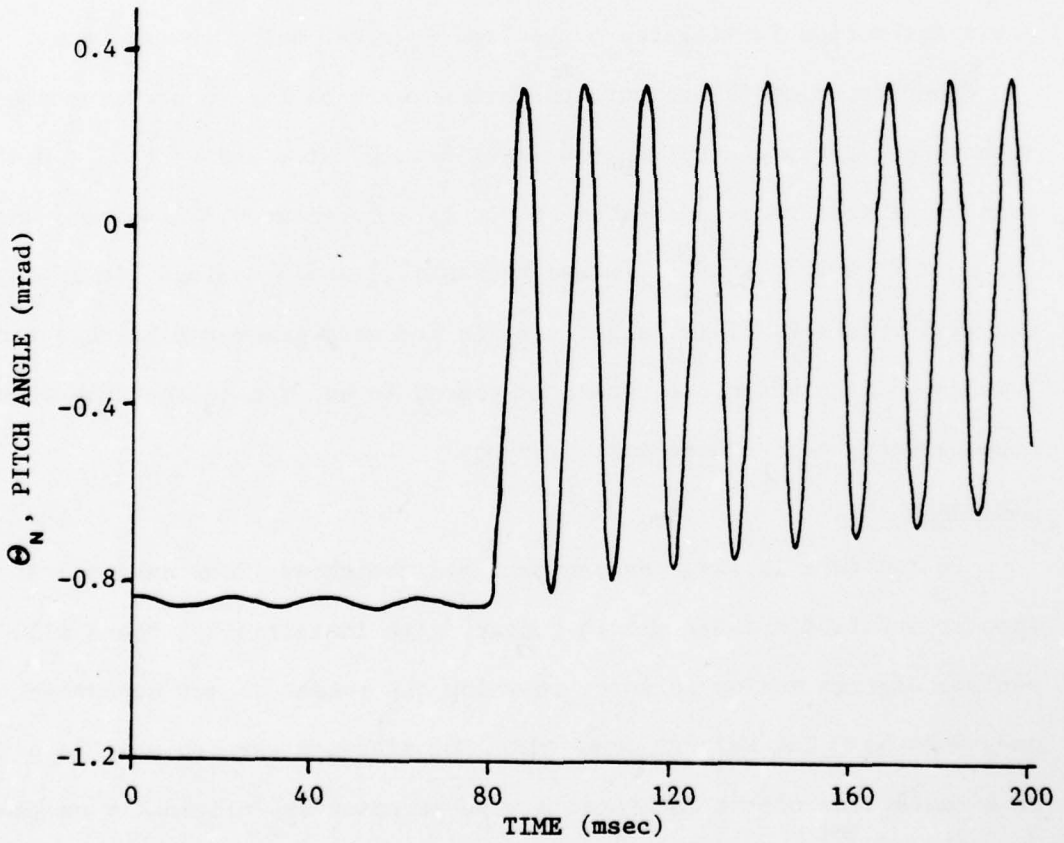


Fig. 21. Effect of flexible supports.

motion is unstable; i.e., the bending oscillations increase in amplitude as time progresses. Fig. 22 shows the time histories of $\Theta_N$ and $\Psi_N$ obtained using the above stated values of parameters and friction coefficients $\mu_P = \mu_Q = 0.05$. The mean transverse rate at EOG is greater than with no friction,but is still less than 0.8 mrad/sec.

The mean transverse rate is much larger for the case of $\mu_P = \mu_Q = 0.1$ (see Fig. 23). Its value is about 240 mrad/sec. Larger values of $\mu_P$ and $\mu_Q$ thus produce more bending and larger mean transverse angular rates. In fact, $\mu_P$ and $\mu_Q = 0.2$ produce divergent motion to the extent that the small angle assumption is violated for $\theta_2$ and $\theta_3$ after only 0.05 seconds.

When friction is present, the stiffnesses of the supports become much more important. For $K_P = K_Q = 4.38 \times 10^7$ Nt/m and $\mu_P = \mu_Q = 0.05$, the mean transverse rate, as stated above, is only about 0.8 mrad/sec; whereas, for $K_P = K_Q = 1.75 \times 10^8$ Nt/m and the same $\mu_P$ and $\mu_Q$ values, it is approximately 2 mrad/sec. This larger rate is probably generated because the "violence" with which the rocket is forced to and fro in the tube when the tube is very stiff causes more bending.

Clearance

If the tube is large enough that all the shoes (four assumed) at each support location are not all in contact with it initially, there will be periods of time during guidance in which the rocket is not supported at one, or both, of the support locations. The distance through which a point on a centerline of the rocket,at a support point and originally on the centerline of the tube,must move for a shoe to contact the tube wall is denoted by $\varepsilon$. In the work we have done, $\varepsilon$ has been assumed to be the same at the fore and aft support points.

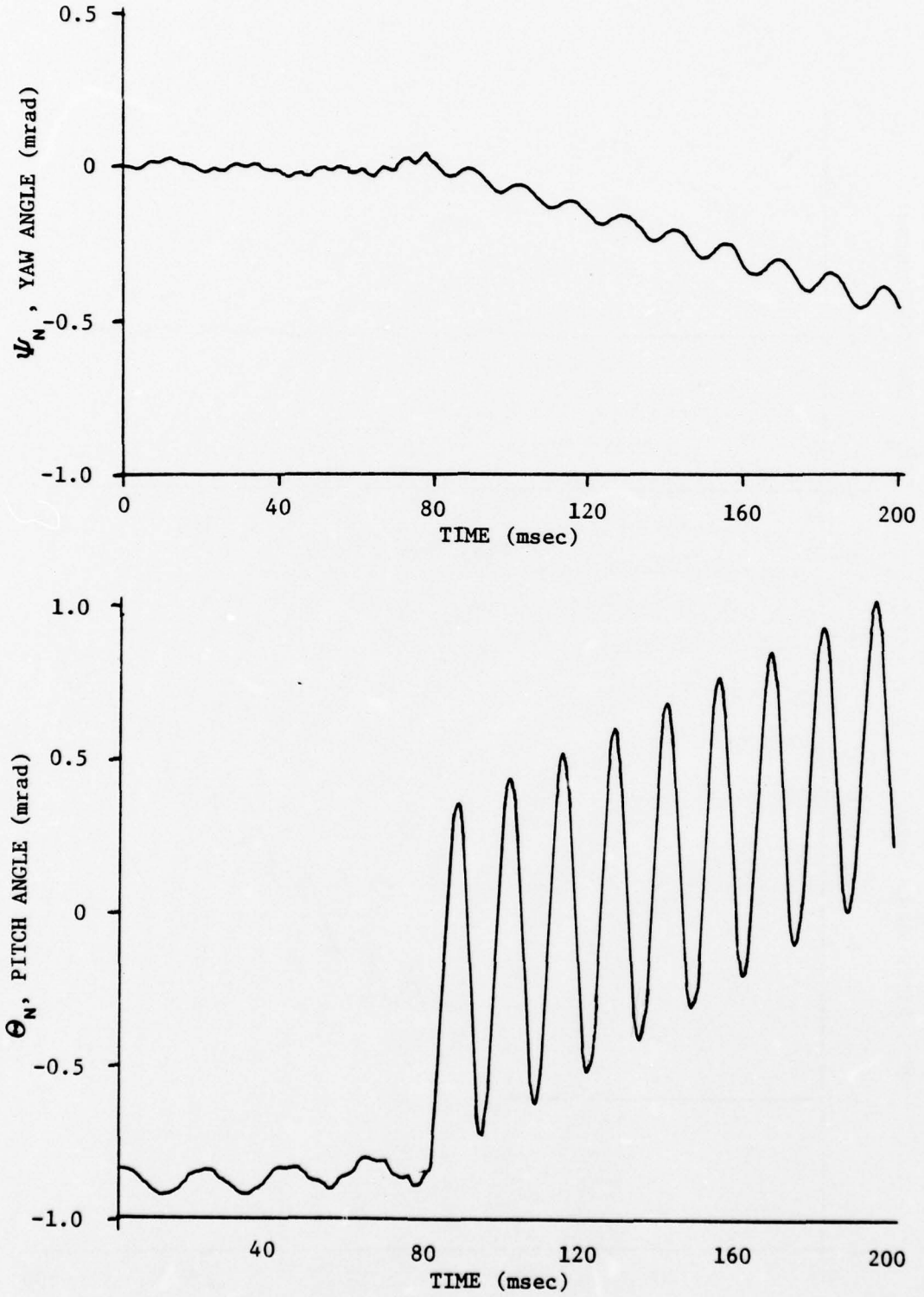


Fig. 22. Effects of flexible supports and friction - $\mu_P = \mu_Q = 0.05$.

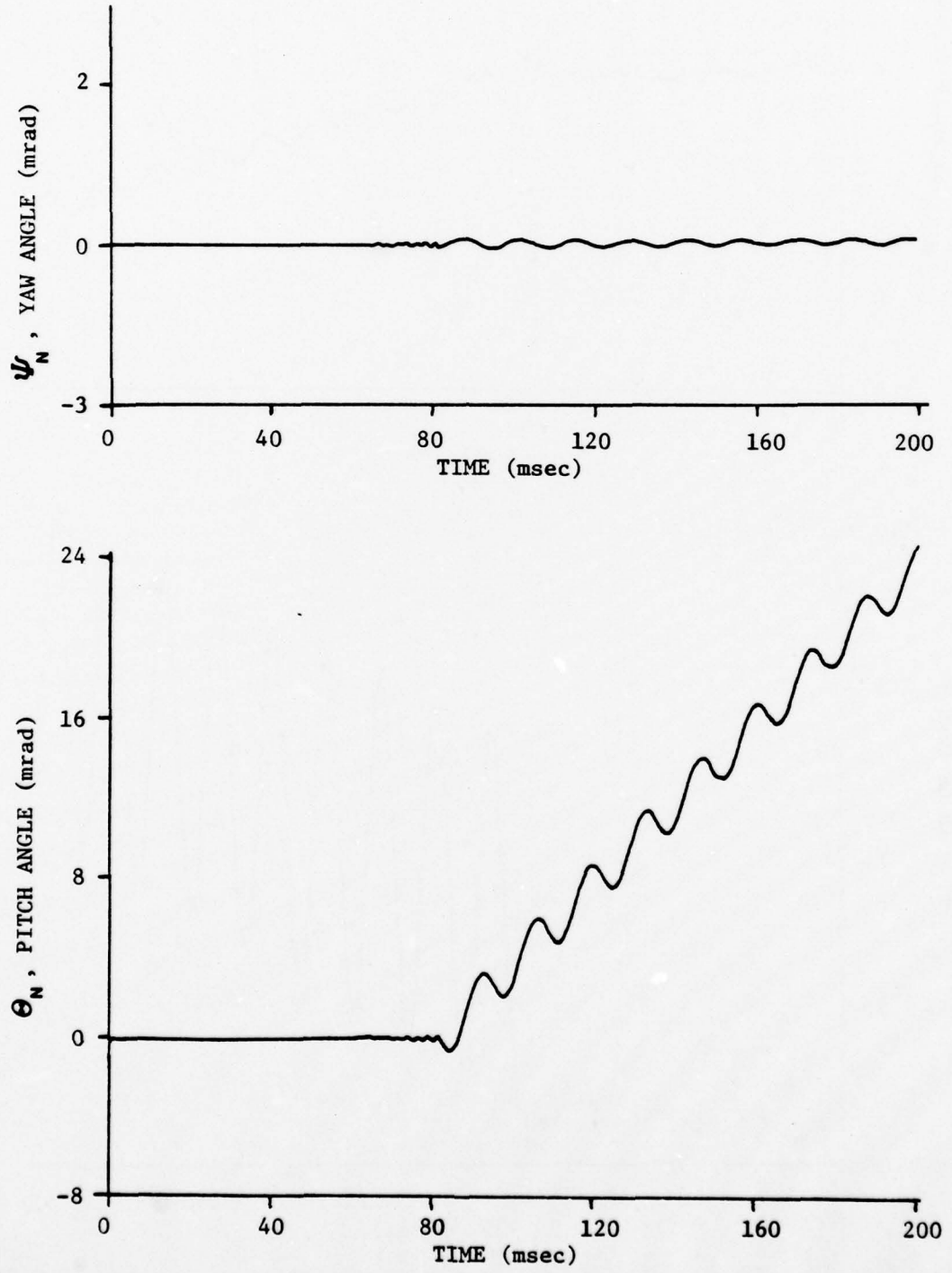


Fig. 23. Effects of flexible supports and friction - $\mu_P = \mu_Q = 0.1$.

We have found that a nonzero $\varepsilon$, say 0.31 mm, with no friction, will result in a slightly greater mean transverse rate at EOG than would otherwise be present.

An example of the attitude motion of the rocket's nose that occurs when $K_P = K_Q = 8.76 \times 10^7$ Nt/m, $\mu_P$ and $\mu_Q = 0.05$ and $\varepsilon = 0.31$ mm is shown in Fig. 24. The irregularity of the time histories of $\Psi_N$ and $\Theta_N$ during the guidance phase is due to the clearance. During certain intervals of time, the rocket is actually in free-flight within the tube.

Forward Support Location

If the forward support is moved from its nominal ($\ell_2 = -0.335$ m) location on the rocket, the equilibrium pitch angle of the nose changes. For the two-body model, if the support is moved so that $\ell_2 = 0.54$ m (the value found in Section 2 which makes the constant factor of Eq. (1) zero, then the equilibrium pitch angle of the rocket's nose is about 0.24 mrad. For $\ell_2 = 0.54$ m, $K_P = K_Q = 8.76 \times 10^7$ Nt/m, $\mu_P = \mu_Q = 0.05$, $\varepsilon = 0$ mm, and all other values of parameters the nominal ones, we get the result shown in Fig. 25. The mean transverse rate is not zero, but is approximately 12 mrad/sec. It is not zero because the support points P and Q are moving at EOG in such a way that there is a transverse angular rate of the rocket's principal axes in addition to the rate produced by transverse vibrations. Hence, the suggested method for reducing the adverse effects of transverse vibration, i.e., placing the supports properly, does not necessarily produce zero transverse angular rate when other factors, such as tube flexibility, are present.

Combined Effects

As a final example of the effects of friction clearance and support location, we offer Fig. 26. The results shown in Fig. 26 were obtained

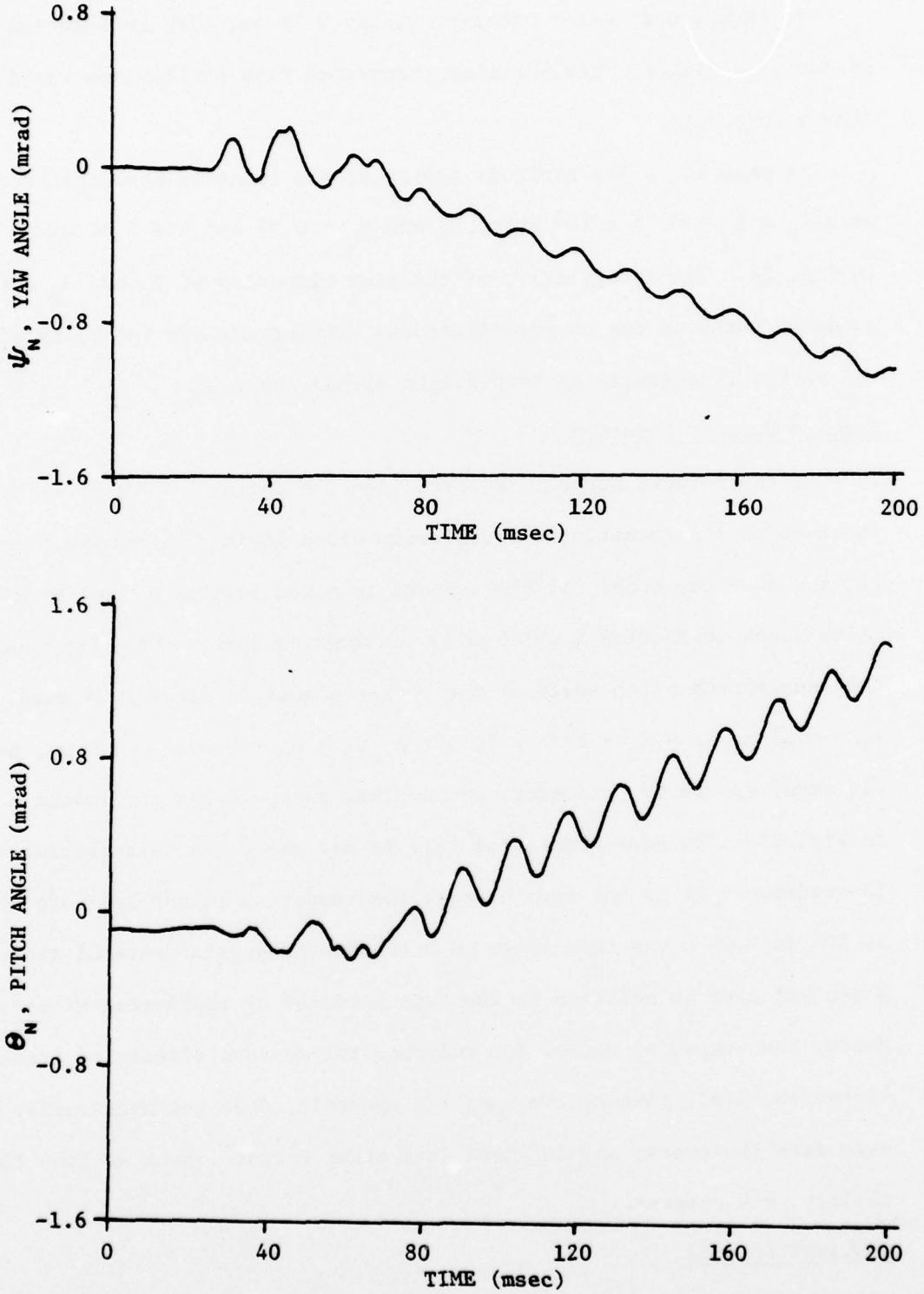


Fig. 24. Effects of flexible supports, friction and clearance - $\mu_P = \mu_Q = 0.05$ and = 0.31 mm.

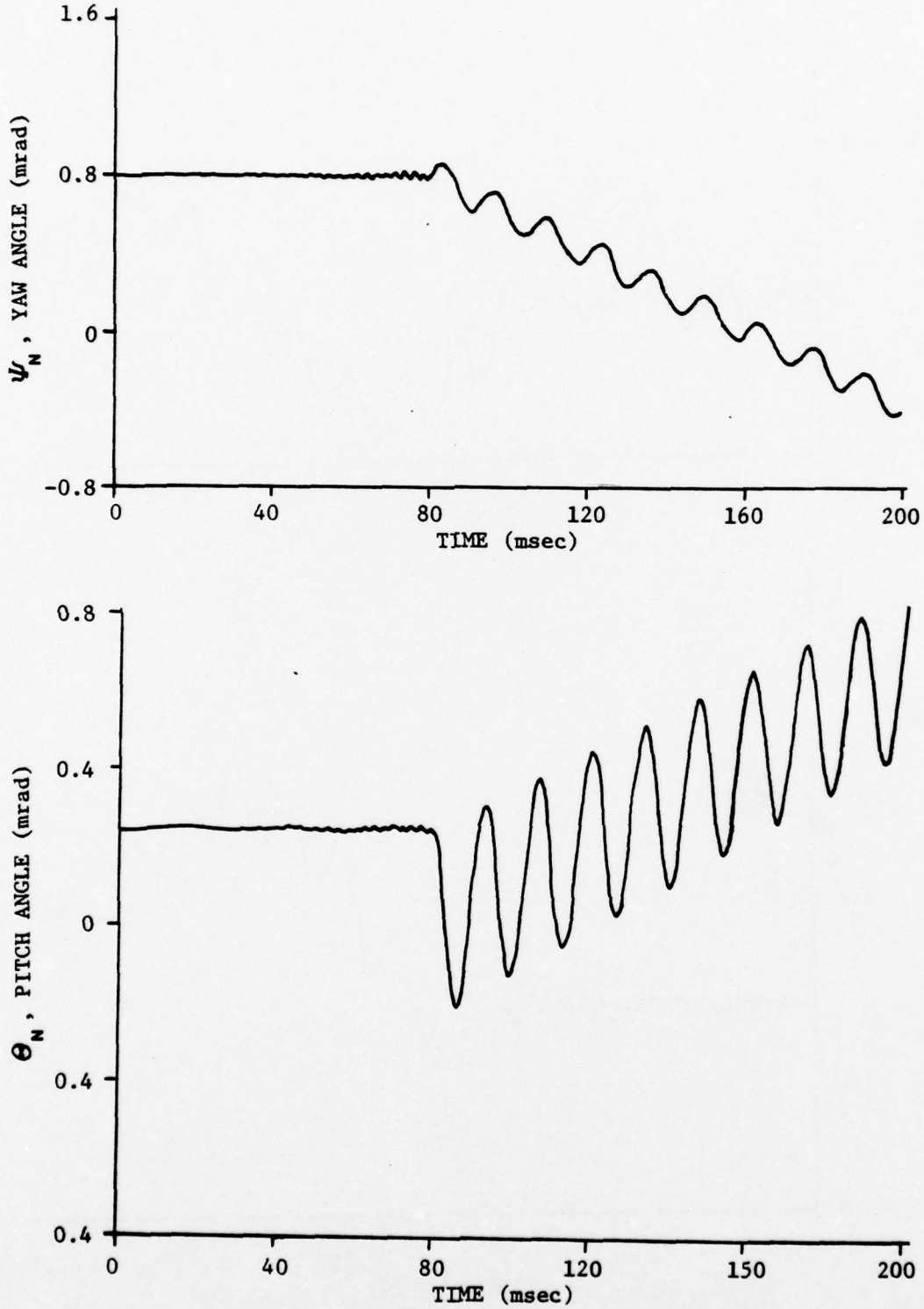


Fig. 25. Effect of forward support location.

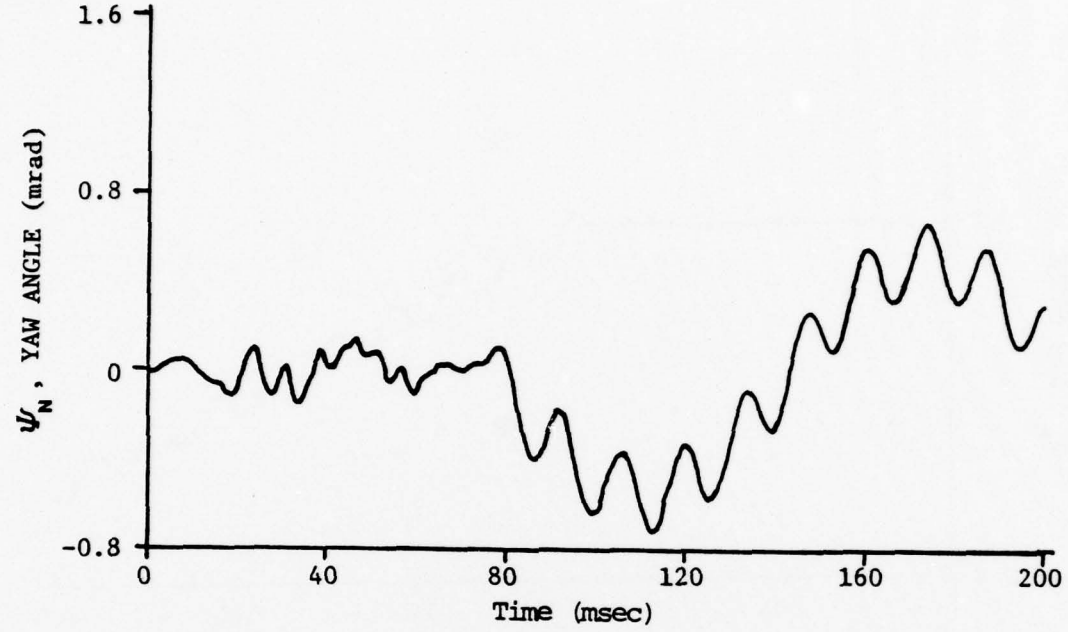


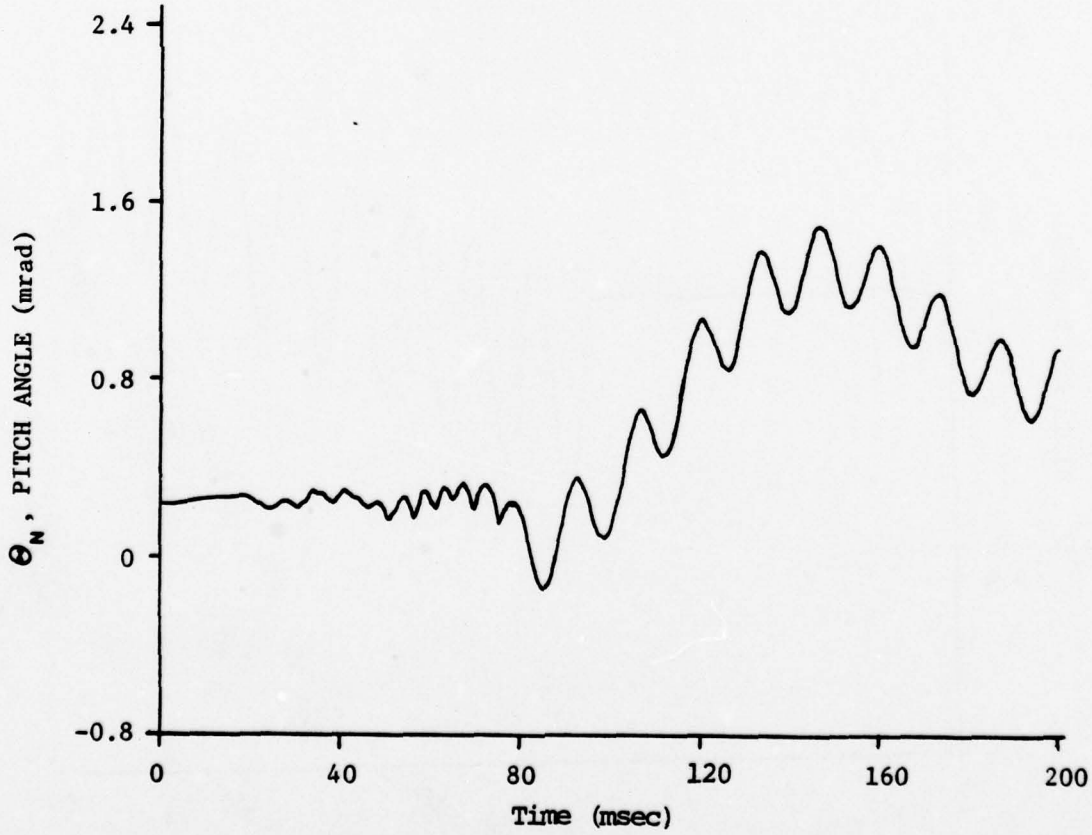


Fig. 26. A combined effects example.

using $\ell_2 = 0.54$ m, $K_P = K_Q = 8.76 \times 10^7$ Nt/m, $\mu_P = \mu_Q = 0.05$, $\varepsilon = 0.31$ mm and the thrust misalignment angles $\alpha_y = \alpha_z = 1$ mrad. In this case, the transverse rate is less than that which would be present if only thrust misalignment existed.

The qualitative similarity between the pitch and yaw time histories shown in Fig. 26 during the guidance phase and the optical lever results shown in Figs. 16, 17, 18 or 19 should be noted. This is encouraging, as it indicates that a mathematical model which includes the flexibilities of the rocket and its supporting structure, clearance, friction, thrust misalignment, dynamic imbalance and possibly only a few more characteristics could be used successfully in analyses of free-flight rocket motion during both the guidance and free-flight phases.

Comments on Angular Momentum

That the transverse component of angular momentum may represent a substantial portion of $\underline{H}$, the total angular momentum of a flexible rocket about its center of mass at EOG was verified by using the extended two-body model. The Body 1-fixed (Cxyz frame) and space-fixed components of $\underline{H}$ were computed along with the rocket's state. The transverse component of $\underline{H}$ at EOG was found, for example, to be $0.633\ |\underline{H}|$ for the combined effects case.

The space-fixed angular momentum components also served as checks on the numerical integration procedure. If there are no external torques subsequent to EOG, they should remain constant. Constancy to four significant figures was, in fact, achieved.

## SECTION 5. CONCLUSIONS AND RECOMMENDATIONS

### 5.1 Conclusions

On the basis of results of this investigation we have reached the following conclusions:

1. The two-body model and assumed-modes model computer codes are correct as far as programming is concerned.

2. The assumed-modes computer code allows one to model a flexible free-flight rocket in more detail than is possible with the two-body computer code. The changes in amplitudes and frequencies of transverse vibrations obtained using the assumed-modes code are qualitatively the same as those which are often observed in optical lever data.

3. The graphical method presented is useful in getting order of magnitude information.

4. The two-body model is a valid representation of a spinning, flexible free-flight rocket to the extent that it can be used to analyze optical lever data which contain evidence of transverse vibration.

5. The methods for analyzing optical lever data which are given in the body of this report provide useful information concerning the effects of transverse vibrations. They also can be used to detect the presence of "other" factors which cause transverse angular rates of free-flight rockets at EOG.

6. Transverse vibration of a spinning flexible free-flight rocket during the guidance phase can result in transverse angular rates of the rocket as a whole at EOG. These rates are of the same magnitude as those caused by several milli-radians angular thrust misalignment, generally being on the order of 10 to 100 mrad/sec.

7. The transverse angular rate due to bending vibrations can be reduced by placement of the rocket supports in such a way that rotational motion of the time-varying centroidal principal axes of the rocket is reduced.

8. A probable cause of transverse bending of some of the GEM series rockets was the use of an "intermittent" third support.

9. Coulomb friction acting axially and circumferentially on a spinning, flexible rocket at its points, or areas, of support may cause considerable transverse bending, the magnitude of which depends on the coefficient of friction, clearance and other factors. Friction is another probable cause of bending vibrations of the GEM series rockets.

10. If the points of support of a spinning, flexible rocket are not constrained to translate in a fixed direction during guidance, then, although the transverse rate due to bending vibrations may be reduced by choosing the support points properly, the transverse angular rate of the rocket's principal axes may still be large due to the transverse motions of the support points.

11. Additional work is needed to provide a complete understanding of the causes and effects of transverse vibration of spinning, flexible rockets supported and guided by flexible launchers. The results presented herein should provide a basis for such work.

Conclusions 1 and 2 are based on the results of comparisons of the two-body and assumed modes computer codes. Conclusion 3 is an obvious result of the successful use of the graphical method in analyzing GEM #8 data in Section 3. Conclusion 4 is reached in light of the success achieved in Refs. 2 and 3 and herein in "fitting" optical lever data with the two-body results. There is still some question about uniqueness of the parameter set needed to "fit" the data.

The analysis presented in Section 3 justifies Conclusion 5. From results given in Sections 2 and 3, it is apparent that transverse vibration during guidance is a significant cause of transverse angular rates subsequent to EOG, as concluded in 6, above. Results given herein also indicate that if the rotational motion of the time-varying centroidal principal axes of a flexible rocket is due only to bending of the rocket, such rotation can be reduced (Conclusion 7). Conclusions 8, 9 and 10 follow from the results of Section 4.

Although it is felt that considerable progress has been made since the work reported in Ref. 2 was begun, the problem of determining the motion of a general, flexible free-flight rocket while it is being supported and guided by a general flexible launcher has obviously not been solved. A complete solution is apparently not attainable. However, as Conclusion 11 indicates, much more can and needs to be done. We consider this next.

## 5.2 Recommendations

Several problem areas should be more carefully explored in the near future. These are considered in the following recommendations.

1. Additional work is recommended with the goal of developing a more accurate and efficient method for correlating theoretical and experimental results for spinning, flexible free-flight rocket motion. More general mathematical models for both the launcher and rocket should be developed so that the simultaneous effects of launcher motion, launcher flexibility and aerodynamic effects (including blow-by) can be studied. Such models coupled with a statistical parameter estimation algorithm would be very useful in analyzing test results.

2. Although it is now agreed by many that transverse vibration of a free-flight rocket during guidance does generally produce a transverse angular rate of the rocket as a whole (gross motion) subsequent to EOG, the experimental confirmation of this phenomenon is currently based on optical lever data acquired without a priori consideration of transverse bending as a possible error source. It is recommended that a test program be conducted to verify that transverse bending vibrations are as significant as theoretically predicted and to determine how well the current theories predict their effects. Such a test program would necessarily involve (1) tests to determine the effects of transverse vibration and (2) tests to determine its major causes. The former could be conducted with small reusable experimental rocket models which are propelled by cold gas, or spring mechanisms, and which are caused to vibrate in prescribed fashions. The latter could be conducted with similar experimental rocket models and a launcher for which friction and support stiffness could be controlled.

## REFERENCES


1. Anonymous, Memoranda containing flight test data for rockets GEM #7 (fired 5 Feb. 1976) and GEM #8 (fired 2 March 1976). U.S. Army Missile Research and Development Command, Redstone Arsenal, Alabama.

2. Cochran, J. E., Jr., Evans, C. D., and McCurry, J. B., "Effects of Transverse Bending on the Motion of Free-Flight Rockets," Technical Report T-CR-78-21, Final Report under Contract DAAK40-77-C-0125 for the U.S. Army Missile Research and Development Command, Redstone Arsenal, Alabama, September 1978.

3. Cochran, J. E., Jr., and Christensen, D. E., "Post-Launch Effects of Transverse Bending of a Spinning Free-Flight Rocket During the Guidance Phase," AIAA Paper No. 79-1668, Presented at the AIAA Atmospheric Flight Mechanics Conference, Boulder, Colorado, August 7-9, 1979.

4. Booker, D. L., "Free Flight Rocket Spin Technique Development," Technical Report T-78-30, U.S. Army Missile Research and Development Command, Redstone Arsenal, Alabama, January 1978.

5. Golden, T., Private communication, August 1979.

6. Smith, T. A., "Preliminary Evaluation of Spike Motor Case Angular Deflections due to Postulated Circumferential Variation in Motor Case Thickness," Working paper only, U.S. Army Missile Laboratory, Redstone Arsenal, Alabama, October 29, 1979, revised November 20, 1979.

## APPENDIX A

## TWO-BODY MATHEMATICAL MODEL FOR FREE FLIGHT

### Introduction

The mathematical model developed on the basis of the two-body physical model described in Ref. 2 and in the body of this report is given here for the convenience of the reader and also for the purpose of correcting some errors which appear in Ref. 2. The derivation of Ref. 2 should be consulted regarding the nonlinear equations of motion, since only the linearized versions are given here.

### Equations of Motion

The linearized version of the equations which govern the rotational motion of the system of two bodies can be expressed in the form of four first-order, scalar, ordinary differential equations and a first-order matrix equation. The scalar equations are

$$\dot{\Omega}_1 = T_s/I_A \quad , \tag{A-1a}$$

$$\dot{\Phi} = \Omega_1 \quad , \tag{A-1b}$$

$$\dot{\Psi} = \Omega_2 \, s\Phi + \Omega_3 \, c\Phi \tag{A-1c}$$

and

$$\dot{\Theta} = \Omega_2 \, c\Phi - \Omega_3 \, s\Phi \quad , \tag{A-1d}$$

where the $\Omega_j$, j=1,2,3, are the $x_1$-, $y_1$- and $z_1$-components, respectively, of the angular velocity of Body 1 (the "aft" body), $T_s$ is the spin torque; $I_A$ is the moment of inertia of the undeformed system of two bodies about the $x_1$-axis; $\Phi$ is the roll angle of Body 1; $\dot{\Psi}$ and $\dot{\Theta}$ are the yaw and pitch angles of Body 1.

The matrix equation can be written as follows:

$$\underline{\underline{I}}\ \dot{\underline{x}} = \underline{\underline{B}}\ \underline{x} + \underline{T}\ , \tag{A-2}$$

where

$$\underline{x} = (\Omega_2\ \Omega_3\ \omega_2\ \omega_3\ \theta_2\ \theta_3)^T; \tag{A-3}$$

$\underline{\underline{I}}$ is a 6x6 matrix with <u>non-zero</u> elements,

$$I_{11} = A_2 + B_2 + \sigma(\ell_1+r_2)^2, \tag{A-4a}$$

$$I_{13} = B_2 + \sigma\ r_2(\ell_1+r_2), \tag{A-4b}$$

$$I_{22} = I_{11}, \tag{A-4c}$$

$$I_{33} = I_{44} = B_2 + \sigma r_2^{\,2}, \tag{A-4d}$$

$$I_{42} = I_{24} = I_{31} = I_{13}, \tag{A-4e}$$

and

$$I_{55} = I_{66} = 1; \tag{A-4f}$$

$\underline{\underline{B}}$ is a 6x6 matrix with <u>non-zero</u> elements,

$$B_{12} = \Omega_1[A_2 + B_2 + \sigma(\ell_1+r_2)^2 - A_1-B_1]\ , \tag{A-5a}$$

$$B_{14} = \Omega_1[2B_2 - B_1 + 2\ \sigma\ r_2(\ell_1+r_2)], \tag{A-5b}$$

$$B_{15} = \mu r_2 F_T + \Omega_1^{\,2}[B_2-B_1 + \sigma r_2(\ell_1+r_2)]\ , \tag{A-5c}$$

$$B_{16} = \dot{\Omega}_1[B_2-B_1 + \sigma r_2(\ell_1+r_2)]\ , \tag{A-5d}$$

$$B_{21} = -\ B_{12}, \tag{A-5e}$$

$$B_{23} = B_{14}, \tag{A-5f}$$

$$B_{25} = B_{16}, \tag{A-5g}$$

$$B_{26} = B_{15}, \tag{A-5h}$$

$$B_{32} = \Omega_1[B_2-B_1 + \sigma r_2(\ell_1+r_2)], \tag{A-5i}$$

$$B_{33} = -c, \tag{A-5j}$$

$$B_{34} = \Omega_1[2\ B_2-B_1 + 2\sigma r_2^2], \tag{A-5k}$$

$$B_{35} = \mu r_2 F_T + \Omega_1^2[B_2-B_1 + \sigma r_2^2] - k \tag{A-5ℓ}$$

and

$$B_{36} = \dot{\Omega}_1[B_2-B_1 + \sigma r_2^2]\ ; \tag{A-5m}$$

$\underline{T}$ is the 6x1 matrix,

$$\underline{T} = (-\alpha_y\ F_T\ \ell_c \quad -\alpha_z F_T \ell_c \quad 0\ \ 0\ \ 0\ \ 0)^T. \tag{A-6}$$

In the above Eq. (A-3), $\omega_2$ and $\omega_3$ are, respectively, the $y_2$- and $z_2$-components of the angular velocity of Body 2 relative to Body 1 and $\theta_2$ and $\theta_3$ are the transverse angles of rotation of Body 2 relative to Body 1. Also, in Eqs. (A-4) and (A-5), $A_1$ and $A_2$ are, respectively, the axial and transverse centroidal moments of inertia of Body 1, while $B_1$ and $B_2$ are those for Body 2. Furthermore, with $m_1$ and $m_2$ denoting the masses of Bodies 1 and 2, respectively, $\sigma = m_1 m_2/M$ where $M = m_1+m_2$. Additionally, $\ell_1$ is the distance from the center of mass of Body 1 to the "hinge point" between the bodies, and $r_2$ is the distance from the hinge point to the center of mass of Body 2. Finally, c and k are the inter-body damping and stiffness constants.

In Eq. (A-6), $\alpha_y$ and $\alpha_z$ are thrust misalignment angles; $F_T$ is the thrust magnitude and $\ell_c = [m_1 r_1 + (\ell_1+r_1+r_2)m_2]/M$, where $r_1$ is the distance from the aft end of Body 1 to its center of mass.

Constant Spin Rate Solution

When the spin torque $T_s = 0$, $\Omega_1$ is constant. In this case, if $F_T$ is also a known function of time, a closed-form solution to Eqs. (A-1) and (A-2) can be obtained. Since $F_T$ is fairly constant immediately after "end of guidance" (EOG), it is assumed to be constant herein, thereby simplifying the process of obtaining a particular solution to Eq. (A-2).

In the case of constant spin rate, $\underline{\underline{B}}$ is constant. Hence, the matrix,

$$\underline{\underline{A}} = \underline{\underline{I}}^{-1}\underline{\underline{B}} \ , \tag{A-7}$$

is also constant and Eq. (A-2) can be written as

$$\dot{\underline{x}} = \underline{\underline{A}}\,\underline{x} + \underline{\tau} \ , \tag{A-8}$$

where $\underline{\tau} = \underline{\underline{I}}^{-1}\underline{T}$ .

A particular solution to Eq. (A-8) ($\underline{\tau}$ is constant) is

$$\underline{x}_p = -\,\underline{\underline{A}}^{-1}\underline{\tau} \ , \tag{A-9a}$$

or

$$\underline{x}_p = \underline{\underline{B}}^{-1}\underline{T} \ . \tag{A-9b}$$

The complete general solution to Eq. (A-8) consists of $\underline{x}_p$ and the solution to the homogeneous equation,

$$\dot{\underline{x}}_h = \underline{\underline{A}}\,\underline{x}_h \ , \ \underline{x}_h(0) = \underline{x}_{h0} \ . \tag{A-10}$$

By using the eigenvalues and eigenvectors of $\underline{\underline{A}}$, which for our purposes appear as complex conjugate pairs (three of them), the solution $\underline{x}_h$ can be expressed as

$$\underline{x}_h = \underline{\underline{E}}\,\underline{\underline{D}}\,\underline{\underline{E}}^{-1}\,\underline{x}_{h0} \ , \tag{A-11}$$

where $\underline{\underline{E}}$ is a 6x6 matrix the columns of which are alternately the real and imaginary parts of the eigenvectors corresponding to the eigenvalues of $\underline{\underline{A}}$

with positive imaginary parts. Also, if $n_j$ and $\omega_j$ denote the real and imaginary parts respectively of an eigenvalue $\lambda_j$ which has a positive imaginary part,

$$\underline{\underline{D}} = \begin{bmatrix} \underline{\underline{D}}_{11} & \underline{\underline{0}} & \underline{\underline{0}} \\ \underline{\underline{0}} & \underline{\underline{D}}_{22} & \underline{\underline{0}} \\ \underline{\underline{0}} & \underline{\underline{0}} & \underline{\underline{D}}_{33} \end{bmatrix} , \tag{A-12}$$

where

$$\underline{\underline{D}}_{jj} = \begin{bmatrix} e^{n_j\tau}\cos\omega_j\tau & e^{n_j\tau}\sin\omega_j\tau \\ -e^{n_j\tau}\sin\omega_j\tau & e^{n_j\tau}\cos\omega_j\tau \end{bmatrix} \quad (j=1,2,3) . \tag{A-13}$$

The solutions for the first two elements of $\underline{x}$; i.e., $x_j$, j=1,2, can be written out explicitly and substituted into Eqs. (1c) and (1d) to obtain

$$\begin{bmatrix} \dot{\Theta} \\ \dot{\Psi} \end{bmatrix} = \frac{1}{2}\sum_{i=1}^{3} \begin{bmatrix} \cos p_i\tau & -\sin p_i\tau \\ \sin p_i\tau & \cos p_i\tau \end{bmatrix} \begin{bmatrix} A_{i1}-B_{i2} \\ A_{i2}+B_{i1} \end{bmatrix} e^{n_i\tau}$$

$$+ \frac{1}{2}\sum_{i=1}^{3} \begin{bmatrix} \cos q_i\tau & -\sin q_i\tau \\ \sin q_i\tau & \cos q_i\tau \end{bmatrix} \begin{bmatrix} A_{i1}+B_{i2} \\ A_{i2}-B_{i1} \end{bmatrix} e^{n_i\tau} + \begin{bmatrix} \cos\Phi & -\sin\Phi \\ \sin\Phi & \cos\Phi \end{bmatrix} \begin{bmatrix} x_{1p} \\ x_{2p} \end{bmatrix} , \tag{A-14}$$

where $\Phi = \Omega_1\tau$, $\tau = t-t_o$, $p_i = \Omega_1 - \omega_i$, $q_i = \Omega_1 + \omega_i$ and if $E_{jk}$ is the (j,k) element of $\underline{\underline{E}}$ and $C_j$ is the jth element of $\underline{C} = \underline{\underline{E}}^{-1}\underline{x}_0$,

$$A_{ij} = E_{j,2i-i}\, C_{2i-1} + E_{j,2i}\, C_{21} \tag{A-15a}$$

and

$$B_{ij} = E_{j,2i-1}\, C_{21} - E_{j,2i}\, C_{2i-1} \,. \tag{A-15b}$$

Equation (A-14) can be integrated. The result is

$$\begin{bmatrix} \Theta \\ \Psi \end{bmatrix} = \frac{1}{2} \sum_{i=1}^{3} \frac{e^{n_i \tau}}{n_i^2+p_i^2} \underline{\underline{P}}(\tau) \begin{bmatrix} A_{i1}-B_{i2} \\ A_{i2}+B_{i1} \end{bmatrix} + \begin{bmatrix} \Theta_0 \\ \Psi_0 \end{bmatrix}$$

$$+ \frac{1}{2} \sum_{i=1}^{3} \frac{e^{n_i \tau}}{n_i^2+q_i^2} \underline{\underline{Q}}(\tau) \begin{bmatrix} A_{i1}+B_{i2} \\ A_{i2}-B_{i1} \end{bmatrix} + \begin{bmatrix} \sin\Phi & (\cos\Phi-1) \\ (1-\cos\Phi) & \sin\Phi \end{bmatrix} \begin{bmatrix} x_{1p}/\Omega_1 \\ x_{2p}/\Omega_1 \end{bmatrix}, \tag{A-16}$$

where

$$\underline{\underline{P}}(\tau) = \begin{bmatrix} n_i(cp_i\tau - 1) + p_i sp_i\tau & -[n_i sp_i\tau - p_i\,(cp_i\tau-1)] \\ n_i\, sp_i\tau - p_i(cp_i\tau-1) & n_i(cp_i\tau - 1) + p_i sp_i\tau \end{bmatrix} \tag{A-17}$$

and $\underline{\underline{Q}}(\tau)$ has the same form as $\underline{\underline{P}}(\tau)$, but in $\underline{\underline{Q}}(\tau)$ the $q_i$ take the place of $p_i$.

The pitch and yaw angles of the rocket's nose, $\Theta_N$ and $\Psi_N$, respectively, are given, in the linear approximation, by

$$\begin{bmatrix} \Theta_N \\ \Psi_N \end{bmatrix} = \begin{bmatrix} \Theta \\ \Psi \end{bmatrix} + \begin{bmatrix} \cos\Phi & -\sin\Phi \\ \sin\Phi & \cos\Phi \end{bmatrix} \begin{bmatrix} \theta_2 \\ \theta_3 \end{bmatrix}. \tag{A-18}$$

Initial Conditions

The initial conditions on the $x_j$, $j=1,2,\ldots,6$, and/or $\Theta$ and $\Psi$ are obtained by assuming that the rocket is, at EOG, supported at two points P and Q which do not move transversely. This constraint and the assumption of small angles lead to the following initial conditions:

$$x_{10} = -[(\ell_2+r_2)/(\ell_1+r_1)]\dot{\Theta}_{NO} \quad , \tag{A-19a}$$

$$x_{20} = -[(\ell_2+r_2)/(\ell_1+r_1)]\dot{\Psi}_{NO} \quad , \tag{A-19b}$$

$$x_{30} = [(d/(\ell_1+r_1)][\dot{\Theta}_{NO} + \Omega_1\Psi_{NO}] \quad , \tag{A-19c}$$

$$x_{40} = [(d/(\ell_1+r_1)][\dot{\Psi}_{NO} - \Omega_1\Theta_{NO}] \quad , \tag{A-19d}$$

$$x_{50} = [d/(\ell_1+r_1)]\Theta_{NO} \quad , \tag{A-19e}$$

$$x_{60} = [d/(\ell_1+r_1)]\Psi_{NO} \quad , \tag{A-19f}$$

$$\Theta_0 = -[(\ell_2+r_2)/d]\ x_{50} \tag{A-19g}$$

and

$$\Psi_0 = -[(\ell_2+r_2)/d]\ x_{60} \quad , \tag{A-19h}$$

where $d = \ell_1 + r_1 + \ell_2 + r_2$.

## APPENDIX B

## ASSUMED-MODES MATHEMATICAL MODEL

### Introduction

The mathematical model, developed on the basis of the "continuous" physical model and referred to as the "assumed-mode" model because of the use of assumed mode shapes to model the rocket bending, is given here for the sake of completeness. For additional details, the reader is referred to Refs. 2 and 3.

Actually, two mathematical models of a flexible rocket, one for on-launcher motion and a second for off-launcher motion, are needed. For this reason, two sets of equations of motion as well as the transformation relating the two are given here.

### Equations for On-Launcher Motion

When the rocket is on the launcher, i.e., during the detent and guidance phases, pinned-pinned-free mode shapes, $\psi_j(x)$, j=1,2,3, are used to approximate its bent shape by assuming that the y- and z-displacements (rotating with the rocket) of the rocket centerline are

$$y = \eta + y_0(x) \tag{B-1a}$$

and

$$z = \zeta + z_0(x), \tag{B-1b}$$

where

$$\eta = \sum_{j=1}^{3} p_j(t)\, \psi_j(x) \quad \text{and} \quad \zeta = \sum_{j=1}^{3} q_j(t)\, \psi_j(x)$$

are the parts of y and z, respectively, due to bending of the rocket and $y_0(x)$ and $z_0(x)$ are functions which define its original non-straight

shape if necessary. The $p_j$ and $q_j$ are generalized coordinates which are six of the sixteen (16) state variables which are used to model the rocket's motion.

The equations governing axial rotation are

$$\dot{\Omega}_1 = T_s/I_A \tag{B-2a}$$

and

$$\dot{\Phi} = \Omega_x, \tag{B-2b}$$

where $T_s$ is the spin torque and $I_A$ is the axial moments of inertia of the unbent rocket. Here, $\Omega_x$ is the x-component of the angular velocity of the rocket and $\Phi$ is the rocket roll angle.

Simple equations are also used to model the translational dynamics of the point P (on the centerline of the rocket at its aft end). These are

$$\dot{x}_P = u_P \tag{B-3a}$$

and

$$\dot{u}_P = F_T/M - g \sin \Theta_L, \tag{B-3b}$$

where $F_T$ is the thrust magnitude and $\Theta_L$ is the fixed launcher elevation.

The equations for the $p_j$ and $q_j$ are obtained as explained in Refs. 1 and 2. The results are

$$\underline{\underline{M}}\,(\ddot{\underline{p}} - 2\Omega_x\dot{\underline{q}} - \dot{\Omega}_x\underline{q} - \Omega_x^2\underline{p}) + (\underline{\underline{K}} - F_T\underline{\underline{\Gamma}})\underline{p} - (g \sin \Phi)\underline{m} + F_T\underline{c} - \dot{\Omega}_x\underline{b} - \Omega_x^2\underline{a}$$

$$+ \underline{\underline{D}}\dot{\underline{p}} = \underline{0} \tag{B-4a}$$

and

$$\underline{\underline{M}}(\ddot{\underline{q}} + 2\Omega_x\dot{\underline{p}} + \dot{\Omega}_x\underline{p} - \Omega_x^2\underline{q}) + (\underline{\underline{K}} - F_T\underline{\underline{\Gamma}})\underline{q}$$

$$-(g \cos \Phi)\underline{m} + F_T\underline{d} + \dot{\Omega}_x\underline{a} - \Omega_x^2\underline{b} + \underline{\underline{D}}\dot{\underline{q}} = \underline{0} \tag{B-4b}$$

where $\underline{p} = (p_1\ p_2\ p_3)^T$ and $\underline{q} = (q_1\ q_2\ q_3)^T$. Here also, $\underline{\underline{M}}$ is (currently) a 3x3 matrix with elements

$$m_{ij} = \int_0^L \bar{\sigma}\psi_i\psi_j \, dx \tag{B-5a}$$

where $\bar{\sigma}$ is the mass per unit length of the rocket; $\underline{\underline{K}}$ is a 3x3 matrix with elements

$$K_{ij} = \int_0^L \psi_i(E\ I\ \psi_j'')'' \, dx \ , \tag{B-5b}$$

where $(\ )' = d(\ )/dx$ and EI is the bending stiffness of the rocket at station x; $\underline{\underline{\Gamma}}$ is a 3x3 matrix with elements

$$\gamma_{ij} = \int_0^L \psi_i' \, \psi_j' \quad f(x) \, dx \ , \tag{B-5c}$$

where f(x) is the internal force per unit length; $\underline{m}$ is a 3x1 matrix with elements

$$m_i = \int_0^L \bar{\sigma} \, \psi_i \, dx \ . \tag{B-5d}$$

Furthermore, the matrices $\underline{a}$, $\underline{b}$, $\underline{c}$ and $\underline{d}$ are 3x1 matrices with elements,

$$a_i = \int_0^L \bar{\sigma} \, \psi_i \, y_0 \, dx \ , \tag{B-6a}$$

$$b_i = \int_0^L \bar{\sigma} \, \psi_i \, z_0 \, dx \ , \tag{B-6b}$$

$$c_i = \int_0^L \bar{\sigma} \, \psi_i' \, y_0' \, dx \tag{B-6c}$$

and

$$d_i = \int_0^L \bar{\sigma} \, \psi_i' \, z_0' \, dx \ , \tag{B-6d}$$

respectively. Also, g is the gravitational acceleration magnitude.

The angular rotation of the nose of the rocket is defined by the angles $\Theta_N$ and $\Psi_N$ as in the case of the two-body model. However, for the continuous model these angles are determined by using

$$\Theta_N = \Theta_L + \theta_{2N} \cos \Phi - \theta_{3N} \sin \Phi \tag{B-7a}$$

and

$$\Psi_N = \theta_{2N} \sin \Phi + \theta_{3N} \cos \Phi \, , \tag{B-7b}$$

where

$$\theta_{2N} = -\sum_{i=1}^{3} q_i \, \psi_i'(L) - z_0'(L) \tag{B-8a}$$

and

$$\theta_{3N} = \sum_{i=1}^{3} p_i \, \psi_i'(L) + y_0'(L) \, . \tag{B-8b}$$

Equations for Off-Launcher Motion

The motion of the rocket after end of guidance is modeled by using mode shapes for a free-free uniform beam and using instantaneous principal axes of the deformed rocket in writing the equations for rotational motion. The use of instantaneous principal axes simplifies the equation of rotational motion so that it is simply

$$\underline{\underline{I}}_C \, \dot{\underline{\omega}} + \tilde{\underline{\omega}} \, \underline{\underline{I}}_C \, \underline{\omega} = \underline{T} \, , \tag{B-9}$$

where $\underline{\underline{I}}_C$ is the principal centroidal inertia matrix, $\underline{\omega} = (\omega_1 \; \omega_2 \; \omega_3)^T$ is the matrix of $u_1$-, $u_2$- and $u_3$-components of the angular velocity of the principal $(Cu_1u_2u_3)$ system,

$$\tilde{\underline{\omega}} = \begin{bmatrix} 0 & -\omega_3 & \omega_2 \\ \omega_3 & 0 & -\omega_1 \\ -\omega_2 & \omega_1 & 0 \end{bmatrix} \tag{B-10}$$

and

$$\underline{T} = \{T_s \quad F_T x_C \, [u_3'(0,t) + u_3(x_M,t)/x_C - \alpha_y]$$

$$- F_T \, x_C \, [u_2'(0,t) + u_2(x_M,t)/x_C + \alpha_z]\}^T \, . \tag{B-11}$$

In Eq. (B-11), $x_C$ is the distance from point P to the center of mass of the rocket, $x_M$ is the distance from P to the head end of the rocket motor, $u_2'(0,t)$ and $u_3'(0,t)$ are the slope of the bent (and bending) centerline of the rocket at P and $\alpha_y$ and $\alpha_z$ are constant mechanical thrust misalignment angles.

The translational motion of the rocket is governed by the equation,

$$\dot{\underline{V}} = - \tilde{\underline{\omega}}\, \underline{V} + \underline{F}_T/M + \underline{g} \ , \tag{B-12}$$

where $\underline{V}$ is the 3x1 matrix of $u_1$- , $u_2$- and $u_3$-components of the velocity of the center of mass C, g is a 3x1 matrix of similar components of the acceleration of gravity and

$$\underline{F}_T = F_T[\ 1 \quad u_3'(0,t)+\alpha_z \quad u_2'(0,t) - \alpha_y\ ]^T. \tag{B-13}$$

In addition to Eqs. (B-9) and (B-12), the following kinematic equations are needed to complete the gross motion equations:

Rotation

$$\dot{\phi} = \omega_1 + (\omega_2 \sin \phi + \omega_3 \cos \phi) \tan \theta \tag{B-14a}$$

$$\dot{\theta} = \omega_2 \cos \phi - \omega_3 \sin \phi \tag{B-14b}$$

$$\dot{\psi} = (\omega_2 \sin \phi + \omega_3 \cos \phi)/\cos \theta \tag{B-14c}$$

Translation

$$\begin{bmatrix} \dot{X}_C \\ \dot{Y}_C \\ \dot{Z}_C \end{bmatrix} = \begin{bmatrix} c\psi & -s\psi & 0 \\ s\psi & c\psi & 0 \\ 0 & 0 & 1 \end{bmatrix} \begin{bmatrix} c\theta & 0 & s\theta \\ 0 & 1 & 0 \\ -s\theta & 0 & c\theta \end{bmatrix} \begin{bmatrix} 1 & 0 & 0 \\ 0 & c\phi & -s\phi \\ 0 & s\phi & c\phi \end{bmatrix} \begin{bmatrix} u \\ v \\ w \end{bmatrix} . \tag{B-15}$$

As in the case of on-launcher motion, it is assumed that the rocket may be non-straight before any bending occurs. Hence, the functions $u_2(x,t)$ and $u_3(x,t)$ are expressed as follows:

$$u_2(x,t) = u_{20}(x) + \sum_{j=1}^{3} P_j(t)\phi_j(x) \tag{B-16a}$$

and

$$u_3(x,t) = u_{30}(x) + \sum_{j=1}^{3} Q_j(t)\phi_j(x), \tag{B-16b}$$

where $u_{20}(x)$ and $u_{30}(x)$ are the counterparts of $y_0(x)$ and $z_0(x)$ and the $P_j$ and $Q_j$ are <u>new</u> generalized coordinates, i.e., they are <u>not necessarily</u> such that $P_1 = p_1$, etc.

The ways in which the $P_j$ and $Q_j$ change with time are determined by solving the equations,

$$\begin{aligned} \underline{\underline{M}}_f \, (\ddot{\underline{P}} - 2\omega_1 \dot{\underline{Q}} - \dot{\omega}_1 \underline{Q} - \omega_1{}^2 \underline{P}) + (\underline{\underline{K}}_f - F_T \underline{\underline{\Gamma}})\underline{P} + \underline{\underline{D}}\dot{\underline{P}} \\ + (\dot{\omega}_3 + \omega_1\omega_2)\underline{\ell}_f - \dot{\omega}_1 \underline{b}_f - \omega_1^2 \, \underline{a}_f + F_T \underline{c}_f \\ - F_T \, [u_2'(0,t) + \alpha_z] \, \underline{\phi}(0) + (F_T/M)_2 \, \underline{m}_f = \underline{0} \end{aligned} \tag{B-17a}$$

and

$$\begin{aligned} \underline{\underline{M}}_f \, (\ddot{\underline{Q}} + 2\omega_1 \dot{\underline{P}} + \dot{\omega}_1 \underline{P} - \omega_1{}^2 \underline{Q}) + (\underline{\underline{K}}_f - F_T \underline{\underline{\Gamma}}_f)\underline{Q} + \underline{\underline{D}}\dot{\underline{Q}} \\ + (\omega_3 \, \omega_1 - \dot{\omega}_2)\underline{\ell}_f + \dot{\omega}_1 \, \underline{a}_f - \omega_1{}^2 \underline{b}_f + F_T \, \underline{d}_f \\ + F_T[u_3'(0,t) + \alpha_y] + (F_T/M)_3 \, \underline{m}_f = \underline{0}, \end{aligned} \tag{B-17b}$$

where a subscript f is used to denote "free-flight."

The matrices appearing in Eqs. (B-17) are defined as follows:

$\underline{P}$ and $\underline{Q}$ are 3x1, i.e.,

$$\underline{P} = (P_1 \; P_2 \; P_3)^T \tag{B-18a}$$

and

$$\underline{Q} = (Q_1 \; Q_2 \; Q_3)^T \tag{B-18b}$$

$\underline{\underline{M}}_f$ is 3x3, with elements,

$$m_{ij_f} = \int_0^L \bar{\sigma}\, \phi_i\, \phi_j \, dx \,, \tag{B-18c}$$

$\underline{\underline{K}}_f$ is 3x3, with elements,

$$K_{ij_f} = \int_0^L \phi_i \, [E\, I\, \phi_j'']'' \, dx, \tag{B-18d}$$

$\underline{\underline{\Gamma}}_f$ is 3x3, with elements,

$$\gamma_{ij_f} = \int_0^L \phi_i' \phi_j' f(x) \, dx \,, \tag{B-18e}$$

$\underline{a}_f$, $\underline{b}_f$, $\underline{c}_f$, $\underline{d}_f$, $\underline{\ell}_f$ and $\underline{m}_f$ are 3x1, with elements,

$$a_{i_f} = \int_0^L \bar{\sigma}\, \phi_i\, u_{20} \, dx \,, \tag{B-19a}$$

$$b_{i_f} = \int_0^L \bar{\sigma}\, \phi_i\, u_{30} \, dx \,, \tag{B-19b}$$

$$c_{i_f} = \int_0^L \bar{\sigma}\, \phi_i\, u_{20}' \, dx \,, \tag{B-19c}$$

$$d_{i_f} = \int_0^L \bar{\sigma}\, \phi_i\, u_{30}' \, dx \,, \tag{B-19d}$$

$$\ell_{i_f} = \int_0^L \bar{\sigma}\, \phi_i (x - x_c) \, dx \tag{B-19e}$$

and

$$m_{i_f} = \int_0^L \bar{\sigma}\, \phi_i \, dx \,, \tag{B-19f}$$

respectively.

Also in Eqs.(B-17),

$$(F_T/M)_2 = (F_T/M)[u_2(0,t) + \alpha_z] \tag{B-20a}$$

and

$$(F_T/M)_3 = (F_T/M)[u_3(0,t) - \alpha_y] \ . \tag{B-20b}$$

Transformation Required at End of Guidance

Since two sets of equations of motion are used, one for the guidance phase and one for the free-flight phase, it is necessary that the solutions to these equations be matched at the EOG. Hence, we require that the positions and velocities of points P and Q and of the center of mass be continuous at $t_{EOG}$, the time of EOG. Since three mode shapes are used during each phase, we can also require that the angular orientation and angular velocity of the nose of the rocket be continuous at $t_{EOG}$.

To enforce the desired continuity of state, we must first determine the orientation and angular velocity of the centroidal principal axes of the rocket, because the bending during free-flight is referenced to those axes. The centroidal principal axes are oriented with respect to the Pxyz system by using the angles $\mu_2$ and $\mu_3$ which are defined as follows:

$$\mu_2 = -[\int_0^L \bar{\sigma}(z_0+\zeta-z_C)(x-x_C)dx]/I_T \tag{B-21a}$$

and

$$\mu_3 = [\int_0^L \bar{\sigma}(y_0+\eta-y_C)(x-x_C)dx]/I_T \ , \tag{B-21b}$$

where $x_C = [\int_0^L \bar{\sigma}x dx]/M$, $y_C = [\int_0^L \bar{\sigma}(y_0+\eta)dx]/M$ and $z_C = [\int_0^L \bar{\sigma}(z_0+\zeta)dx]/M$.

The orientation of the $Cu_1u_2u_3$ system in space is defined by the angles $\psi$, $\theta$ and $\phi$(3-2-1 sequence). At EOG, these angles can be expressed in terms of $\Phi$ (the roll angle of the Pxyz system) $\mu_2$ and $\mu_3$ by equating

elements of equivalent direction cosine matrices. The required expressions are

$$\psi = \tan^{-1} \{(\mu_3 c\Phi + \mu_2 s\Phi)/[c\theta_L + (\mu_3 s - \mu_2 c\Phi)s\theta_L]\}, \tag{B-22a}$$

$$\theta = \sin^{-1}[s\theta_L + (\mu_2 c\Phi - \mu_3 s\Phi)c\theta_L] \tag{B-22b}$$

and

$$\phi = \tan^{-1} \{(-\mu_3 s\theta_L + s\Phi c\theta_L)/(-\mu_2 s\theta_L + c\Phi c\theta_L)\}. \tag{B-22c}$$

Since the angular velocity of the $cu_1u_2u_3$ system is that of the Pxyz system plus the angular velocity of the $cu_1u_2u_3$ system relative to the Pxyz system,

$$\underline{\omega} \simeq [\ \Omega_x \quad \dot{\mu}_2 - \mu_3\Omega_x \quad \dot{\mu}_3 + \mu_2\Omega_x\ ]^T . \tag{B-23}$$

The position and velocity of the center of mass C are obtained by using the definitions of $x_C$, $y_C$ and $z_C$ given above. The space-fixed coordinates $X_C$, $Y_C$ and $Z_C$ of C while the rocket is guided are found from the equation,

$$\begin{bmatrix} X_C \\ Y_C \\ Z_C \end{bmatrix} = \begin{bmatrix} c\Theta_L & 0 & s\Theta_L \\ 0 & 1 & 0 \\ -s\Theta_L & 0 & c\Theta_L \end{bmatrix} \begin{bmatrix} 1 & 0 & 0 \\ 0 & c\Phi & -s\Phi \\ 0 & s\Phi & c\Phi \end{bmatrix} \begin{bmatrix} x_C + X_P \\ Y_C \\ Z_C \end{bmatrix} . \tag{B-24}$$

Furthermore the $u_j$-components of the velocity of C are, during guidance,

$$u = \dot{X}_P , \tag{B-25a}$$

$$v = -\mu_3 u + \dot{y}_C - \Omega_x z_C \tag{B-25b}$$

and

$$w = \mu_2 u + \dot{z}_C + \Omega_x y_C . \tag{B-25c}$$

Because only a limited number of mode shapes are used, the position and velocity of each particle of the rocket cannot be forced to be

continuous at EOG. However, if three mode shapes are used, the position and velocities of three points on the rocket's centerline can be made continuous at EOG. Alternatively, the positions and velocities of <u>two</u> points on the rocket's centerline and the slope and time rate of change of slope of a third point can be made continuous at EOG. The latter approach is taken because it is desired that the pitch and yaw angles of the nose of the rocket and their time rates of change be continuous at EOG. Also, to model the effects of the constraints during guidance, the positions of points P and Q are forced to be continuous at EOG.

If we let $x_Q$ be the position of the forward support and define the matrices

$$\underline{\underline{\Phi}} = \begin{bmatrix} \phi_1(0) & \phi_2(0) & \phi_3(0) \\ \phi_1(x_Q) & \phi_2(x_Q) & \phi_3(x_Q) \\ \phi_1'(L) & \phi_2'(L) & \phi_3'(L) \end{bmatrix}, \tag{B-26a}$$

$$\underline{b}_y = \begin{bmatrix} -\mu_3 x_c \\ (x_Q - x_C)\mu_3 - y_c \\ \mu_3 + \eta'(L,t) + y_0'(L) \end{bmatrix}_{t=t_{EOG}}, \tag{B-26b}$$

$$\underline{b}_z = \begin{bmatrix} \mu_2 x_C \\ -\mu_2 (x_Q - x_C) - z_C \\ -\mu_2 + \zeta'(L,t) + z_0'(L) \end{bmatrix}_{t=t_{EOG}}, \tag{B-26c}$$

$$\dot{\underline{b}}_y = \begin{bmatrix} -\dot{\mu}_3 x_C \\ (x_Q - x_C)\dot{\mu}_3 - \dot{y}_C \\ \dot{\mu}_3 + \dot{\eta}'(L,t) \end{bmatrix}_{t=t_{EOG}} \tag{B-26d}$$

and

$$\dot{\underline{b}}_z = \begin{bmatrix} \dot{\mu}_2 \\ -\dot{\mu}_2(x_Q - x_C) - \dot{z}_C \\ -\dot{\mu}_2 + \dot{\zeta}'(L,t) \end{bmatrix}_{t=t_{EOG}} , \tag{B-26e}$$

then,

$$\underline{P}(t_{EOG}) = \underline{\underline{\Phi}}^{-1} \underline{b}_y , \tag{B-27a}$$

$$\underline{Q}(t_{EOG}) = \underline{\underline{\Phi}}^{-1} \underline{b}_z , \tag{B-27b}$$

$$\dot{\underline{P}}(t_{EOG}) = \underline{\underline{\Phi}}^{-1} \dot{\underline{b}}_y \tag{B-27c}$$

and

$$\dot{\underline{Q}}(t_{EOG}) = \underline{\underline{\Phi}}^{-1} \dot{\underline{b}}_z . \tag{B-27d}$$

The above "initial" conditions (those at EOG) on $X_C$, $Y_C$, $Z_C$, u, v, w, $\psi$, $\theta$, $\phi$, $\underline{\omega}$, $\underline{P}$ and $\underline{Q}$ can be used to continue the solution of the equations of motion during the free-flight phase.

# APPENDIX C

# PRINCIPAL AXES ROTATIONS DUE TO TRANSVERSE VIBRATION

## Introduction

Due to slenderness of most free-flight rockets, there is generally little coupling of their transverse vibrational and rotational motions subsequent to end-of-guidance (EOG) if aerodynamic forces are not significant. Hence, as explained in the body of this report, the free-flight motion of a slender free-flight rocket which is caused by bending vibrations prior to EOG is essentially composed of a uniform, transverse rotational motion of the rocket about its centroidal principal axes, a vibrational motion with respect to those axes, and a translation of the rocket's center of mass. In this appendix, we present an approximate method for determining the transverse angular velocity of the rocket's principal axes at EOG and, hence, the transverse rate due to transverse vibration. The two-body model described in Ref. 2 and herein (see Section 2 and Appendix A) is used.

## Principal Axes of the Two-Body Model

The orientation of the centroidal principal (see Fig. C-1) reference frame Cx'y'z' relative to the Cxyz reference frame (which is parallel to the Body 1-fixed $C_1x_1y_1z_1$ reference frame) can be defined in terms of the inertia characteristics of the bodies and the angles $\theta_2$ and $\theta_3$.

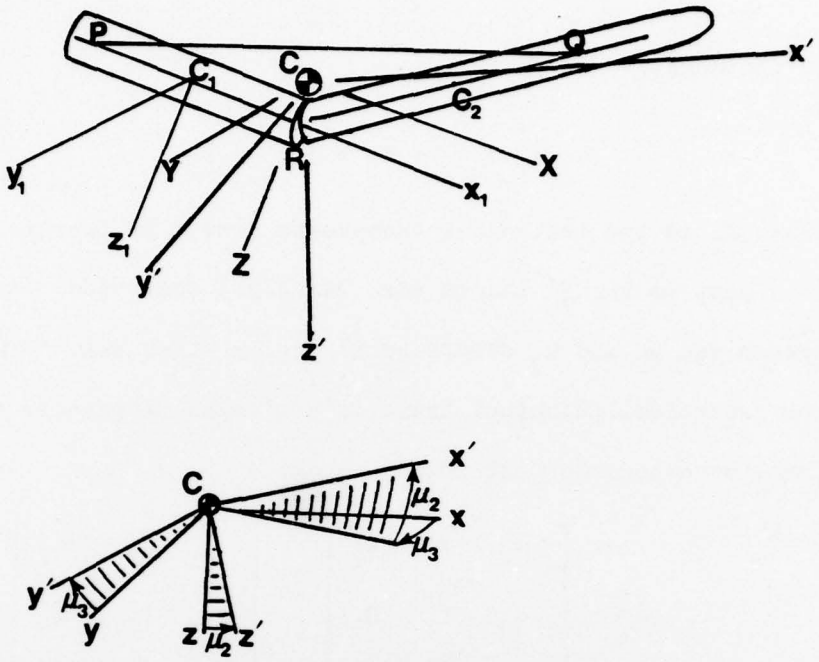


Fig. C-1. Principal axes of the two-body model.

The inertia matrix of the system of two bodies using the Cxyz frame as the reference is, through first order in $\theta_2$ and $\theta_3$,

$$\underline{\underline{I}} = \begin{bmatrix} I_A & -\theta_3 J & \theta_2 J \\ -\theta_3 J & I_T & 0 \\ \theta_2 J & 0 & I_T \end{bmatrix} , \qquad \text{(C-1)}$$

where

$$I_A = A_1 + B_1 , \qquad \text{(C-2)}$$

the sum of the axial moments of inertia of Bodies 1 and 2, and

$$J = B_2 - B_1 + \sigma\, r_2(\ell_1 + r_2) . \qquad \text{(C-3)}$$

In Eq. (C-3), $B_2$ is the centroidal transverse moment of inertia of Body 2, $\sigma = m_1 m_2/(m_1+m_2)$ where $m_j$ is the mass of Body j, $r_2 = |\underline{r}_2|$ and $\ell_1 = |\underline{\ell}_1|$.

Furthermore,

$$I_T = A_2 + B_2 + \sigma(\ell_1+r_2)^2, \tag{C-4}$$

where $A_2$ is the centroidal transverse moment of inertia of Body 1.

Now, we let $\underline{\underline{I}}'$ denote the principal centroidal inertia matrix of the system and $\mu_2$ and $\mu_3$ denote small angles which define the orientation of the centroidal principal frame Cx'y'z' with respect to the Cxyz frame. Then, by using the fact that

$$\underline{\underline{I}} \simeq \begin{bmatrix} 1 & -\mu_3 & \mu_2 \\ \mu_3 & 1 & 0 \\ -\mu_2 & 0 & 1 \end{bmatrix} \underline{\underline{I}}' \begin{bmatrix} 1 & \mu_3 & -\mu_2 \\ -\mu_3 & 1 & 0 \\ \mu_2 & 0 & 1 \end{bmatrix},$$

we get, through first order in $\mu_2$ and $\mu_3$,

$$\mu_2 = [J/(I_T-I_A)]\theta_2 \tag{C-5a}$$

and

$$\mu_3 = [J/(I_T-I_A)]\theta_3 . \tag{C-5b}$$

Angular Velocity of the Principal Frame

The angular velocity of the principal frame Cx'y'z', as resolved in terms of components in that frame, is

$$\underline{\omega}' = \begin{bmatrix} 1 & \mu_3 & -\mu_2 \\ -\mu_3 & 1 & 0 \\ \mu_2 & 0 & 1 \end{bmatrix} \begin{bmatrix} \Omega_1 \\ \Omega_2 \\ \Omega_3 \end{bmatrix} + \begin{bmatrix} 0 \\ \dot{\mu}_2 \\ \dot{\mu}_3 \end{bmatrix}, \tag{C-6}$$

where $\Omega_1$, $\Omega_2$ and $\Omega_3$ are the x-, y- and z-components, respectively, of the angular velocity of the Cxyz reference frame. By neglecting terms which are second order in $\mu_2$, $\mu_3$, $\dot{\mu}_2$ and $\dot{\mu}_3$, we get the following expressions for the components of $\underline{\omega}'$:

$$\omega_1' = \Omega_1 \ , \tag{C-7a}$$

$$\omega_2' = \Omega_2 - \mu_3\Omega_1 + \dot{\mu}_2 \tag{C-7b}$$

and

$$\omega_3' = \Omega_3 + \mu_2\Omega_1 + \dot{\mu}_3 \ . \tag{C-7c}$$

Equations (7) may be used at any time, provided the assumptions of small angles and angular rates made above are valid. We are, however, most interested in the angular velocity of the principal axes reference frame at the time of EOG, since if there is no thrust misalignment and negligible aerodynamic torque, the angular rates in pitch and yaw present at EOG will persist during free-flight.

If the constraints adopted are such that points P and Q (see Fig. A1) can only translate along a fixed straight line during the guidance phase, then at the EOG when $t=t_{EOG}$ (and letting a subscript 0 denote the value of a variable at that time)

$$\Omega_{20} = -(k_1/k_2)\dot{\Theta}_{NO} \ , \tag{C-8a}$$

$$\Omega_{30} = -(k_1/k_2)\dot{\Psi}_{NO} \ , \tag{C-8b}$$

$$\dot{\theta}_{20} = \omega_{20} = k_1(\Omega_1\Psi_{NO} + \dot{\Theta}_{NO}) \ , \tag{C-8c}$$

$$\dot{\theta}_{30} = \omega_{30} = k_1(-\Omega_1\Theta_{NO} + \dot{\Psi}_{NO}) \ , \tag{C-8d}$$

$$\Theta_0 = -(k_1/k_2)\Theta_{NO} \ , \tag{C-8e}$$

$$\Psi_0 = -(k_1/k_2)\Psi_{NO} \ , \tag{C-8f}$$

$$\theta_{20} = k_1\,\Theta_{NO} \tag{C-8g}$$

and

$$\theta_{30} = k_1\,\Psi_{NO} \tag{C-8h}$$

In Eqs. (8),

$$k_1 = d/d_1 \tag{C-9a}$$

and

$$k_2 = d/d_2, \tag{C-9b}$$

where

$$d = d_1 + d_2 , \tag{C-10a}$$

$$d_1 = \ell_1 + r_1 \tag{C-10b}$$

and

$$d_2 = \ell_2 + r_2 .^{\dagger} \tag{C-10c}$$

From Eqs. (C-5) and Eqs. (C-8) we find that at EOG, the values of $\mu_2$ and $\mu_3$ are

$$\mu_{20} = \delta\, k_1\, \Theta_{NO} \tag{C-11a}$$

and

$$\mu_{30} = \delta\, k_1\, \Psi_{NO}, \tag{C-11b}$$

respectively, where

$$\delta = J/(I_T - I_A) , \tag{C-12}$$

and the values of $\dot{\mu}_2$ and $\dot{\mu}_3$ are

$$\dot{\mu}_{20} = \delta\, k_1 (\Omega_1\, \Psi_{NO} + \dot{\Theta}_{NO}) \tag{C-13a}$$

and

$$\dot{\mu}_{30} = \delta\, k_1 (-\Omega_1\, \Theta_{NO} + \dot{\Psi}_{NO}) , \tag{C-13b}$$

respectively. By using Eqs. (C-11) and (C-13) in Eqs. (C-7), we get the following expressions for the values of $\omega_2'$ and $\omega_3'$ at EOG:

$$\omega_{20}' = (\delta k_1 - k_1/k_2)\dot{\Theta}_{NO} \tag{C-14a}$$

$$\omega_{30}' = (\delta k_1 - k_1/k_2)\dot{\Psi}_{NO} \tag{C-14b}$$

---

$^{\dagger}$Note: Here, $\ell_2$ is such that $\underline{\ell}_2 = \ell_2\, \hat{i}_2$; i.e., it is the $x_2$-component of the vector from $C_2$ to Q. Hence, it may be negative.

The transverse angular rate due to transverse vibrations is therefore

$$\omega_t = (\delta k_1 - k_1/k_2)\sqrt{\dot{\Theta}_{NO}^2 + \dot{\Psi}_{NO}^2}\,. \qquad \text{(C-15)}$$

Also, the aim change due to transverse vibration is

$$\Theta_t = \delta k_1 \sqrt{\Theta_{NO}^2 + \Psi_{NO}^2}\,. \qquad \text{(C-16)}$$

# APPENDIX D

# TWO-BODY MATHEMATICAL MODEL WITH FLEXIBLE SUPPORTS

## Introduction

Since the structure which supports a rocket until end of guidance (EOG) is in reality not rigid, the issue of whether the flexibility of this structure contributes to the bending of the supported rocket needs to be addressed. Furthermore, the effects of frictional forces, which necessarily act on the rocket at its points of support, must be considered as a possible mechanism for causing transverse vibration of the rocket. To this end, the two-body model presented in Appendix A was extended to include the effects of support flexibility and friction.

## Extended Model

The physical model is depicted in Fig. D-1. It is identical with that used in deriving the equations given in Appendix A, except the rocket is supported in such a manner that forces are exerted on it through small "shoes." The shoes in the present model are not constrained to move on rails, but are assumed to slide on the interior of a "smooth" tube. Although the tube is smooth, it is not perfectly so; hence, frictional forces are assumed present at the rocket/tube interface.

## Equations of Motion

Because the points P and Q can move transversely as well as longitudinally, a general equation for motion of the mass centers of the two-body

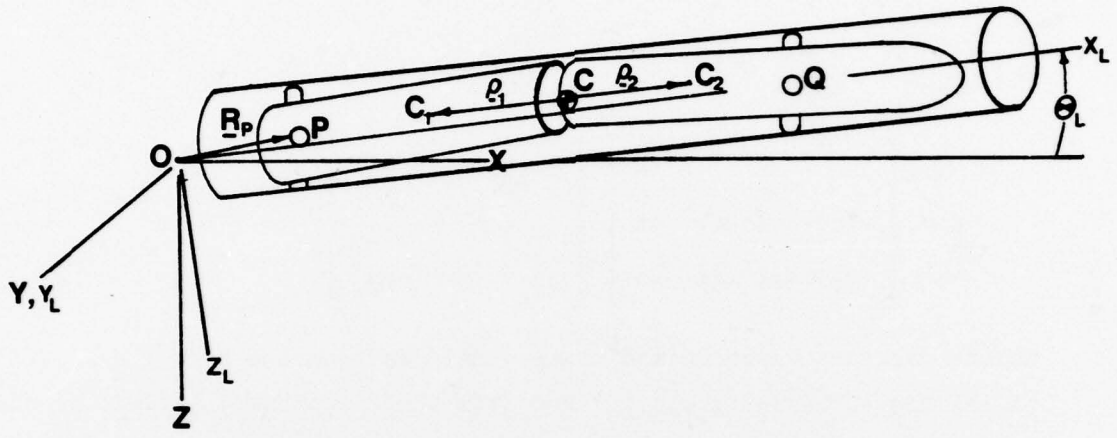


Fig. D.1. Two-body model in flexible tube.

system is required. The center of mass C is located by the vector,

$$\underline{R}_C = \underline{R}_P = \mu(\underline{\ell}_1+\underline{r}_2) + \underline{r}_1, \tag{D-1}$$

where $\mu = m_2/(m_1+m_2)$ and $m_j$ is the mass of Body j. Here (as in Appendix A), the aft body is Body 1. The acceleration of C is

$$\ddot{\underline{R}}_C = \ddot{\underline{R}}_P + \mu\left[ \frac{{}^1d\underline{\Omega}}{dt} \times (\underline{\ell}_1+\underline{r}_1) + \underline{\Omega}\times[\underline{\Omega}\times(\underline{\ell}_1+\underline{r}_1)]\right] + \mu\left[\frac{{}^2d\underline{\omega}}{dt} \times \underline{r}_2 + \underline{\omega}\times(\underline{\omega}\times\underline{r}_2)\right] \tag{D-2}$$

where $\underline{\Omega}$ is the angular velocity of Body 1, $\underline{\omega}$ is the angular velocity of Body 2 and ${}^jd(\ )/dt$ denotes the derivative with respect to time of ( ), treating the unit vectors associated with $C_j x_j y_j z_j$ as non-rotating.

If we let

$$\underline{\underline{A}} = \begin{bmatrix} 1 & \theta_3 & -\theta_2 \\ -\theta_3 & 1 & 0 \\ \theta_2 & 0 & 1 \end{bmatrix} \tag{D-3}$$

and

$$\underline{\underline{C}} = \begin{bmatrix} 1 & \Psi & -\Theta \\ -\Psi c\Phi+\Theta s\Phi & c\Phi & s\Phi \\ \Psi s\Phi+\Theta c\Phi & -s\Phi & c\Phi \end{bmatrix} \begin{bmatrix} c\Theta_L & 0 & -s\Theta_L \\ 0 & 1 & 0 \\ s\Theta_L & 0 & c\Theta_L \end{bmatrix} \tag{D-4}$$

denote matrices which define transformations from the Body-1 basis $(\hat{\underline{i}}_1, \hat{\underline{j}}_1, \hat{\underline{k}}_1)$ to the Body-2 basis $(\hat{\underline{i}}_2, \hat{\underline{j}}_2, \hat{\underline{k}}_2)$ and from the fixed basis $(\hat{\underline{I}}, \hat{\underline{J}}, \hat{\underline{K}})$ to the launcher basis $(\hat{\underline{i}}_L, \hat{\underline{j}}_L, \hat{\underline{k}}_L)$, respectively, then Eq. (D-2) can be replaced by the matrix equation (launcher basis),

$$\ddot{\underline{R}}_{P_L} = -\underline{\underline{C}}^T \mu[\tilde{\underline{\Omega}}\tilde{\underline{\Omega}}\underline{\ell}_1 + \underline{\underline{A}}^T\tilde{\underline{\omega}}\tilde{\underline{\omega}}\,\underline{r}_2 + \underline{\underline{A}}^T\tilde{\underline{r}}_2\underline{\omega}_{2/1}\,\underline{\underline{A}}\,\underline{\Omega} - (\tilde{\underline{\ell}}_1+\underline{\underline{A}}^T\,\tilde{\underline{r}}_2\underline{\underline{A}})\dot{\underline{\Omega}}$$
$$-\underline{\underline{A}}^T\,\tilde{\underline{r}}_2\,\dot{\underline{\omega}}_{2/1}] + \underline{F}_P/M + \underline{F}_Q/M + \underline{F}_T/M + \underline{g} + \underline{\underline{C}}^T\,\tilde{\underline{r}}_1\,\dot{\underline{\Omega}}\,\underline{\underline{C}}^T\,\tilde{\underline{\Omega}}\tilde{\underline{\Omega}}\underline{r}_1, \tag{D-5}$$

where $\underline{\Omega} = (\Omega_1\ \Omega_2\ \Omega_3)^T$, $\underline{\ell}_1 = (\ell_1\ \ 0\ \ 0)^T$, $\underline{\omega} = \underline{\omega}_{2/1} + \underline{\underline{A}}\underline{\Omega}$, $\underline{\omega}_{2/1} = (0\ \ \dot{\theta}_2\ \ \dot{\theta}_3)^T$

$\underline{r}_2 = (r_2\ \ 0\ \ 0)^T$, $\underline{F}_P = (F_{P_{x_L}}\ F_{P_{y_L}}\ F_{P_{z_L}})^T$, $\underline{F}_Q = (F_{Q_{x_L}}\ F_{Q_{y_L}}\ F_{Q_{z_L}})^T$,

$\underline{F}_T = (F_T\ \alpha_z F_T\ -\alpha_y F_T)^T$, $M = m_1+m_2$ and $\underline{g} = (-\ g \sin\Theta_L\ \ 0\ \ g\cos\Theta_L)^T$.

Here, $\alpha_y$ and $\alpha_z$ are thrust misalignment angles. Also,

$$\ddot{\underline{R}}_{P_L} = (\ddot{x}_P\ \ \ddot{\delta}_{P_{y_L}}\ \ \ddot{\delta}_{P_{z_L}})^T, \tag{D-6}$$

where $\delta_{P_{y_L}}$ and $\delta_{P_{z_L}}$ are the displacements of P in the $y_L$- and $z_L$-directions, respectively.

Equation (D-5) can be used to find $\delta_{P_{y_L}}$ and $\delta_{P_{z_L}}$, if $\underline{F}_P$, $\underline{F}_Q$, $\underline{F}_T$, $\dot{\underline{\omega}}_{2/1}$ and $\dot{\underline{\Omega}}$ are expressed in terms of the state variables, $\psi,\theta,\phi,\theta_2,\theta_3,x_p$, $\delta_{P_{y_L}}$, $\delta_{P_{z_L}}$, $\Omega_1$, $\Omega_2$, $\Omega_3$, $\omega_2 = \dot{\theta}_2$, $\omega_3 = \dot{\theta}_3$, $\dot{x}_P$, $\dot{\delta}_{P_{y_L}}$ and $\dot{\delta}_{P_{z_L}}$ and time. We shall consider $\underline{F}_P$ and $\underline{F}_Q$ later.

The equations for the rotational motion of the system of two bodies about their center of mass are the same as in the "free" case considered in Appendix A, except an additional torque is now applied to the two-body system. It is due to the forces on the system at P and Q which produce transverse and axial ($x_1$-axis) torque components and can be expressed as

$$\underline{T}_{sys_{add}} = (\underline{\rho}_1 - \underline{r}_1) \times \underline{F}_P + (\underline{\rho}_2 + \underline{\ell}_2) \times \underline{F}_Q + \underline{T}_P + \underline{T}_Q \ , \qquad \text{(D-7)}$$

where $\underline{T}_P$ and $\underline{T}_Q$ are torques about P and Q, respectively. They are assumed to be axial and due to friction.

Additional terms must also be added to the equations which govern the rotation of Body 2 relative to Body 1. These can be found by considering the equation for rotational motion of Body 2 about the accelerating point R. We have

$$\dot{\underline{H}}_{2/R} = \underline{T}_R - m_2 \, \underline{r}_2 \times \underline{a}_R \ , \qquad \text{(D-8)}$$

where $\dot{\underline{H}}_{2/R}$ is the time rate of change of the angular momentum of Body 2 due to rotation about R, $\underline{T}_R$ is the torque about R, and $\underline{a}_R$ is the absolute acceleration of R. The acceleration $\underline{a}_R$ can be expressed in the form,

$$\underline{a}_R = \ddot{\underline{R}}_P + \ddot{\underline{r}}_1 + \ddot{\underline{\ell}}_1 \ . \qquad \text{(D-9)}$$

Also,

$$\underline{T}_R = \underline{T}_{2/1} + \underline{T}_Q + (\underline{r}_2+\underline{\ell}_2) \times \underline{F}_Q + m_2\underline{r}_2 \times \underline{g} \quad , \tag{D-10}$$

where $\underline{T}_{2/1}$ is the torque on Body 2 due to the torsional springs and dampers used to represent the flexibility of the rocket being modeled.

Now, the acceleration $\ddot{\underline{R}}_P$ can be expressed as [see Eq. (D-1)],

$$\ddot{\underline{R}}_P = \ddot{\underline{R}}_C - \ddot{\underline{r}}_1 - (\ddot{\underline{\ell}}_1+\ddot{\underline{r}}_2) \quad , \tag{D-11}$$

where $\mu = m_2/M$. Obviously,

$$\ddot{\underline{a}}_R = \ddot{\underline{R}}_C - (\ddot{\underline{\ell}}_1+\ddot{\underline{r}}_2). \tag{D-12}$$

However, we also have, from Newton's second law,

$$\ddot{\underline{R}}_C = \underline{g} + (\underline{F}_T + \underline{F}_P + \underline{F}_Q)/M, \tag{D-13}$$

and by using this result along with Eq. (D-10) in Eq. (D-8), we get

$$\dot{\underline{H}}_{2/R} = \underline{T}_{2/1} + \underline{T}_Q - \mu\, \underline{r}_2 \times(\underline{F}_T + \underline{F}_P) + [(1-\mu)\underline{r}_2 + \underline{\ell}_2] \times \underline{F}_Q \quad . \tag{D-14}$$

The additional torque on Body 2 due to the flexible supports and friction is therefore

$$\underline{T}_{2_{add}} = \underline{T}_Q - \mu\underline{r}_2 \times(\underline{F}_T+\underline{F}_P) + [(1-\mu)\underline{r}_2+\underline{\ell}_2] \times \underline{F}_Q \quad . \tag{D-15}$$

Definition of the Forces and Torques at P and Q

The forces at P and Q are assumed to be caused by deformation of the supporting structure, e.g., tube, and coulomb friction. The possibility that the supporting structure will not always be in contact with the rocket at either, or both, points P and Q is allowed for by simply enclosing the rocket in a deadspace "cylinder" of thickness $\varepsilon$. For the purpose of illustrating how the forces at P and Q are defined, figures which imply the

rocket is within a tube are used. However, the model of the forces is also representative of other types of launchers.

In Fig. D-2, the displacement of point P from the launch axis ($x_L$-axis) is represented by $\delta_{P_{y_L}}$ and $\delta_{P_{z_L}}$ in the $\hat{j}_L$ ($y_L$-axis) and $\hat{k}_L$ ($z_L$-axis) directions, respectively. Let

$$\underline{\delta}_P = \delta_{P_{y_L}} \hat{\underline{j}}_L + \delta_{P_{z_L}} \hat{\underline{k}}_L \quad . \tag{D-16}$$

We say that if

$$|\underline{\delta}_P \cdot \hat{\underline{j}}| > \varepsilon, \tag{D-17}$$

where $\hat{\underline{j}}$ is a unit vector which rotates with the rocket, then the component of the elastic restoring force in the y-direction is

$$N_{P_y} = - K_P \underline{\delta}_P \cdot \hat{\underline{j}} \ , \tag{D-18a}$$

where $K_P$ is a constant in this study, but could be considered a function of the distance traveled along the tube. Similarly, the z-component of the restoring force is

$$N_{P_z} = - K_P \underline{\delta}_P \cdot \hat{\underline{k}} \ , \tag{D-18b}$$

if $|\underline{\delta}_P \cdot \hat{\underline{k}}| > \varepsilon$, where $\hat{\underline{k}}$ also rotates with the rocket.

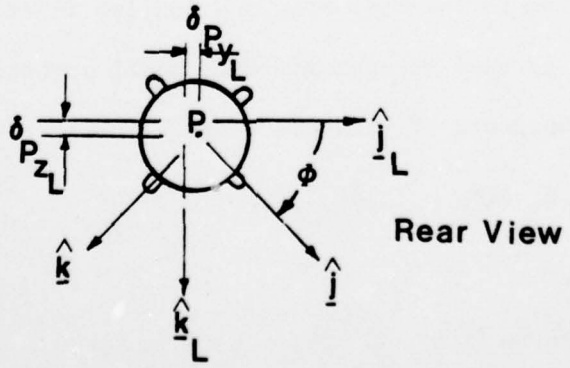


Fig. D.2. Displacement of point P.

AD-A080 606 AUBURN UNIV ALA DEPT OF AEROSPACE ENGINEERING F/G 19/4
AN ANALYSIS OF THE EFFECTS OF TRANSVERSE VIBRATION ON THE ATTIT--ETC(U)
DEC 79 J E COCHRAN, G A CASTLEBERRY, S D REW DAAK40-79-C-0030
UNCLASSIFIED DRSMI/RL-CR-80-2 NL

2 OF 2
AD
A080606

END
DATE
FILMED
3 - 80
DDC

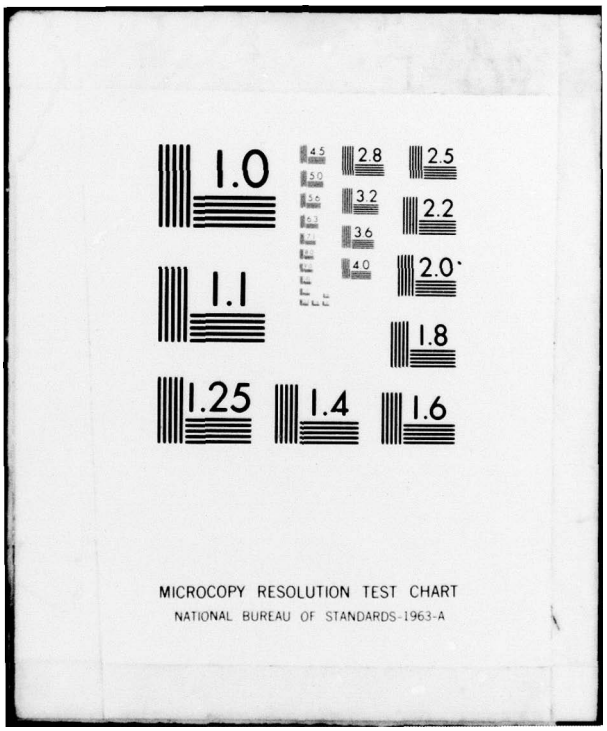
1.0
1.1
1.25
1.4
1.6
1.8
2.0
2.2
2.5
2.8
3.2
3.6
4.0
4.5
5.0
MICROCOPY RESOLUTION TEST CHART
NATIONAL BUREAU OF STANDARDS-1963-A

Referring to Fig. D-3, if $\dot{\phi}$ (the spin rate) is nonzero, frictional forces which oppose such spin are present if the rocket is in contact with the supporting structure. If $\mu_P \neq 0$, $\dot{\phi} > 0$ and $\mu_P = 0$ for $\dot{\phi} = 0$, we have the transverse frictional force components,

$$f_{P_y} = - \mu_P N_{P_z} \tag{D-19b}$$

and

$$f_{P_z} = \mu_P N_{P_y} \quad . \tag{D-19c}$$

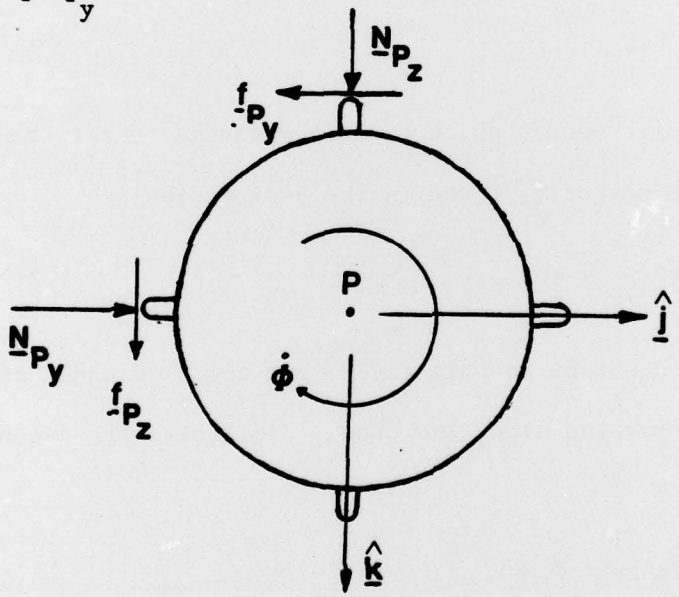


Fig. D.3. Normal and frictional forces.

In addition to the restoring and coulomb friction forces, a viscous damping force is used to approximately model structural damping. The transverse components of this force are

$$d_{P_y} = -\zeta_P K_P \, d(\underline{\delta}_P \cdot \hat{\underline{j}})/dt \tag{D-20a}$$

and

$$d_{P_z} = - \zeta_P \, K_P \, d(\underline{\delta}_P \cdot \hat{\underline{k}})/dt \quad , \tag{D-20b}$$

where $\zeta_P$ is a constant, and the axial component is zero.

If the rocket is translating in the $x_L$ direction, then an additional force due to friction acts at P in the negative $x_L$-direction. The x-component of this force is

$$F_{P_x} = \mu_P[\,|N_{P_y}| + |N_{P_y}|\,] \quad , \quad (\dot{x}_P > 0) . \tag{D-21}$$

The forces acting at Q have the same forms as those acting at P; hence, if the subscript P is changed to Q in Eqs. (D-18) through (D-21) the forces acting at Q are obtained. However, the displacement of the point Q transversely is more complicated than that for point P, since the rotations of both Bodies 1 and 2 contribute to displacement of Q. The displacement components $\delta_{Q_{y_L}}$ and $\delta_{Q_{z_L}}$ (launcher basis) are given by the equation,

$$\begin{bmatrix} 0 \\ \delta_{Q_{y_L}} \\ \delta_{Q_{z_L}} \end{bmatrix} = \begin{bmatrix} 0 \\ \delta_{P_{y_L}} \\ \delta_{P_{z_L}} \end{bmatrix} + \underline{\underline{E}}_{23} \begin{bmatrix} 1 & -\Psi c\Phi+\Theta s\Phi & \Psi s\Phi+\Theta c\Phi \\ \Psi & c\Phi & -s\Phi \\ -\Theta & s\Phi & c\Phi \end{bmatrix} [\underline{\ell}_1 + \underline{r}_1 + \underline{\underline{A}}^T(\underline{r}_2+\underline{\ell}_2)], \tag{D-22}$$

where

$$\underline{\underline{E}}_{23} = \begin{bmatrix} 0 & 0 & 0 \\ 0 & 1 & 0 \\ 0 & 0 & 1 \end{bmatrix} . \tag{D-23}$$

Thus, if products of small angles are neglected,

$$\delta_{Q_{y_L}} = \delta_{P_{y_L}} + \Psi(r_1+\ell_1+r_2+\ell_2) + [\theta_3 c\Phi+\theta_2 s\Phi](r_2+\ell_2) \tag{D-24a}$$

and

$$\delta_{Q_{z_L}} = \delta_{P_{z_L}} - \Theta(r_1+\ell_1+r_2+\ell_2) + [\theta_3 s\Phi - \theta_2 c\Phi](r_2+\ell_2) \tag{D-24b}$$

The torques on Bodies 1 and 2 due to all additional (those not present in free flight) sources can be found by using Eqs. (D-7) and (D-14).

The total torque on the system about its center of mass, obtained assuming that $\Psi$, $\Theta$, $\theta_2$ and $\theta_3$ are small angles, can be expressed as

$$\underline{T}_C = T_A \hat{\underline{i}}_1 + T_1 \hat{\underline{j}}_1 + T_2 \hat{\underline{k}}_1 , \tag{D-25}$$

where

$$T_A = \{T_P + T_Q + T_s - \mu r_2[\theta_2 F_{P_y} + \theta_3 F_{P_z}] + [(1-\mu)r_2 + \ell_2][\theta_2 F_{Q_y} + \theta_3 F_{Q_z}]\} , \tag{D-26a}$$

$$T_1 = \{\underline{\mu\theta_2 r_2 F_{P_x}} + [r_1 + \mu(\ell_1 + r_2)]F_{P_z} - [(1-\mu)r_2 + \ell_2]\theta_2 F_{Q_x}$$
$$- [(1-\mu)r_2 + \ell_2]F_{Q_z} - \alpha_y x'_C F_T + \mu_P r_s N_{P_z}$$
$$+ \mu_Q r_s N_{Q_z} \tag{D-26b}$$

and

$$T_2 = \{\underline{\mu\theta_3 r_2 F_{P_x}} - [r_1 + \mu(\ell_1 + r_2)]F_{P_y} - [(1-\mu)r_2 + \ell_2]\theta_3 F_{Q_x}$$
$$+ [(1-\mu)r_2 + \ell_2] F_{Q_y} - \alpha_z x_C F_T - \mu_P r_s N_{P_y}$$
$$- \mu_Q r_s N_{Q_y}\} , \tag{D-26c}$$

where $T_P$ and $T_Q$ are axial torque components due to friction at P and Q, respectively, $T_s$ is the spin torque, assumed to be applied by an eroding spin turbine,

$$F_{P_y} = \begin{cases} N_{P_Y} & , \dot{\Phi} = 0 , \\ N_{P_y} - \mu_P N_{P_z} & , \dot{\Phi} > 0 \end{cases} \tag{D-27a}$$

and

$$F_{P_z} = \begin{cases} N_{P_z} & , \dot{\Phi} = 0 , \\ N_{P_z} + \mu_P N_{P_y} & , \dot{\Phi} > 0. \end{cases} \tag{D-27b}$$

Force components with Q subscripts are of the same form as those with subscripts. The underlined terms in Eqs. (D-26) are zero if $\dot{x}_P = 0$. They

represent the "couple" parts of torque components due to frictional forces acting axially at P and Q, whereas, the terms involving $F_{P_x}$ and $F_{Q_x}$ represent the remainders of the components. Here $r_s$ is the distance from the rocket centerline to the end of a "shoe."

In a similar manner the transverse torque on Body 2 can be expressed as

$$\underline{T}_{2_{trans}} = T_3 \hat{\underline{j}}_1 + T_4 \hat{\underline{k}}_1 , \qquad \text{(D-28)}$$

where

$$T_3 = \{\mu r_2[\theta_2 \underline{F_{P_x}} + F_{P_z}] - [(1-\mu)r_2+\ell_2][\theta_2 \underline{F_{Q_x}} + F_{Q_z}] - c\dot{\theta}_2 - k\theta_2 + \mu_Q r_s N_{Q_z}\} \qquad \text{(D-29a)}$$

and

$$T_4 = \{\mu r_2[\theta_3 \underline{F_{P_x}} - F_{P_y}] - [(1-\mu)r_2+\ell_2][\theta_3 \underline{F_{Q_x}} - F_{Q_y}] - c\dot{\theta}_3 - k\theta_3 - \mu_Q r_s N_{Q_y}\} \qquad \text{(D-29b)}$$

where again the underlined terms are zero if $\dot{x}_P=0$. Here, as in Appendix A, k is the stiffness of the torsional springs which connect the two bodies and c is the viscous damping coefficient.

Final Form of the Mathematical Model

The complete mathematical model used to obtain the results presented in this report regarding the effects of support flexibility and friction as follows:

Equations of Motion

$$\dot{\Phi} = \Omega_1, \tag{D-30a}$$

$$\dot{\Theta} = \Omega_2 \cos\Phi - \Omega_3 \sin\Phi, \tag{D-30b}$$

$$\dot{\Psi} = \Omega_2 \sin\Phi + \Omega_3 \cos\Phi, \tag{D-30c}$$

$$\dot{x}_p = u_p, \tag{D-30d}$$

$$\dot{\delta}_{P_{y_L}} = \xi_{P_{y_L}}, \tag{D-30e}$$

$$\dot{\delta}_{P_{z_L}} = \xi_{P_{z_L}}, \tag{D-30f}$$

$$\dot{\Omega}_1 = T_A/I_A \quad [T_A \text{ given by Eq. (D-26a)}], \tag{D-30g}$$

$$\dot{\underline{x}} = \underline{\underline{I}}^{-1} \underline{\underline{B}}\, \underline{x} + \underline{\underline{I}}^{-1} \underline{T}, \tag{D-30h}$$

where

$\underline{\underline{I}}$ = inertia matrix defined in Appendix A,

$\underline{\underline{B}}$ = coefficient matrix defined in Appendix A,

$$\underline{x} = (\Omega_2 \quad \Omega_3 \quad \omega_2 \quad \omega_3 \quad \theta_2 \quad \theta_3)^T, \tag{D-30i}$$

and

$$\underline{T} = (T_1 \quad T_2 \quad T_3 \quad T_4 \quad 0 \quad 0)^T \quad T_j,\ j=1,2,3,4$$

defined by Eqs. (D-26b), (D-26c), (D-29a) and (D-29b), respectively.

$$\dot{\xi}_{P_{y_L}} = b\cos\Phi - c\sin\Phi + [(F_{P_y} + F_{Q_y})\cos\Phi - (F_{P_z} + F_{Q_z})\sin\Phi]/M + (F_T/M)[\Psi + \alpha_z \cos\Phi + \alpha_y \sin\Phi] \tag{D-30j}$$

$$\dot{\xi}_{P_{z_L}} = b\sin\Phi + c\cos\Phi + [(F_{P_z} + F_{Q_z})\cos\Phi + (F_{P_y} + F_{P_z})\sin\Phi]/M - (F_T/M)[\Theta - \alpha_z \sin\Phi + \alpha_y \cos\Phi] + g, \tag{D-30k}$$

where

$$b = -[r_1 + \mu(\ell_1+r_2)][\Omega_1\Omega_2 + \dot{\Omega}_3]$$

$$- \mu r_2[2\Omega_1\omega_2 - \theta_3\Omega_1^2 + \theta_2\dot{\Omega}_1 + \dot{\omega}_3]$$

and

$$c = -[r_1 + \mu(\ell_1+r_2)][\Omega_1\Omega_3 - \dot{\Omega}_2]$$

$$- \mu r_2[2\Omega_1\omega_3 + \theta_2\Omega_1^2 + \theta_3\dot{\Omega}_1 - \dot{\omega}_2] .$$

Equation for Angular Momentum

$$\underline{H} = H_1 \hat{\underline{i}}_1 + H_2 \hat{\underline{j}}_1 + H_3 \hat{\underline{k}}_1 , \qquad \text{(D-31)}$$

where

$$H_1 = (A_1+B_1)\Omega_1 , \qquad \text{(D-32a)}$$

$$H_2 = -\theta_3[B_2 + \sigma r_2(\ell_1+r_2) - B_1]\Omega_1 + [B_2 + \sigma r_2(\ell_1+r_2)]\omega_2$$

$$+ [A_2 + B_2 + \sigma(\ell_1+r_2)^2]\Omega_2 \qquad \text{(D-32b)}$$

and

$$H_3 = \theta_2[B_2 + \sigma r_2(\ell_1+r_2) - B_1]\Omega_1$$

$$+ [B_2 + \sigma r_2(\ell_1+r_2)]\omega_3 + [A_2 + B_2 + \sigma(\ell_1+r_2)^2]\Omega_3 . \qquad \text{(D-32c)}$$

Equations for the Angles $\Theta_N$ and $\Psi_N$

$$\Theta_N = \Theta + \theta_2 \cos\Phi - \theta_3 \sin\Phi \qquad \text{(D-33a)}$$

and

$$\Psi_N = \Psi + \theta_2 \sin\Phi + \theta_3 \cos\Phi . \qquad \text{(D-33b)}$$

# DISTRIBUTION

| | No. of Copies |
|---|---|
| Defense Technical Information Center<br>Cameron Station<br>Alexandria, VA 22314 | 2 |
| Commander<br>US Army Missile Command | |
| Attn: DRSMI-O | 3 |
| DRSMI-R, Dr. Kobler | 1 |
| DRSMI-RLH, Mr. Christensen | 7 |
| DRSMI-ICBB, Mr. Edwards | 1 |
| DRSMI-RPT | 2 |
| DRSMI-RPR | 2 |
| DRSMI-LP, Mr. Voigt | 1 |
| Redstone Arsenal, AL 35809 | |
| Office of Naval Research<br>Atlanta Area Office<br>Attn: Mr. Henry Cassall<br>Georgia Institute of Technology<br>325 Hinman Research Bldg.<br>Atlanta, GA 30332 | 1 |
| US Army Material Systems Analysis Activity<br>Attn: DRXSY-MP<br>Aberdeen Proving Ground, MD 21005 | 1 |
| IIT Research Institute<br>Attn: GACIAC<br>10 West 35th Street<br>Chicago, IL 60616 | 1 |